International
Progress Report

IPR-05-33

Äspö Hard Rock Laboratory

DECOVALEX

Uniaxial compression tests of intact rock specimens at dry condition and at saturation by three different liquids: distilled, saline and formation water

Lars Jacobsson
SP Swedish National Testing and Research Institute
Borås, Sweden

Ann Bäckström
Berg Bygg Konsult AB
Solna, Sweden

December 2005

Svensk Kärnbränslehantering AB
Swedish Nuclear Fuel
and Waste Management Co
Box 5864
SE-102 40 Stockholm Sweden
Tel 08-459 84 00
+46 8 459 84 00
Fax 08-661 57 19
+46 8 661 57 19

Äspö Hard Rock
Laboratory

Report no.
IPR-05-33
No.
F84K
Author
Lars Jacobsson
Ann Bäckström
Date
December 2005
Checked by
Rolf Christiansson
Date
January 2006
Approved
Anders Sjöland
Date
2006-02-07

Äspö Hard Rock Laboratory

DECOVALEX

Uniaxial compression tests of intact rock specimens at dry condition and at saturation by three different liquids: distilled, saline and formation water

Lars Jacobsson
SP Swedish National Testing and Research Institute
Borås, Sweden

Ann Bäckström
Berg Bygg Konsult AB
Solna, Sweden

December 2005

Keywords: Rock mechanics, Uniaxial compression test, Elasticity parameters, Stress-strain curve, Post-failure behaviour

Abstract

Uniaxial compression tests, containing the complete loading response beyond compressive failure, so called post-failure tests, were carried out on 20 cylindrical specimens of intact rock from boreholes KF0066A01 and KF0069A01 in Äspö. The specimens were taken from drill cores at two depth levels ranging between 25-36 m (KF0066A01) and 41-47 m (KF0069A01). Moreover, the rock type was Äspö diorite. The effect of different salinity in liquids on the mechanical strength has been investigated. The wet density of the rock specimens was determined .The specimens were prepared differently, 5 specimens were dried and the remaining 15 specimens, with 5 specimens of each type, were water saturated with distilled, formation and saline water, respectively. The elastic properties, represented by the Young's modulus and the Poisson ratio, and the uniaxial compressive strength were deduced from these tests. The specimens were documented by photographing the specimens before and after the mechanical testing.

The measured densities for the water saturated specimens were in the range 2660-2690 kg/m^3 and had a mean value of 2672 kg/m^3 and the peak values of the axial compressive stress were in the range 232.8- 335.8 MPa with a mean value of 272.1 MPa. The elastic parameters were determined at load corresponding to 50 % of the failure load and it was found that Young's modulus was in the range of 65.1-73.4 GPa with a mean value of 69.5 GPa and the Poisson ratio was in the range of 0.26-0.34 with a mean value of 0.29. It was seen from the mechanical tests that the material in the specimens responded in a brittle way.

Sammanfattning

Enaxiella kompressionsprov med belastning upp till brott och efter brott, så kallade ”post-failure tests”, har genomförts på 20 cylindriska provobjekt av intakt berg. Proverna är tagna från två borrkärnor från borrhålen KF0066A01 och KF0069A01 i Äspö vid två djupnivåer 25-36 m (KF0066A01) och 41-47 m (KF0069A01). Bergtypen vid dessa nivåer var Äspö diorit. Effekten av olika vätskors salinitet på den mekaniska hållfastheten har undersökts. Densiteten hos bergproverna i vått tillstånd mättes upp. Proverna förbereddes på olika sätt, 5 prover torkades och de återstående 15 proven vattenmättades, med 5 prover vardera, med destillerat, formations- och saltvatten. De elastiska egenskaperna, representerade av elasticitetsmodulen och Poissons tal, har bestämts ur försöken. Provobjekten fotograferades före och efter de mekaniska proven.

Den uppmätta densiteten hos de vattenmättade proven var mellan 2660-2690 kg/m^3 med ett medelvärde på 2672 kg/m^3. Toppvärdena för den kompressiva axiella spänningen låg mellan 232,8- 335,8 MPa med ett medelvärde på 272,1 MPa. De elastiska parametrarna bestämdes vid en last motsvarande 50 % av topplasten vilket gav en elasticitetsmodul mellan 65,1-73,4 GPa med ett medelvärde på 69,5 GPa och Poissons tal mellan 0,26-0,34 med ett medelvärde på 0,29. Vid belastningsförsöken kunde man se att materialet i provobjekten hade ett sprött beteende.

Contents

1 Introduction

When building an underground facility, a disturbance in the equilibrium between solid and liquid phases can be created. In Precambrian shield areas, the salinity of the ground water increases with depth. This is the case of the Äspö HRL /Louvat, et al., 1999; Laaksoharju, 2003/, of the Stripa deep rock laboratory and of the Canadian AECL's underground research laboratory (URL). The water inflow into the tunnels is removed using elaborate and efficient pumping systems. But by removing the water in the tunnel, an upwards motion of highly saline water from larger depth can result in an increase of the salinity of the water inflow. Saline water is known to be highly corrosive to iron structures whereas the corrosive effect of saline water on crystalline rock is not very extensively investigated.

Mechanical test conducted on crystalline rocks and other rock types indicate reduction in strength of the rock when submerged in saline water solutions /e.g. Feng et al., 2001; Seto et al, 1998; Feucht and Logan, 1990/. Unfortunately, the combined water effect of acidity and salinity has been studied in the tests on crystalline rocks. In the tests reported in this text, the pH was close to 7 for all waters, this will hopefully facilitate the identification of the effect of salinity differences. It is known that water has a reducing effect on the strength of the rock and it is likely that this effect is induced either by chemical of physical alteration of the matrix /e.g. Hoek, 1968/. The effect of water can clearly be seen on the shear strength of rock /Feucht and Logan, 1990/. For sandstone samples the same authors show an increased weakening with stronger saline solution. Similarly, from earlier experiments on Gosford sandstone and Western Australian granite by Seto et al. /1998/ it has been found that the tensile strength and zeta potential are functions of ionic concentrations. With stronger ionic concentrations and zeta potential close to 0, the tensile strength decreases.

The effect of different chemical solutions on uniaxial compressive peak strength of different rock types has been investigated by Feng et al. /2001/. The results indicated that chemical corrosion induced reduction of uniaxial compressive peak load. This indicates that with stronger alkalescence and acidity of chemical solution, the reduction of the strength increases.

Uniaxial compression tests, with loading beyond the failure point into the post-failure regime, have been conducted on dry and water-saturated specimens sampled from boreholes KF0066A01 and KF0069A01 in Äspö. These tests belong to one of the activities performed as part of the project DECOVALEX IV, Task B (HMC Studies of the Excavation Disturbed Zone (EDZ) in Crystalline rock) lead by the Swedish Nuclear Fuel and Waste Management Co (SKB). The tests were carried out in the material and rock mechanics laboratories at the department of Building Technology and Mechanics at the Swedish National Testing and Research Institute (SP). All work is carried out in accordance with the activity plan AP TDF 84-05-011 (SKB internal controlling document) and is controlled by SP-QD 13.1 (SP internal quality document).

2 Objective and scope

The purpose of the testing is to investigate the effect of liquids with different salinity on the uniaxial compressive strength of intact rock specimens of Äspö diorite. The specimens originate from boreholes KF0066A01 and KF0069A01 in Äspö. The results will lead to a better understanding on how the mechanical properties of rock is affected by chemical processes. Moreover, the results are going to be used in models for simulating the deterioration of the rock due to chemical processes.

The loading is carried out into the post-failure regime in order to study the mechanical behaviour of the rock after cracking, thereby enabling determination of the brittleness and residual strength.

3 Procedure

SKB supplied SP with rock cores and they arrived at SP in two batches, in April and June 2005 and were tested during August 2005. Cylindrical specimens were cut from the cores and selected based on the preliminary core logging with the strategy to primarily investigate the properties of the dominant rock types. The method description SKB MD 190.001, version 2.0 (SKB internal controlling document) was followed for the sampling and for the uniaxial compression tests and the method description SKB MD 160.002, version 2.0 (SKB internal controlling document) was followed when the density was determined. As to the specimen preparation, the end surfaces on the specimens were grinded in order to comply with the required shape tolerances and then put in water and kept stored in water, with a minimum of 7 days, whereupon the density was measured. This yields a water saturation, which is intended to resemble the in-situ moisture condition. The specimens were stored in water until the uniaxial compression tests were carried out, except for the specimens that were aimed to be tested in dry conditions. The specimens aimed to be tested in dry conditions were dried according to /SS-EN 1936/. Additional density measurements according to and porosity measurements according to /SS-EN1936/ on the same specimens are reported by /Savukoski, 2005/. The specimens were photographed before and after the mechanical testing.

The uniaxial compression tests were carried out using radial strain as the feed back signal in order to obtain the complete response in the post-failure regime on brittle specimens as is described in the method description SKB MD 190.001, version 2.0 (SKB internal controlling document) and in the ISRM suggested method /ISRM, 1999/. The axial ε_a and radial strain ε_r together with the axial stress σ_a were recorded during the test. The peak value of the axial compressive stress σ_c was determined at each test. Furthermore, two elasticity parameters, Young's modulus E and Poisson ratio ν, were deduced from the tangent properties at 50 % of the peak load. Diagrams with the volumetric and crack volumetric strain versus axial stress are reported. These diagrams can be used to determine crack initiation stress σ_i and the crack damage stress σ_d, cf. /Martin and Chandler, 1994; Eberhardt et al., 1998/.

4 Equipment

4.1 Specimen preparation and density measurement

A circular saw with a diamond blade was used to cut the specimens to their final lengths. The surfaces were then grinded after cutting in a grinding machine in order to achieve a high-quality surface for the axial loading that complies with the required tolerances. The measurements of the specimen dimensions were made with a sliding calliper. Furthermore, the tolerances were checked by means of a dial indicator and a stone face plate. The specimen preparation is carried out in accordance with ASTM 4543-01 /ASTM 4543-01, 2001/.

The specimens and the water were weighed using a scale weighing machine. A thermometer was used for the water temperature measurement. The calculated wet density was determined with an uncertainty of ± 4 kg/m^3.

4.2 Mechanical testing

The mechanical tests were carried out in servo controlled testing machine specially designed for rock tests, see Figure 3-1. The system contains of a load frame, a hydraulic pump unit, a controller unit and various sensors. The communication with the controller unit is accomplished by means of special testing software running on a PC that is connected to the controller. The load frame has a high stiffness and a fast responding actuator, cf. the ISRM suggested method /ISRM, 1999/.

Figure 3-1: *Rock testing system. From left: Digital controller unit, pressure cabinet (used for triaxial tests) and load frame. The PC with the test software (not shown in the picture) is placed on the left hand side of the controller unit.*

The stiffness of the various components in the loading chain in the load frame has been optimized in order to obtain a high total stiffness. This includes, the load frame, load cell, load platens and piston, as well as minimizing the amount of hydraulic oil in the cylinder. Furthermore, the sensors, the controller and the servo valve are fast responding components. The axial load is determined using a load cell, which has a maximum capacity of 1.5 MN. The uncertainty of the load measurement is less than 1%.

The axial and circumferential (radial) deformations of the rock specimens were measured. The rock deformation measurement systems are based on miniature LVDTs, which have a measurement range of +/- 2.5 mm. The relative error for the LVDTs are less than 0.6 % within a 1 mm range for the axial deformation measurements and less than 1.3 % within a 3 mm range for the circumferential deformation measurement. The LVDTs have been calibrated by means of a micrometer.

Two independent systems were used for the axial deformation measurement in order to obtain two comparative results. The first system (S1), see Figure 3-2, comprises two aluminium rings that are attached on the specimen placed at ¼ and ¾ of the specimen height. Two LVDTs mounted on the rings are used to measure the distance change between the rings on opposite sides of the specimen. As to the attachment, a rubber band made of thin rubber hose with 0.5 mm thickness is first mounted on the specimen right under where the rings are to be mounted. The rings have three adjustable spring-loaded screws each with a rounded tip pointing on the specimen with 120 degrees division. The screw tips are thus pressing on the rubber band. The second system (S2), see Figure 3-3, consists of two aluminium plates that are clamped around the circular loading platens of steel on top and on bottom of the specimen. Two LVDTs, mounted on the plates, measure the distance change between these plates at opposite sides of the specimen at corresponding positions as for the first measurement system (S1).

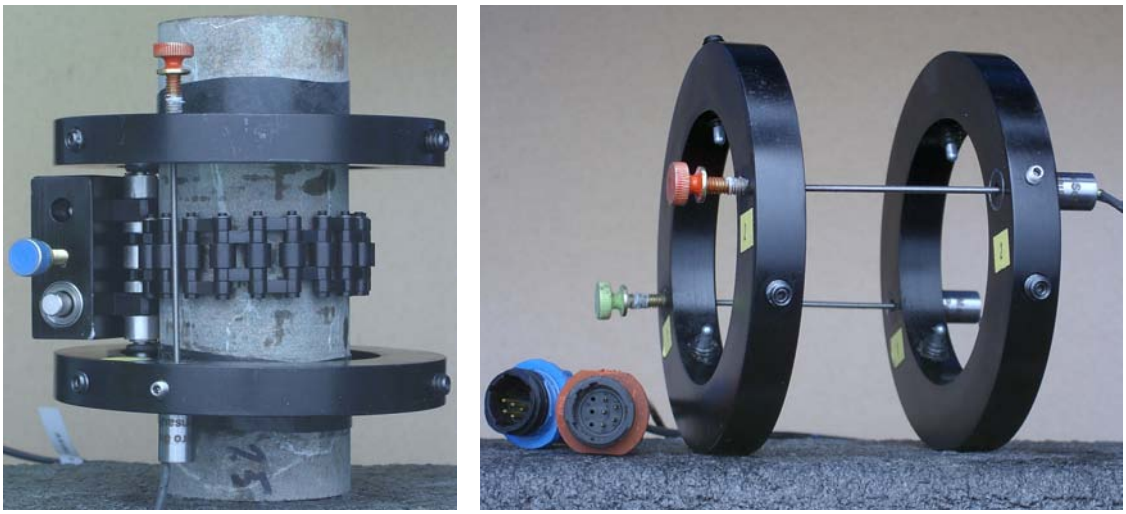

Figure 3-2: *Left: Rings and LVDTs for local axial deformation measurement. Right: Specimen with two rubber bands. Devices for local axial and circumferential deformation measurements attached on the specimen.*

The radial deformation was obtained by using a chain mounted around the specimen at mid-height, see Figures 3-2 and 3-3. The change of the chain-opening gap was measured by means of one LVDT and the circumferential and thereby also the radial deformation could be obtained. See Appendix A.

The specimens were photographed with a 4.0 Mega pixel digital camera at highest resolution and the photographs were stored in a jpeg-format.

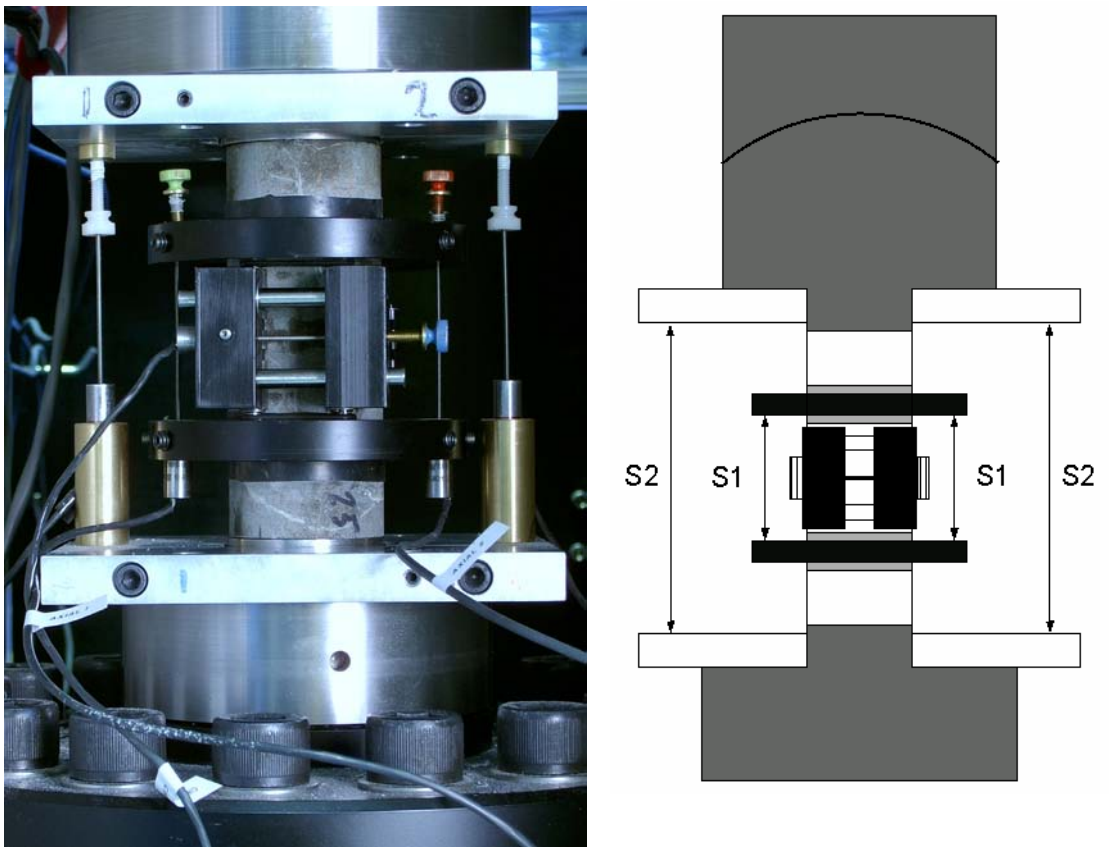

Figure 3-3: *Left: Specimen inserted between the loading platens. The two separate axial deformation measurement devices can be seen: system (S1) that measures the local axial deformation (rings) and system (S2) that measures the deformation between the aluminium plates (total deformation). Right: Principal sketch showing the two systems used for the axial deformation measurements.*

5 Execution

The water saturation and determination of the density of the wet specimens were made in accordance with the method description SKB MD 160.002, version 2.0 (SKB internal controlling document). This includes determination of density in accordance to ISRM /ISRM, 1975/ and water saturation by /SS EN 13755/. The drying of the specimens designated for the tests at dry conditions were carried out according to /SS-EN 1936/. See also the report on additional density measurements and porosity measurements /Savukoski, 2005/. The uniaxial compression tests were carried out according to the method description SKB MD 190.001, version 2.0 (SKB internal controlling document). The test method is based on ISRM suggested method /ISRM, 1999/.

5.1 Description of the samples

The rock type characterisation was made according to Stråhle /Stråhle, 2001/ using the SKB mapping system (Boremap). The rock type is Äspö diorite in all specimens. The borehole name, identification marks, upper and lower sampling depth (Secup and Seclow) and moisture conditions are shown in Table 4-1.

Table 4-1: Borehole, specimen identification, sampling depth for all specimens.

Borehole	Identification	Secup [m]	Seclow [m]	Moisture condition
KF0066A01	6T	26.03	26.16	Dry specimen
KF0066A01	31T	27.80	27.95	Dry specimen
KF0066A01	18T	30.60	30.73	Dry specimen
KF0066A01	25T	35.87	36.00	Dry specimen
KF0069A01	29T	45.58	45.71	Dry specimen
KF0066A01	7D	26.16	26.29	Saturated distilled water
KF0066A01	24D	27.53	27.66	Saturated distilled water
KF0066A01	15D	29.72	29.85	Saturated distilled water
KF0066A01	19D	30.73	30.86	Saturated distilled water
KF0069A01	26D	40.97	41.09	Saturated distilled water
KF0066A01	16F	29.85	29.98	Saturated formation water
KF0066A01	20F	30.86	31.00	Saturated formation water
KF0069A01	27F	41.09	41.22	Saturated formation water
KF0069A01	28F	42.02	42.15	Saturated formation water
KF0069A01	30F	46.36	46.49	Saturated formation water
KF0066A01	4S	25.49	25.62	Saturated saline water
KF0066A01	9S	26.42	26.55	Saturated saline water
KF0066A01	13S	28.63	28.76	Saturated saline water
KF0066A01	17S	30.33	30.46	Saturated saline water
KF0069A01	21S	47.33	47.47	Saturated saline water

5.2 Specimen preparation and density measurement

The temperature of the water was 21.8 °C, which equals to a water density of 998.0 kg/m^3, when the determination of the wet density of the rock specimens was carried out. Further, the specimens had been stored 7 days in water when the density was determined.

An overview of the activities during the specimen preparation is shown in the step-by step description in Table 4-2.

5.3 Mechanical testing

The specimens had been stored 63-66 days in water, except for the dry specimens, when the uniaxial compression tests were carried out. The functionality of the testing system was checked, by carrying out tests on other cores with a similar type rock before the tests described in this report started. A check-list was filled in successively during the work in order to confirm that the different specified steps had been carried out. Moreover, comments were made upon observed things during the mechanical testing that are relevant for the interpretation of the results. The check-list form is a SP internal quality document.

An overview of the activities during the mechanical testing is shown in the step-by step description in Table 4-3.

5.4 Data handling

The test results were exported as text files from the test software and stored in a file server on the SP computer network after each completed test. The main data processing, in which the elastic moduli were computed and the peak stress was determined, has been carried out in the program MATLAB /MATLAB, 2002/. Moreover, MATLAB was used to produce the diagrams shown in Section 5.1 and in Appendix B. The summary of results in Section 5.2 with tables containing mean value and standard deviation of the different parameters and diagrams were produced using MS Excel. MS Excel was also used for reporting data to the SICADA database.

Table 4-2: Activities during the specimen preparation.

Step	Activity
1	The drill cores were marked where the specimens are to be taken.
2	The specimens were cut to the specified length according to markings and the cutting surfaces were grinded.
3	The tolerances were checked: parallel and perpendicular end surfaces, smooth and straight circumferential surface.
4	The diameter and height were measured three times each. The respectively mean value determines the dimensions that are reported.
5	The specimens were then water saturated according to the method described in SKB MD 160.002, version 2.0 (SKB internal controlling document) and were stored for minimum 7 days in water whereupon the wet density was determined.

5.5 Analyses and interpretation

As to the definition of the different results parameters we begin with the axial stress σ_a, which is defined as

$$\sigma_a = \frac{F}{A}$$

where F is the axial force acting on the specimen and A is specimen cross section area. The peak value of the axial stress during a test is representing the uniaxial compressive strength σ_c in the results presentation.

Table 4-3: Activities during the mechanical testing.

Step	Activity
1	Digital photos were taken on each specimen before the mechanical testing.
2	Devices for measuring axial and circumferential deformations were attached to the specimen.
3	The specimen was put in place and centred between the frame loading platens.
4	The core on each LVDT was adjusted by means of a set screw to the right initial position. This was done so that the optimal range of the LVDTs can be used for the deformation measurement.
5	The frame piston was brought down into contact with the specimen with a force corresponding to 0.6 MPa axial stress.
6	A load cycle with loading up to 5 MPa and unloading to 0.6 MPa was conducted in order to settle possible contact gaps in the spherical seat in the piston and between the rock specimen and the loading platens.
7	The centring was checked again.
8	The deformation measurement channels were zeroed in the test software.
9	The loading was started and the initial loading rate was set to a radial strain rate of -0.025 %/min. The loading rate was increased after reaching the post-failure region. This was done in order to prevent the total time for the test to become too long.
10	The test was stopped either manually when the test had proceeded large enough to reveal the post-failure behaviour, or after severe cracking had occurred and it was judged that very little residual axial loading capacity was left in the specimen.
11	Digital photos were taken on each specimen after the mechanical testing.

The average value of the two axial displacement measurements on opposite sides of the specimen is used for the axial strain calculation, cf. Figure 3-3. In the first measurement system (S1), the recorded deformation represents a local axial deformation δ_{local} between the points at ¼ and ¾ height. A local axial strain is defined as

$$\varepsilon_{a,local} = \delta_{local}/L_{local}$$

where L_{local} is the distance between the rings before loading.

In the second measurement system (S2), the recorded displacement corresponds to a total deformation that, in addition to total rock deformation, also contains the local deformations that occur in the contact between the rock and the loading platens and further it also contains the deformation of the steel loading platens at each side of the specimen ends. The average value of the two total deformation measurements on opposite sides of the specimen is defined as the total deformation δ_{total}. An axial strain based on the total of the deformation is defined as

$\varepsilon_{a,total} = \delta_{total}/L_{total}$

where L_{total} is the height of the rock specimen.

The radial deformation is measured by means of a chain mounted around the specimen at mid-height, cf. Figures 3-2 and 3-3. The change of chain opening gap is measured by means of one LVDT. This measurement is used to compute the radial strain ε_r, see Appendix A. Moreover, the volumetric strain ε_{vol} is defined as

$\varepsilon_{vol} = \varepsilon_a + 2\varepsilon_r$

The stresses and the strains are defined as positive in compressive loading and deformation. The elasticity parameters are defined by the tangent Young's modulus E and tangent Poisson ratio ν as

$$E = \frac{\sigma_a(0.60\sigma_c) - \sigma_a(0.40\sigma_c)}{\varepsilon_a(0.60\sigma_c) - \varepsilon_a(0.40\sigma_c)}$$

$$\nu = -\frac{\varepsilon_r(0.60\sigma_c) - \varepsilon_r(0.40\sigma_c)}{\varepsilon_a(0.60\sigma_c) - \varepsilon_a(0.40\sigma_c)}$$

The tangents were evaluated with values corresponding to an axial load between 40 % and 60 % of the axial peak stress σ_c.

Two important observations can be made from the results:

(i) The results based on the total axial deformation measurement (S2) display a lower axial stiffness, i.e. a lower value on Young's modulus, than in the case when the results are based on the local axial deformation measurement (S1). This is due to the additional deformations from the contact interface between the rock specimen and the steel loading platens and also due to the deformation of the loading platens themselves.

(ii) It can be seen that the response differs qualitatively between the results obtained with the local axial deformation measurement system (S1) and the system that measure total axial deformation (S2). In some cases the post-peak response obtained with the local deformation measurement system seems not to be physically correct. This can be due to a number of reasons, e.g. that a crack caused a localized deformation, see Figure 4-1. Another explanation could be that the rings attached to the specimens have slightly slipped or moved for example if a crack was formed nearby one of the attachment points.

It is reasonable to assume that results based on the local axial deformation measurement (S1) are fairly accurate up to the formation of the first macro cracks or up to the peak load, but not after. However, the results obtained with the total axial deformation measurement (S2) seem to be qualitatively correct after failure. We will therefore report the results based on the total axial deformation measurement, but carry out a correction of those results as described below in order to get overall good results.

The total axial deformation δ_{total} measured by (S2) is a summation of several deformations

$$\delta_{total} = \delta_{rock} + \delta_{system} \quad (1)$$

where

$$\delta_{system} = \delta_{interface} + \delta_{loading\ platens}$$

and δ_{rock} is the axial deformation of the whole rock specimen. Assume that the system deformation is proportional to the applied axial force F_a in the loading chain, i.e.

$$\delta_{system} = F_a/K_{system} \quad (2)$$

where K_{system} is the axial stiffness in the system (containing the interface between the rock and loading platens and the deformation of the loading platens). Combining (1) and (2) leads to

$$\delta_{rock} = \delta_{total} - F_a/K_{system} \quad (3)$$

where an expression of the axial deformation in the whole specimen is obtained. This can be viewed as a correction of the measurements made by system (S2). By using δ_{rock} to represent the axial deformation of the specimen that is based on a correction of the results of the total axial deformation will yield good results both in the loading range up to failure and also at loading after failure. However, it is noticed that K_{system} is not known and has to be determined.

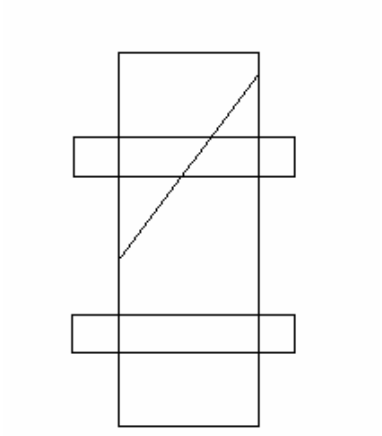

Figure 4-1: *Example of cracking that may cause results that are difficult to interpret with a local deformation measurement.*

It was previously suggested that the local axial deformation measurement represents the real rock deformation well up to the load where the macro cracks forms. Further, it is fair to assume that the axial deformation is homogenous at this part of the loading. Hence, we get

$$\delta_{rock} = \delta_{local} \cdot L_{total}/L_{local}$$

This yields representative values of the total rock deformation for the first part of the loading up to point where macro cracking is taking place. By rewriting (2) we get

$$K_{\text{system}} = \frac{F_{\text{a}}}{\delta_{\text{system}}} \tag{4}$$

It is now possible to determine δ_{system} up to the threshold of macro cracking. We will, however, compute the system stiffness based on the results between 40% and 60% of the axial peak stress σ_c. This means that the Young's modulus and the Poisson ratio will take the same values both when the data from the local axial deformation measurement (S1) and when the data from corrected total axial deformation are used. This means

$$K_{\text{system}} = \frac{F_{\text{a}}(0.60\sigma_{\text{c}}) - F_{\text{a}}(0.40\sigma_{\text{c}})}{\delta_{\text{system}}(0.60\sigma_{\text{c}}) - \delta_{\text{system}}(0.40\sigma_{\text{c}})} \tag{5}$$

where $\delta_{system} = \delta_{total} - \delta_{rock}$ according to (1). The results based on the correction according to (3) and (5) are presented in Section 5.1 whereas the original measured unprocessed data are reported in Appendix B.

A closure of present micro cracks will take place initially during axial loading. Development of new micro cracks will start when the load is further increased and axial stress reaches the crack initiation stress σ_i. The crack growth at this stage is as stable as increased loading is required for further cracking. A transition from a development of micro cracks to macro cracks will take place when the axial load is further increased. At a certain stress level the crack growth becomes unstable. The stress level when this happens is denoted the crack damage stress σ_d, cf. /Martin and Chandler, 1994/. In order to determine the stress levels we look at the volumetric strain.

By subtracting the elastic volumetric strain $\varepsilon_{\text{vol}}^{\text{e}}$ from the total volumetric strain a volumetric strain corresponding to the crack volume $\varepsilon_{\text{vol}}^{\text{cr}}$ is obtained. This has been denoted calculated crack volumetric strain in the literature, cf. / Martin and Chandler, 1994; Eberhardt et al., 1998/. We have thus

$$\varepsilon_{\text{vol}}^{\text{cr}} = \varepsilon_{\text{vol}} - \varepsilon_{\text{vol}}^{\text{e}}$$

Assuming linear elasticity leads to

$$\varepsilon_{\text{vol}}^{\text{cr}} = \varepsilon_{\text{vol}} - \frac{1-2\nu}{E}\sigma_{\text{a}}$$

where $\sigma_r = 0$ was used. Experimental investigations have shown that the crack initiation stress σ_i coincides with the onset of increase of the calculated crack volume, cf. / Martin and Chandler, 1994; Eberhardt et al., 1998/. The same investigations also indicate that the crack damage stress σ_d can be defined as the axial stress at which the total volume starts to increase, i.e. when a dilatant behaviour is observed.

6 Results

The results of the individual specimens are presented in Section 5.1 and a summary of the results is given in Section 5.2. The reported parameters are based both on unprocessed raw data obtained from the testing and processed data and were reported to the SICADA database. These data together with the digital photographs of the individual specimens were handed over to SKB. The handling of the results follows SDP-508 (SKB internal controlling document) in general.

6.1 Description and presentation of the specimen

The cracking is shown in pictures taken on the specimens and comments on observations that appeared during the testing are reported. The elasticity parameters have been evaluated by using the results from the local axial deformation measurements. The data from the adjusted total axial deformation measurements, cf. Section 4.4, are shown in this Section. Red rings are superposed on the graphs indicating every five minutes of the progress of testing.

Diagrams showing the data from both the local and the total axial deformation measurements, system (S1) and (S2) in Figure 3-3, and the computed individual values of K_{system} used at the data corrections are shown in Appendix B. The diagrams actual radial strain rates versus the test time are also presented in Appendix B. The results for the individual specimens are shown in Subsections 5.1.1 to 5.1.4.

6.1.1 Dry specimens

Specimen ID: 6T

Before mechanical test

After mechanical test

Diameter [mm]	Height [mm]	Density [kg/m^3]
50.9	125.4	2660

Comments Spalling on opposite sides along the specimen is observed. Short load oscillations occurred during the testing due to spalling. The specimen had a curvature larger than what is recommended in /ISRM, 1999/.

Specimen ID: 06T

Youngs Modulus (E):	71.6	[GPa]
Poisson Ratio (ν):	0.301	[−]
Axial peak stress (σ_c):	335.8	[MPa]

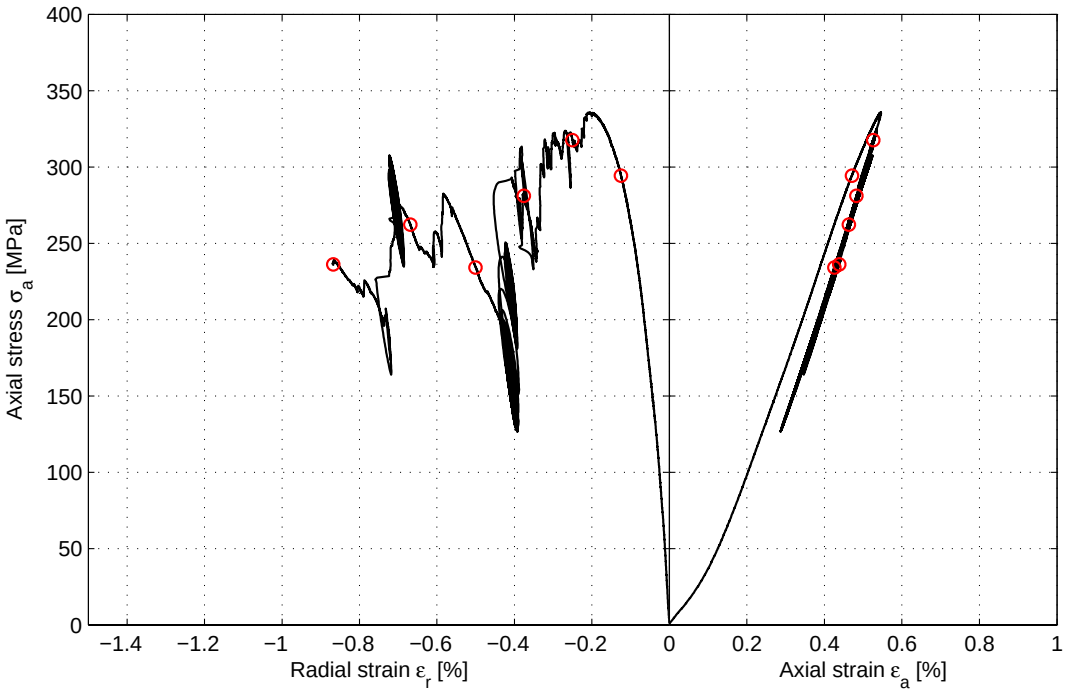

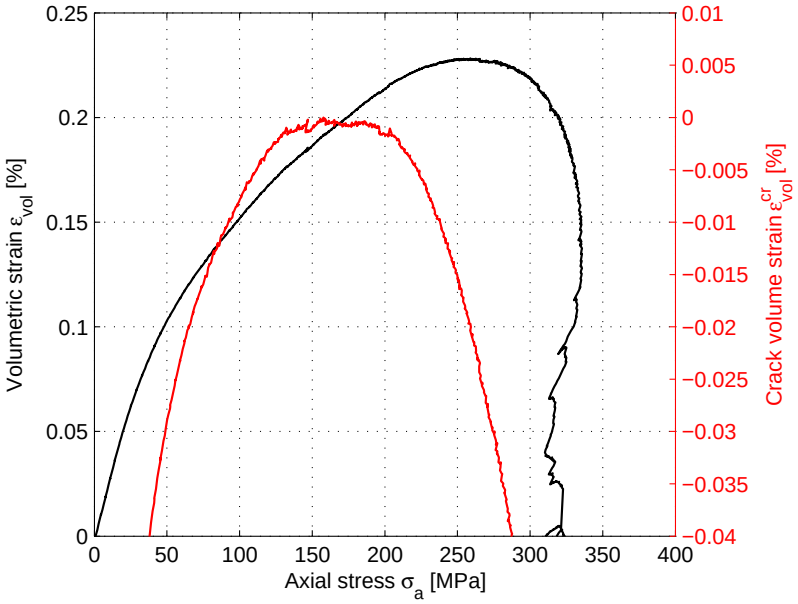

Specimen ID: 31T

Before mechanical test

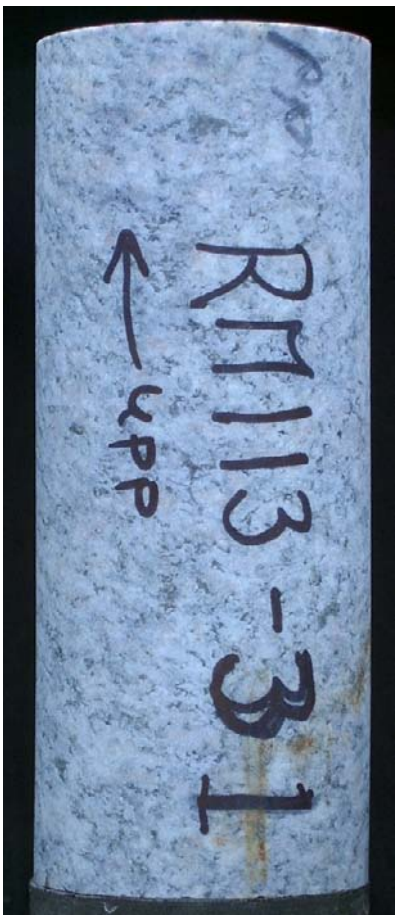

After mechanical test

Diameter [mm]	**Height [mm]**	**Density [kg/m^3]**
50.8	127.5	2680

Comments Spalling on one side along the specimen is observed.

Specimen ID: SKBBBK−113−31T

Youngs Modulus (E):	71.8	[GPa]
Poisson Ratio (ν):	0.274	[−]
Axial peak stress (σ_c):	283.6	[MPa]

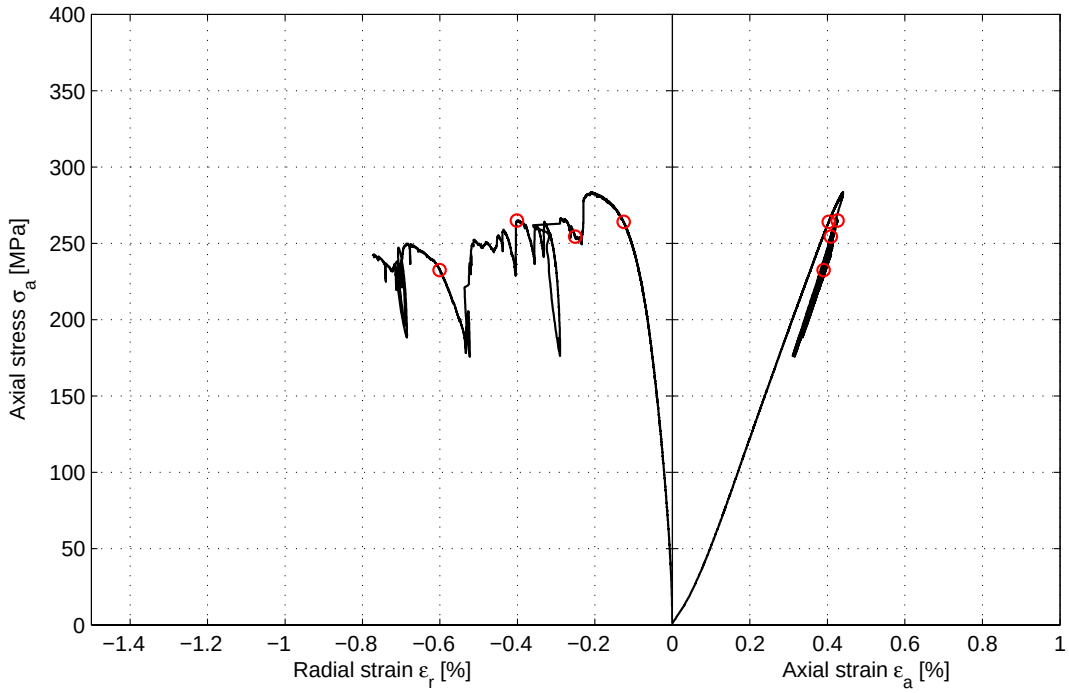

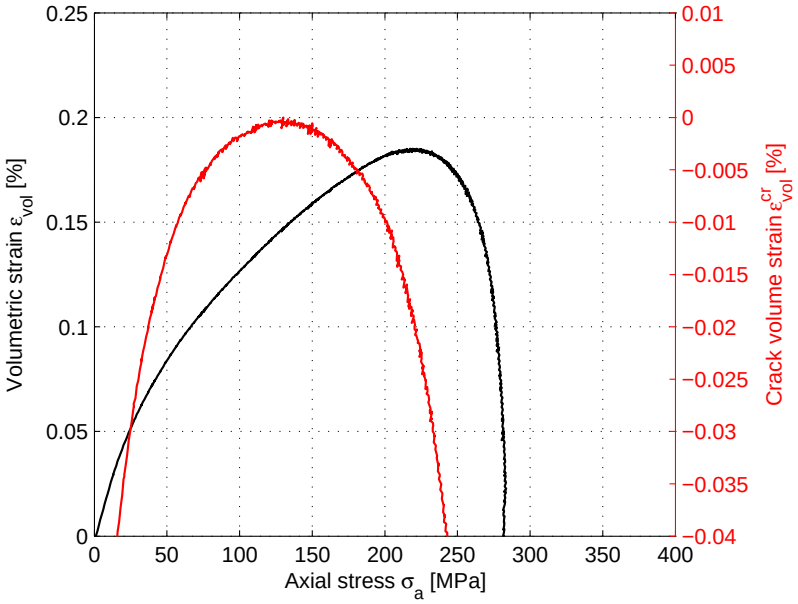

Specimen ID: 18T

Before mechanical test

After mechanical test

Diameter [mm]	Height [mm]	Density [kg/m^3]
50.8	125.4	2680

Comments Spalling on one side along the specimen is observed. The load started to oscillate and the test was stopped. The specimen had a curvature larger than what is recommended in /ISRM,1999/.

Specimen ID: 18T

Youngs Modulus (E):	70.4	[GPa]
Poisson Ratio (ν):	0.285	[−]
Axial peak stress (σ_c):	295.1	[MPa]

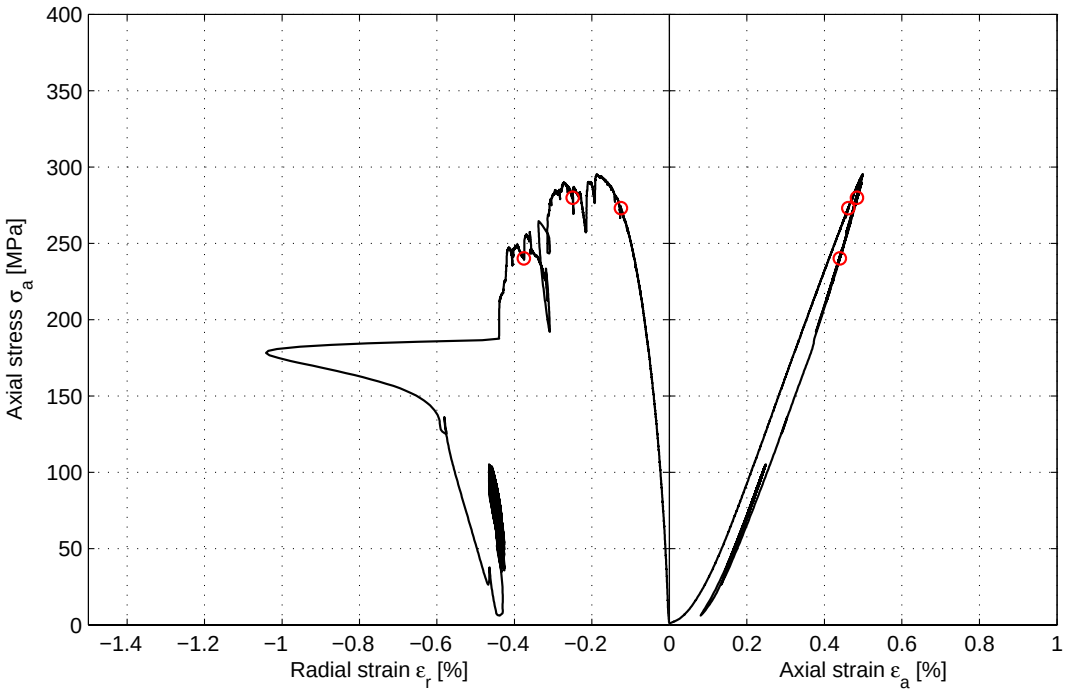

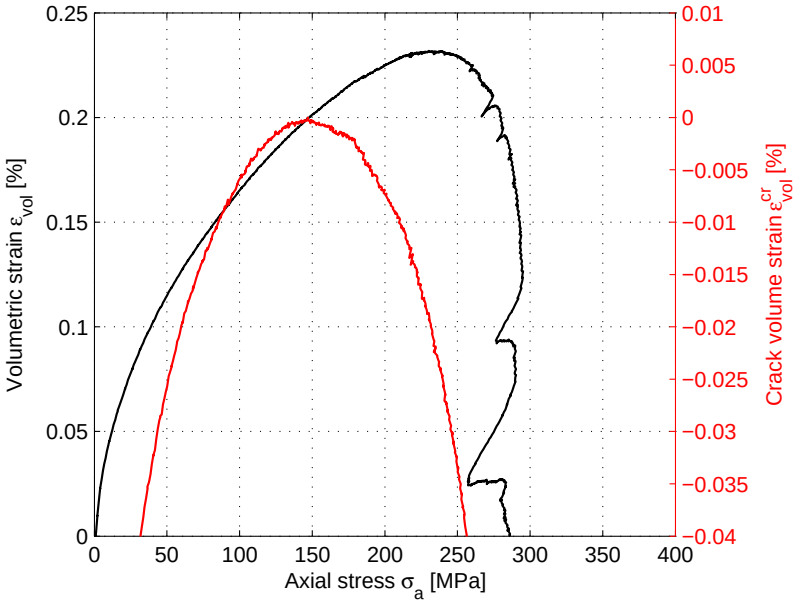

Specimen ID: 25T

Before mechanical test

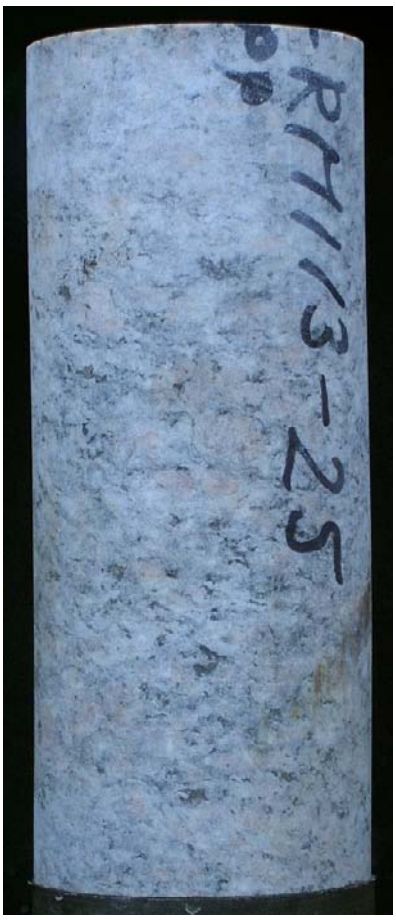

After mechanical test

Diameter [mm]	**Height [mm]**	**Density [kg/m^3]**
50.8	125.4	2690

Comments Spalling on one side along the specimen is observed. A severe cracking caused a sudden increase of the radial strain and the specimen was completely unloaded. The specimen had a curvature larger than what is recommended in /ISRM, 1999/.

Specimen ID: 25T

Youngs Modulus (E):	71.2	[GPa]
Poisson Ratio (ν):	0.285	[−]
Axial peak stress (σ_c):	273.9	[MPa]

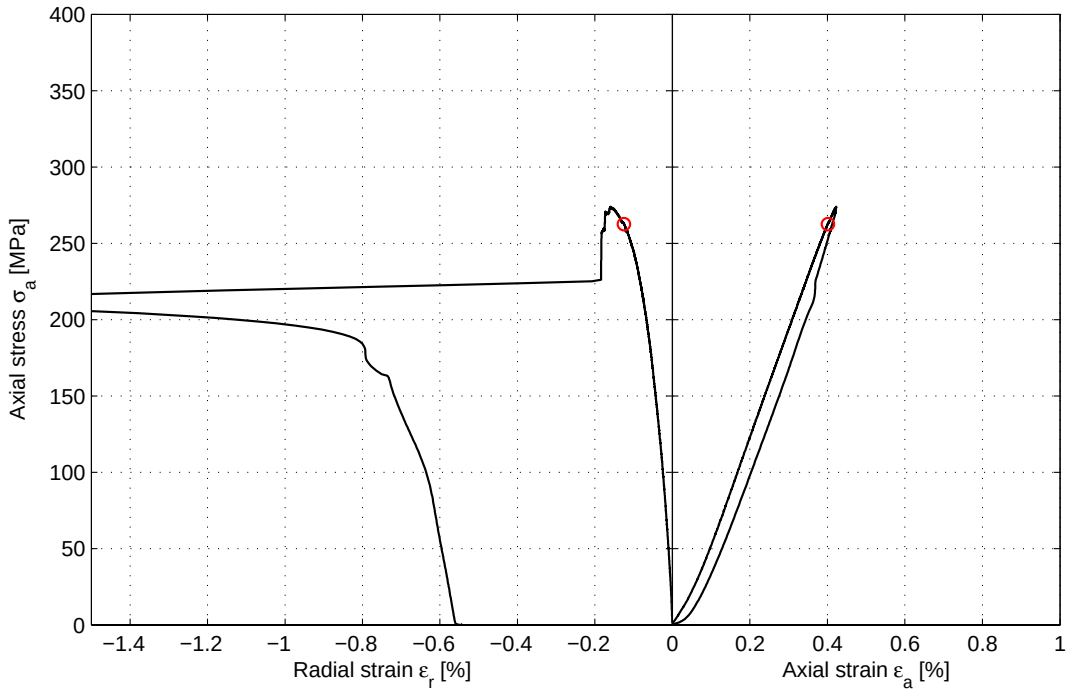

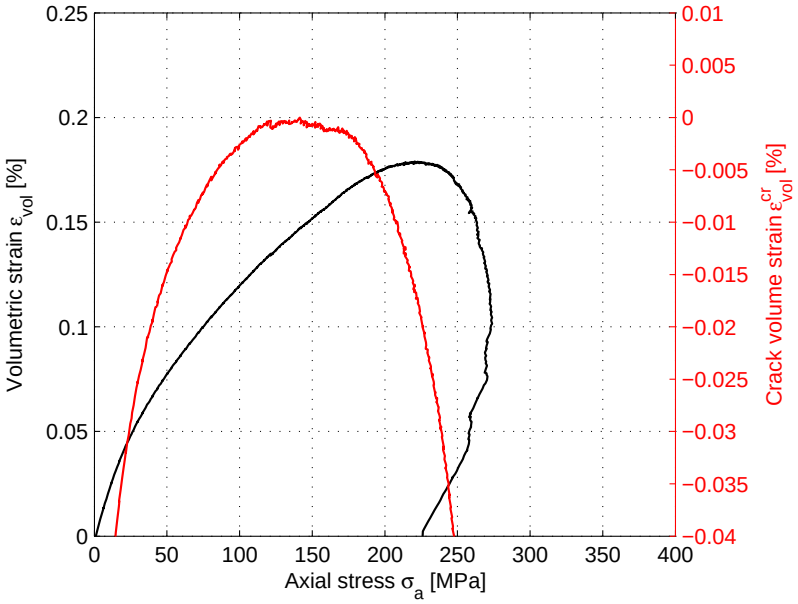

Specimen ID: 29T

Before mechanical test

After mechanical test

Diameter [mm]	Height [mm]	Density [kg/m^3]
50.7	125.4	2680

Comments Spalling on one side along the specimen plus a small local spalling 30 mm from the main cracking is observed. The load started to oscillate and the test was stopped.

Specimen ID: SKBBBK−113−29T

Youngs Modulus (E):	74.3	[GPa]
Poisson Ratio (ν):	0.248	[−]
Axial peak stress (σ_c):	323	[MPa]

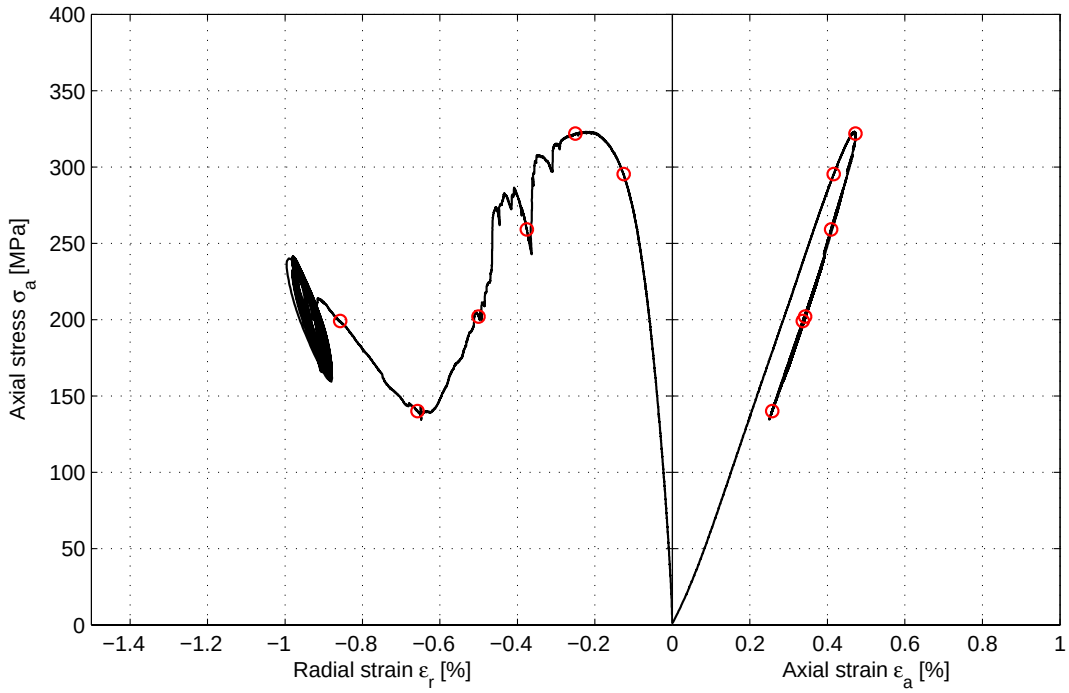

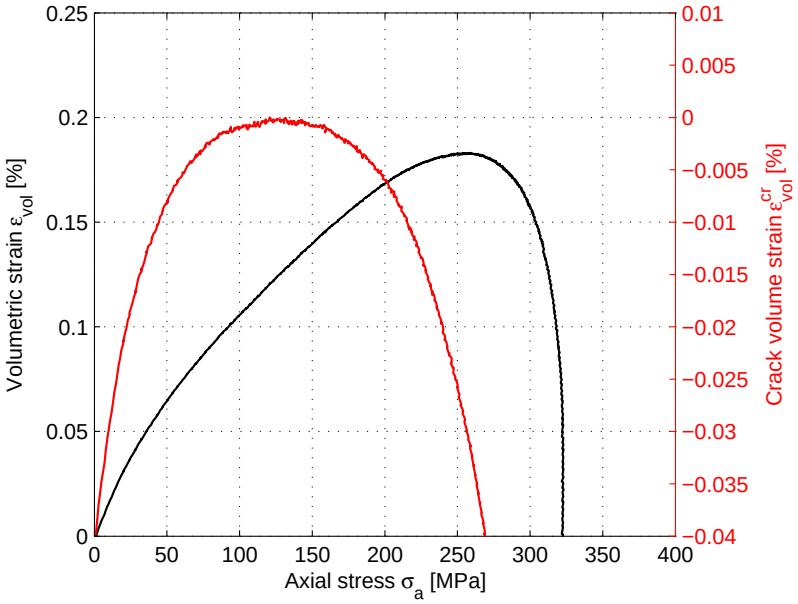

6.1.2 Specimens saturated with distilled water

Specimen ID: 7D

Before mechanical test

After mechanical test

Diameter [mm]	Height [mm]	Density [kg/m^3]
50.8	125.3	2660

Comments Deep spalling on one side along the specimen, with a tendency to piecewise follow the foliation, is observed. The specimen had a curvature larger than what is recommended in /ISRM, 1999/.

Specimen ID: 07D

Youngs Modulus (E):	67.5	[GPa]
Poisson Ratio (ν):	0.299	[−]
Axial peak stress (σ_c):	274.7	[MPa]

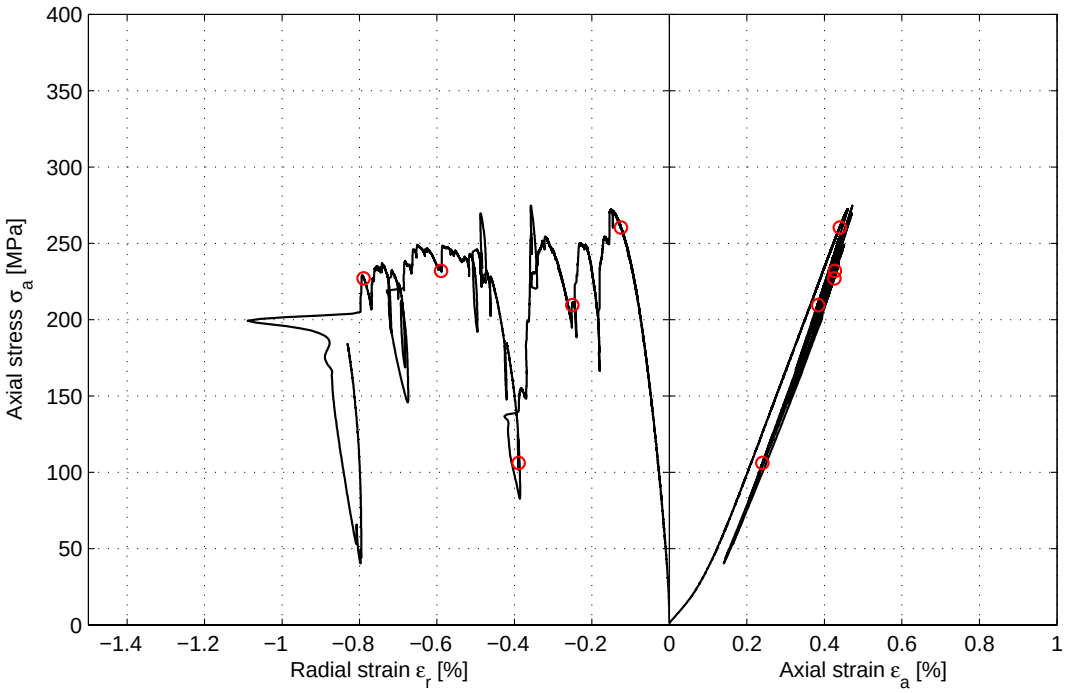

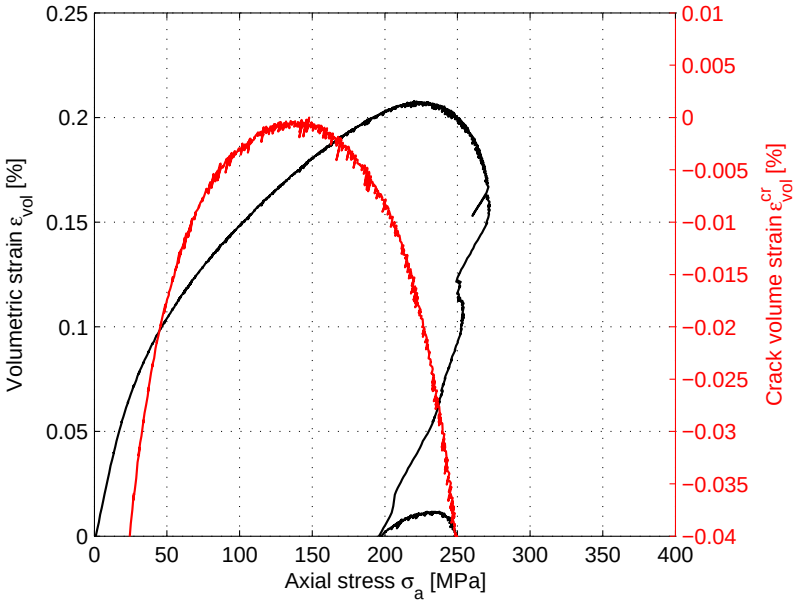

Specimen ID: 24D

Before mechanical test

After mechanical test

Diameter [mm]	**Height [mm]**	**Density [kg/m^3]**
50.8	125.3	2670

Comments Deep spalling on one side and small spalling on the opposite side along the specimen are observed. The specimen had a curvature larger than what is recommended in /ISRM, 1999/.

Specimen ID: 24D

Youngs Modulus (E):	72.1	[GPa]
Poisson Ratio (ν):	0.342	[−]
Axial peak stress (σ_c):	279.1	[MPa]

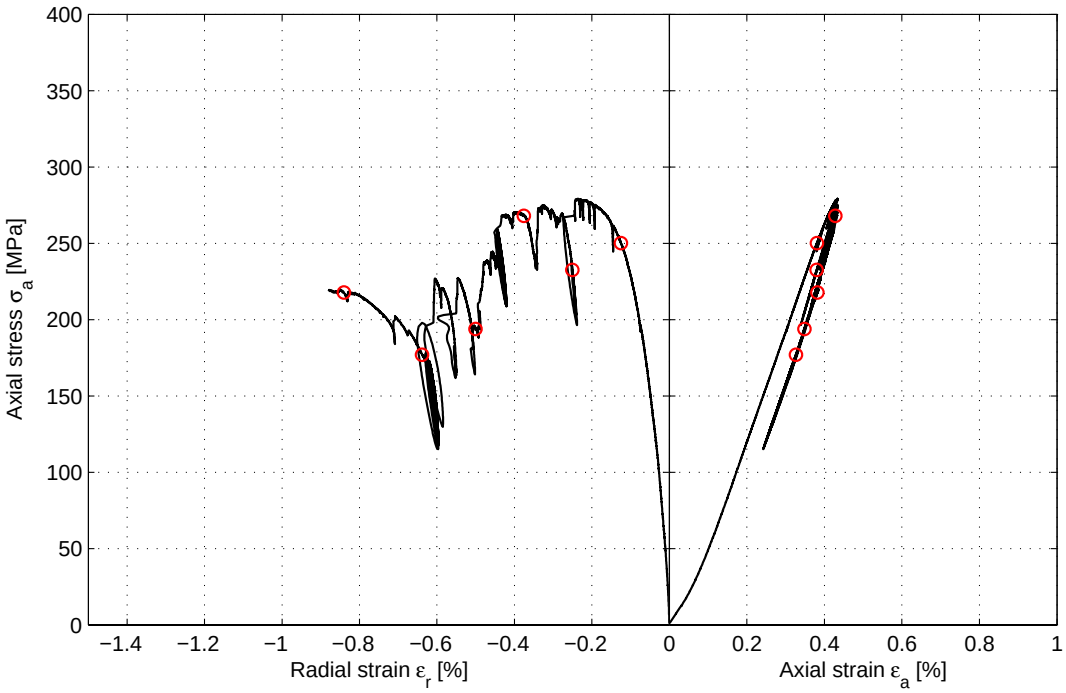

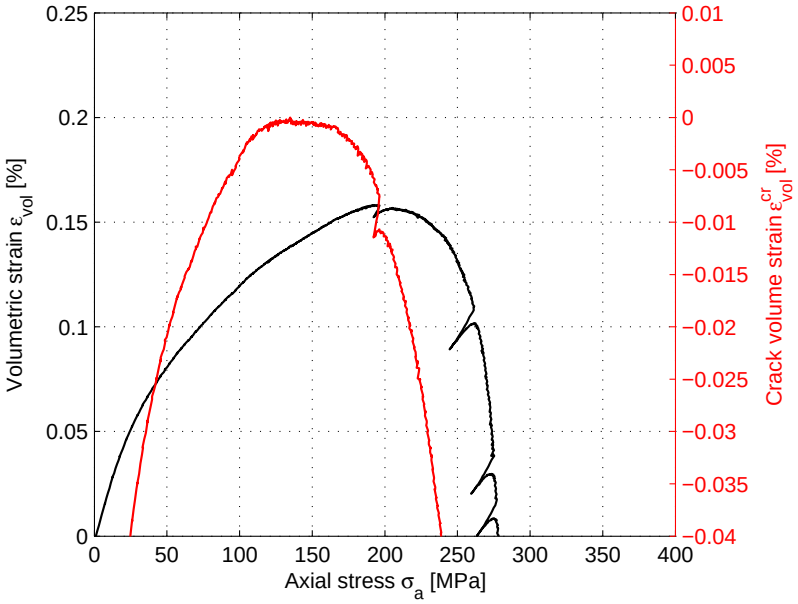

Specimen ID: 15D

Before mechanical test

After mechanical test

Diameter [mm]	**Height [mm]**	**Density [kg/m^3]**
50.7	127.4	2670

Comments Spalling on one side along the specimen is observed. The specimen had a curvature larger than what is recommended in /ISRM, 1999/.

Specimen ID: 15D

Youngs Modulus (E):	69.4	[GPa]
Poisson Ratio (ν):	0.293	[−]
Axial peak stress (σ_c):	249.4	[MPa]

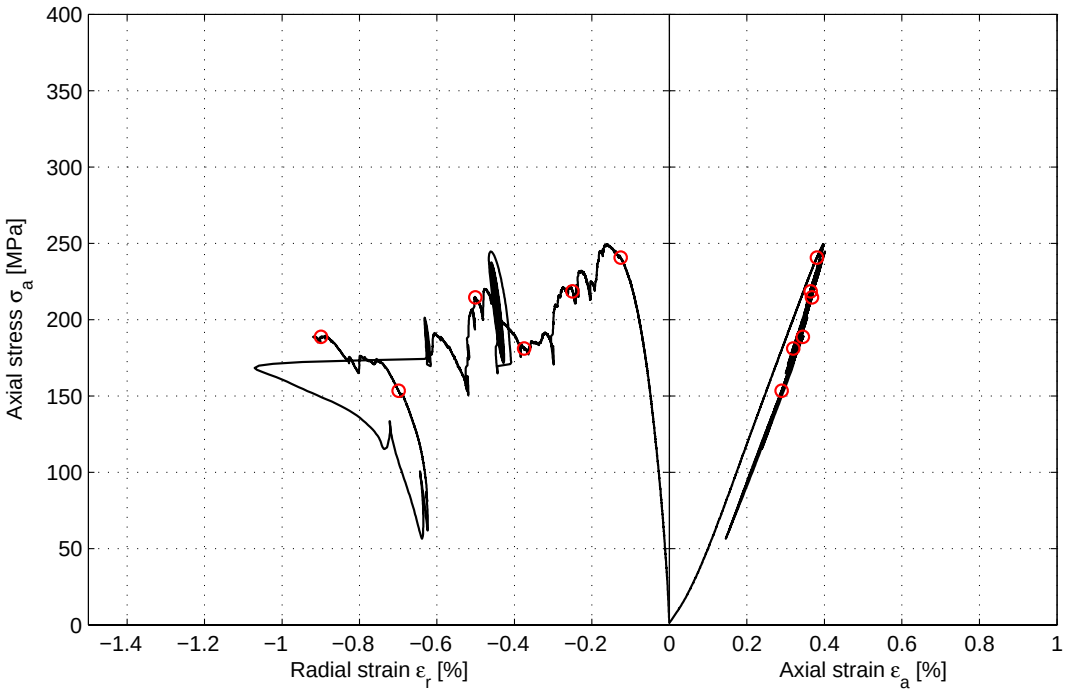

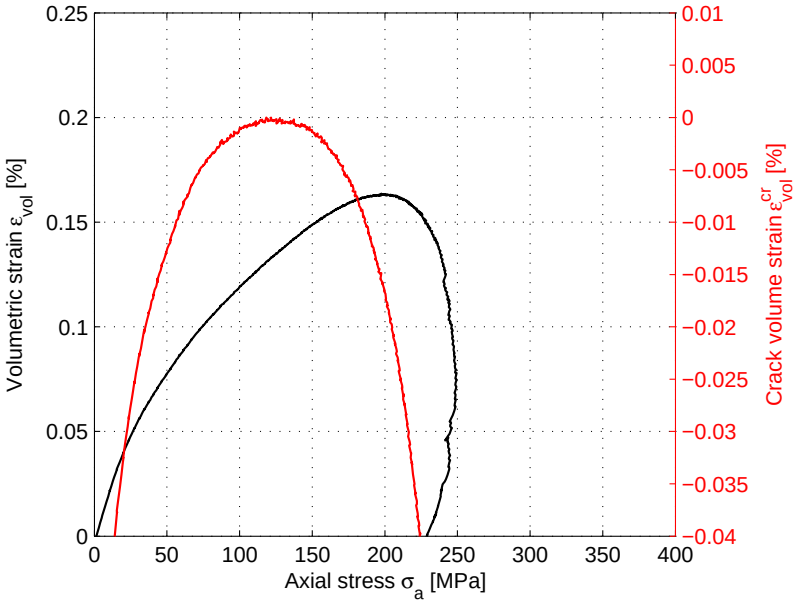

Specimen ID: 19D

Before mechanical test

After mechanical test

Diameter [mm]	**Height [mm]**	**Density [kg/m^3]**
50.8	128.0	2680

Comments Spalling on one side along the specimen is observed. Short load oscillations occurred during the testing.

Specimen ID: 19D

Youngs Modulus (E):	68.5	[GPa]
Poisson Ratio (ν):	0.341	[−]
Axial peak stress (σ_c):	287.4	[MPa]

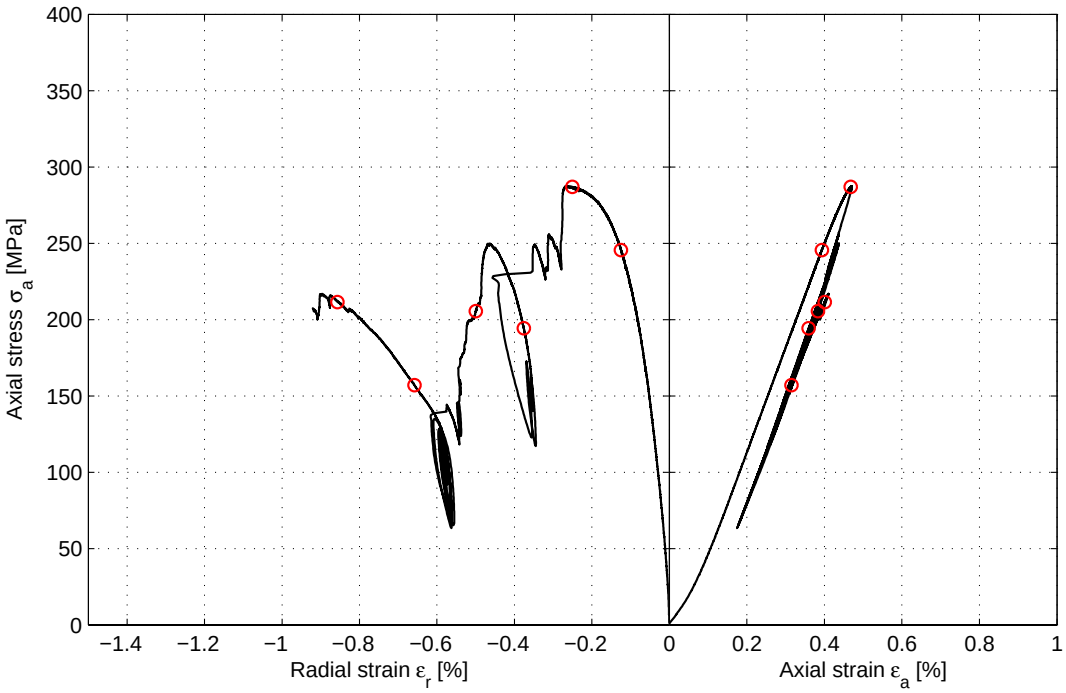

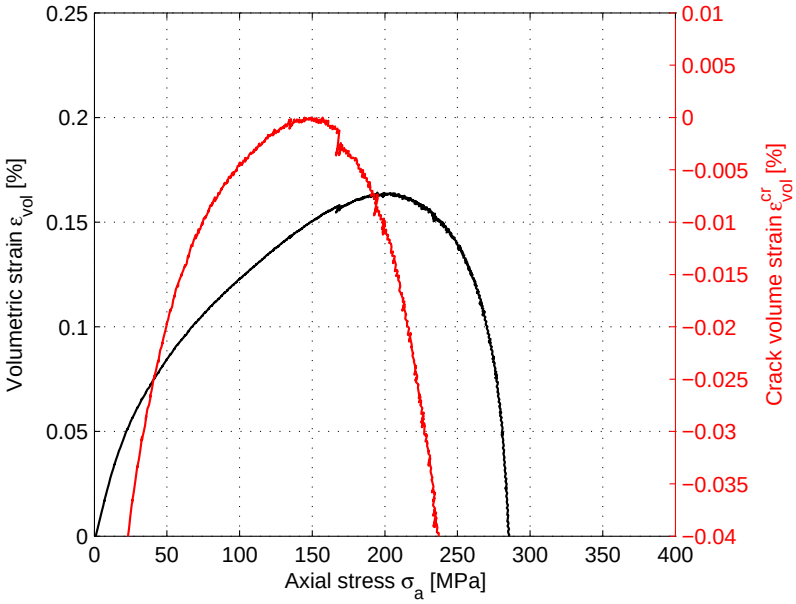

Specimen ID: 26D

Before mechanical test

After mechanical test

Diameter [mm]	Height [mm]	Density [kg/m^3]
50.9	127.9	2660

Comments Vertical cracks going from one of the end surfaces on one side of the specimen is observed. The cracks follow the foliation.

Specimen ID: 26D

Youngs Modulus (E):	72.4	[GPa]
Poisson Ratio (ν):	0.259	[−]
Axial peak stress (σ_c):	262.6	[MPa]

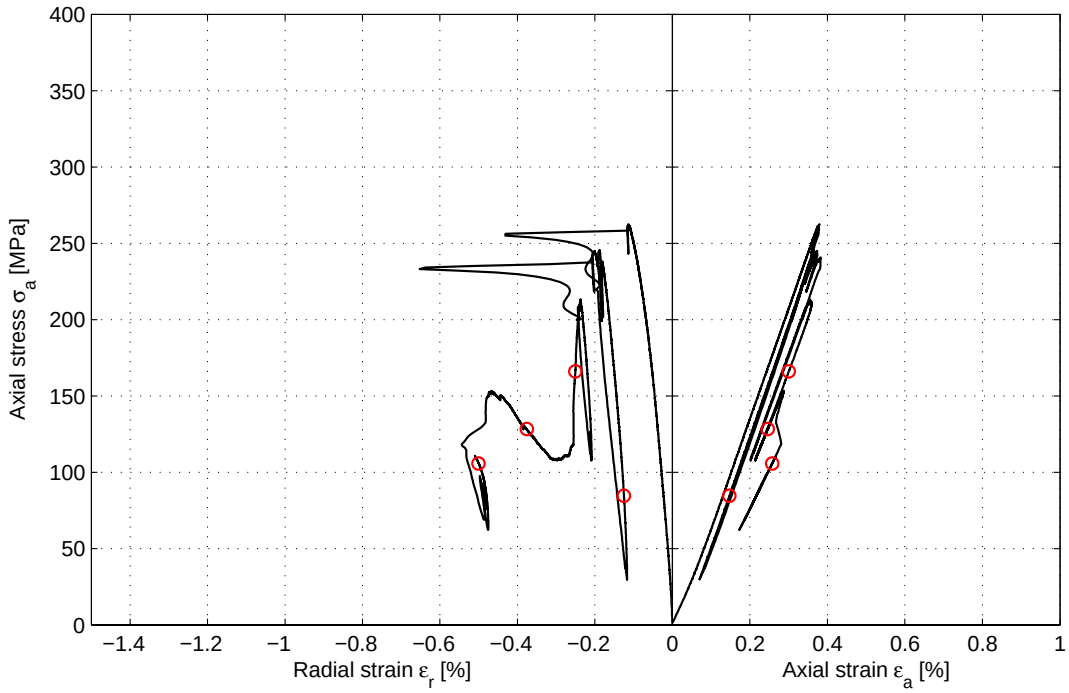

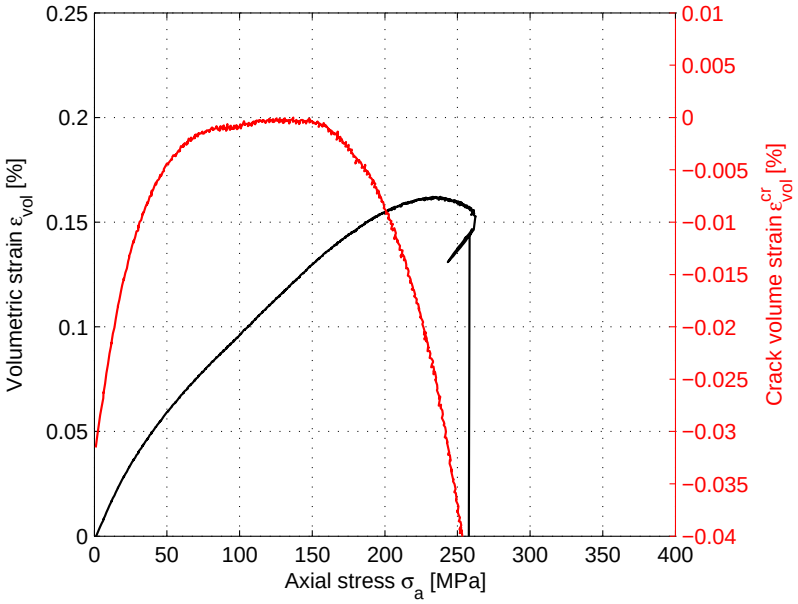

6.1.3 Specimens saturated with formation water

Specimen ID: 16F

Before mechanical test

After mechanical test

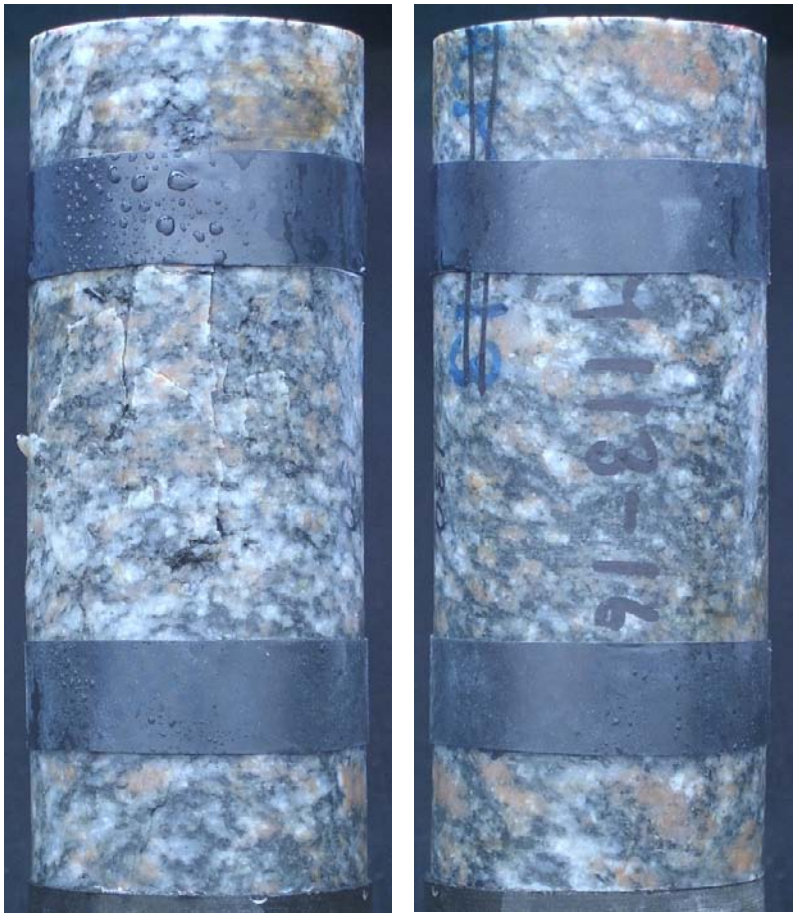

Diameter [mm]	Height [mm]	Density [kg/m^3]
50.8	127.1	2660

Comments Deep spalling on one side along the specimen is observed. The specimen had a curvature larger than what is recommended in /ISRM, 1999/.

Specimen ID: 16F

Youngs Modulus (E):	66.1	[GPa]
Poisson Ratio (ν):	0.314	[−]
Axial peak stress (σ_c):	232.8	[MPa]

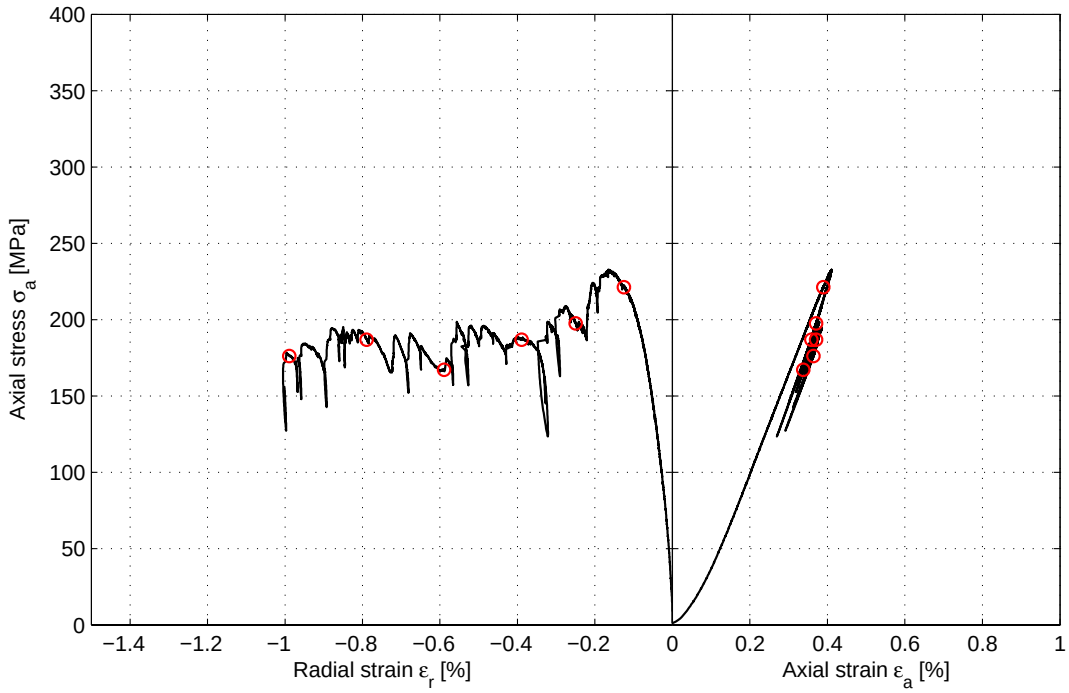

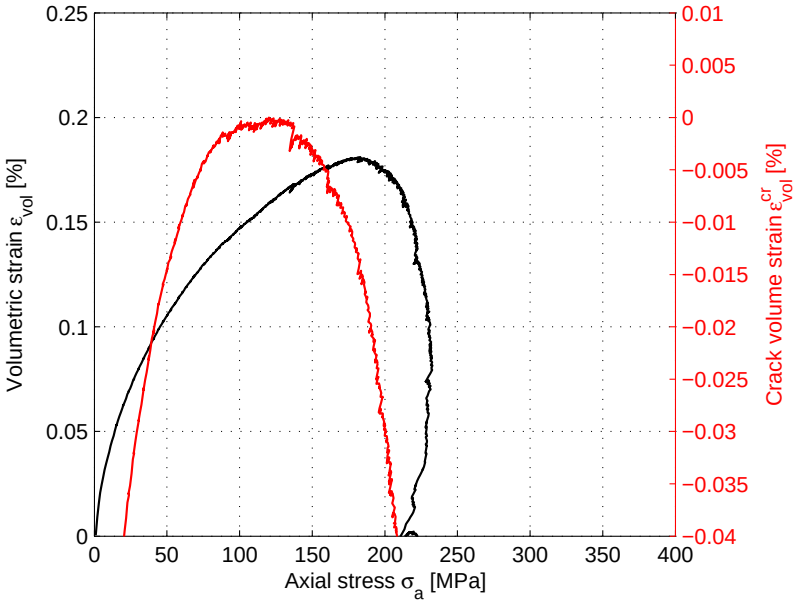

Specimen ID: 20F

Before mechanical test

After mechanical test

Diameter [mm]	Height [mm]	Density [kg/m^3]
50.8	128.1	2670

Comments Spalling on one side along the specimen is observed. The load started to oscillate and the test was stopped.

Specimen ID: 20F

Youngs Modulus (E):	67.2	[GPa]
Poisson Ratio (ν):	0.331	[−]
Axial peak stress (σ_c):	264.2	[MPa]

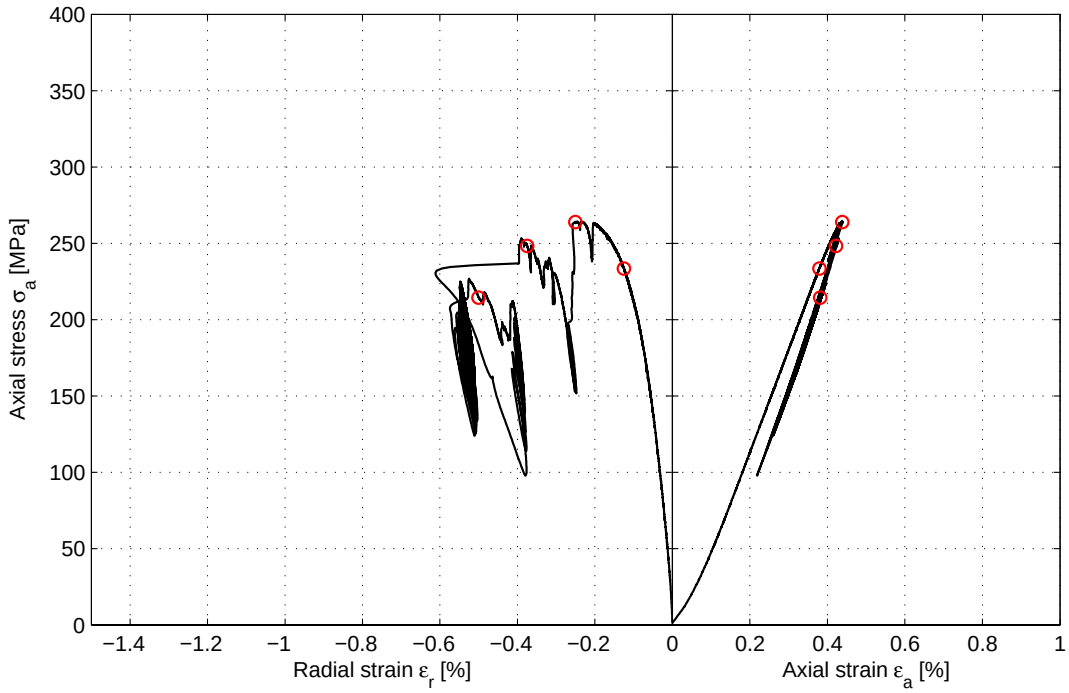

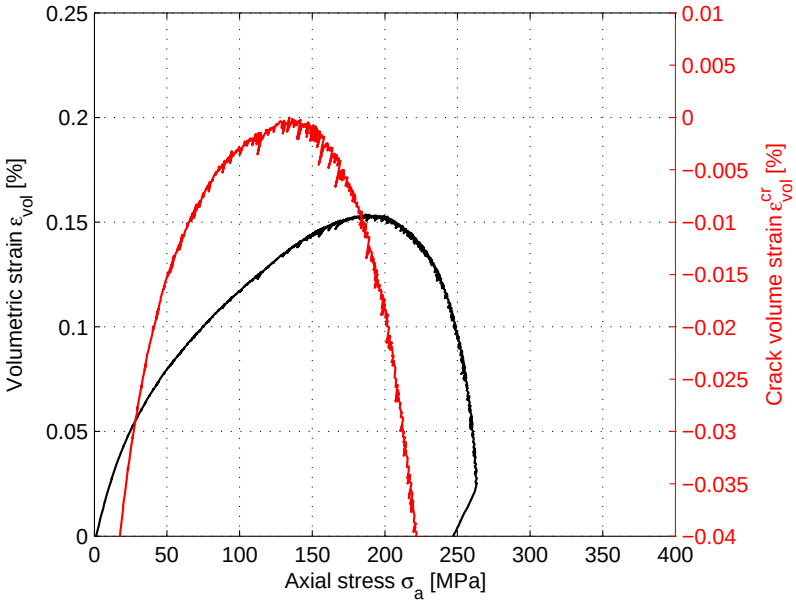

Specimen ID: 27F

Before mechanical test

After mechanical test

Diameter [mm]	Height [mm]	Density [kg/m^3]
50.9	127.8	2660

Comments Spalling on two locations 90 degrees from each other along the specimen is observed. A sudden increase of the radial strain and the specimen was completely unloaded. The test was restarted after this. The registered peak stress was obtained after the test was restarted.

Specimen ID: 27F

Youngs Modulus (E):	73.4	[GPa]
Poisson Ratio (ν):	0.261	[−]
Axial peak stress (σ_c):	305.1	[MPa]

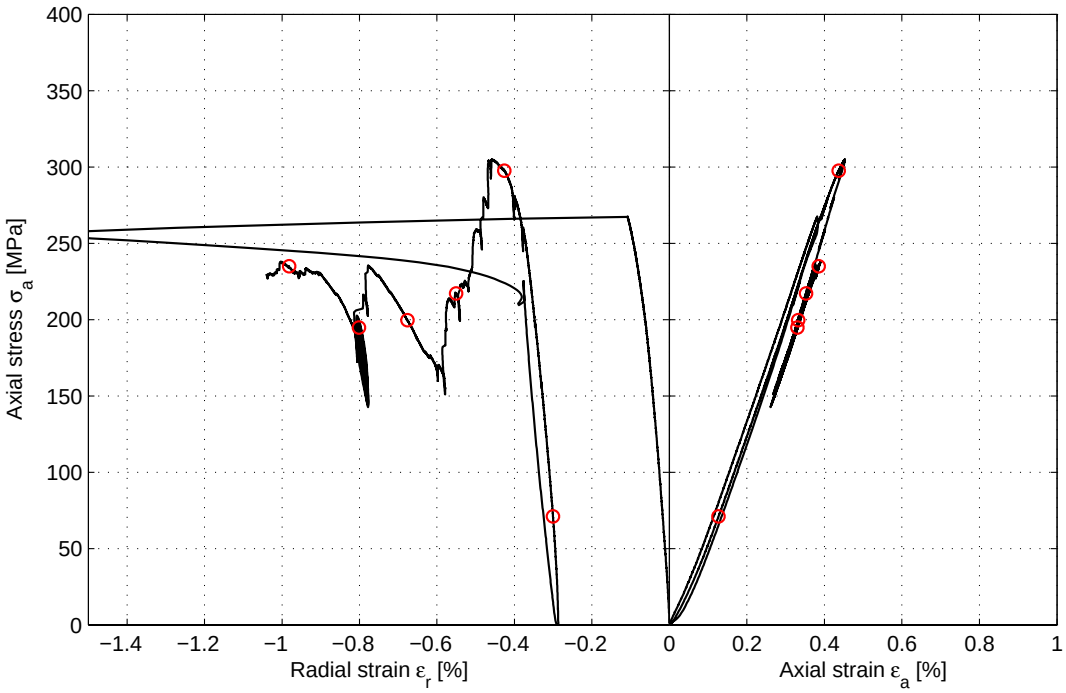

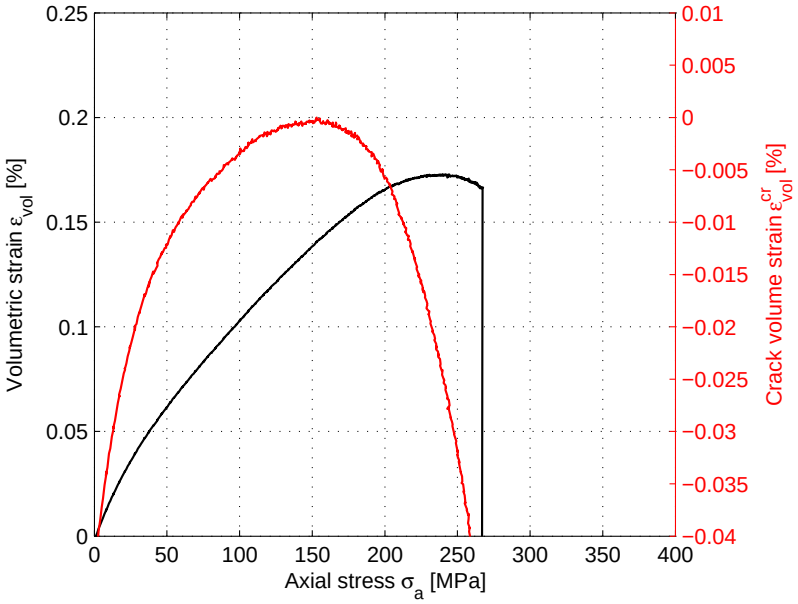

Specimen ID: 28F

Before mechanical test

After mechanical test

Diameter [mm]	Height [mm]	Density [kg/m^3]
50.7	127.8	2670

Comments Spalling on one side along the specimen is observed. The load started to oscillate and the test was stopped.

Specimen ID: 28F

Youngs Modulus (E):	71.8	[GPa]
Poisson Ratio (ν):	0.276	[−]
Axial peak stress (σ_c):	291.6	[MPa]

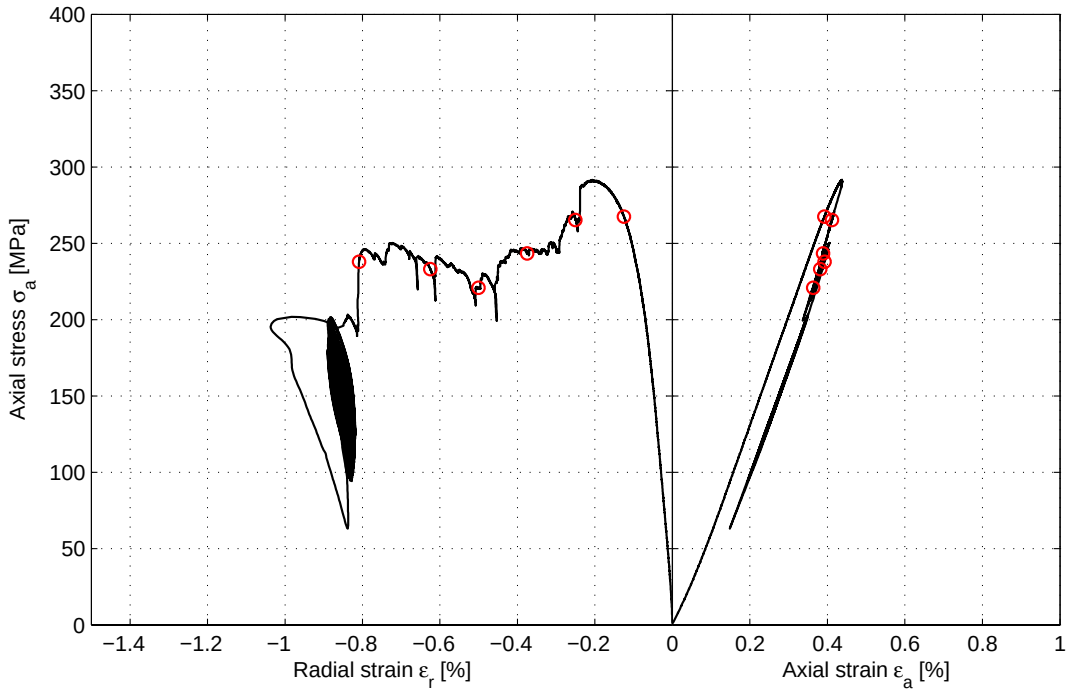

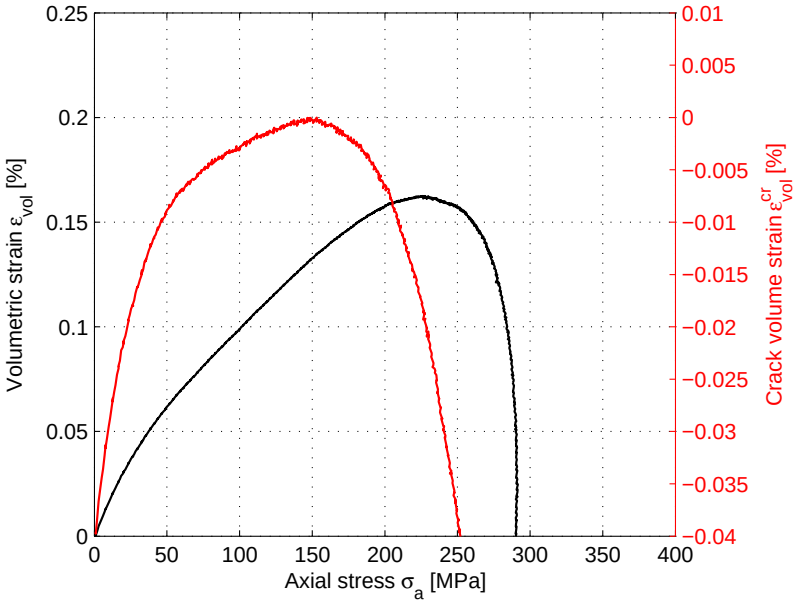

Specimen ID: 30F

Before mechanical test

After mechanical test

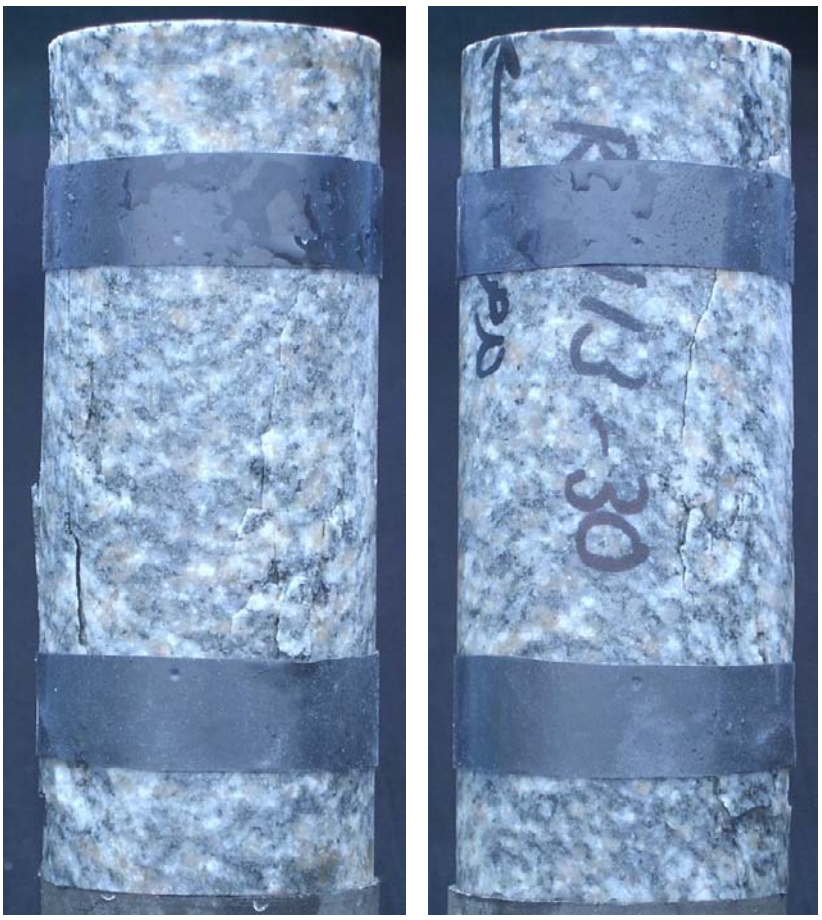

Diameter [mm]	Height [mm]	Density [kg/m^3]
50.7	127.8	2680

Comments Spalling on two locations 90 degrees from each other along the specimen is observed. The load started to oscillate and the test was stopped.

Specimen ID: SKBBBK−113−30F

Youngs Modulus (E):	72.7	[GPa]
Poisson Ratio (ν):	0.279	[−]
Axial peak stress (σ_c):	297.7	[MPa]

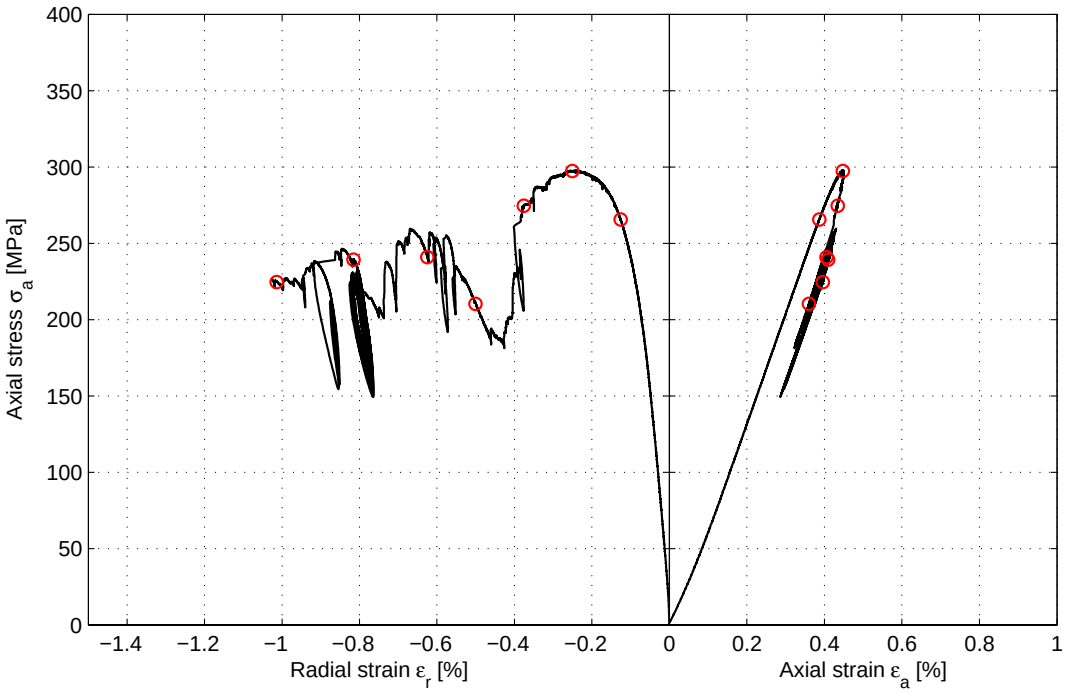

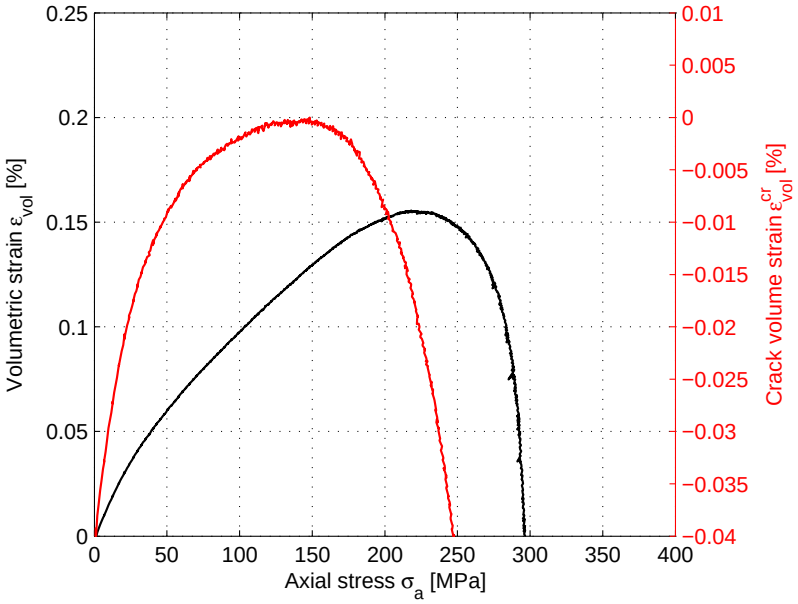

6.1.4 Specimens saturated with saline water

Specimen ID: 4S

Before mechanical test

After mechanical test

Diameter [mm]	Height [mm]	Density [kg/m^3]
51.0	128.4	2670

Comments Spalling with a small slope which seems to follow the foliation on one side along the specimen is observed.

Specimen ID: 04S

Youngs Modulus (E):	67.6	[GPa]
Poisson Ratio (ν):	0.275	[−]
Axial peak stress (σ_c):	220.4	[MPa]

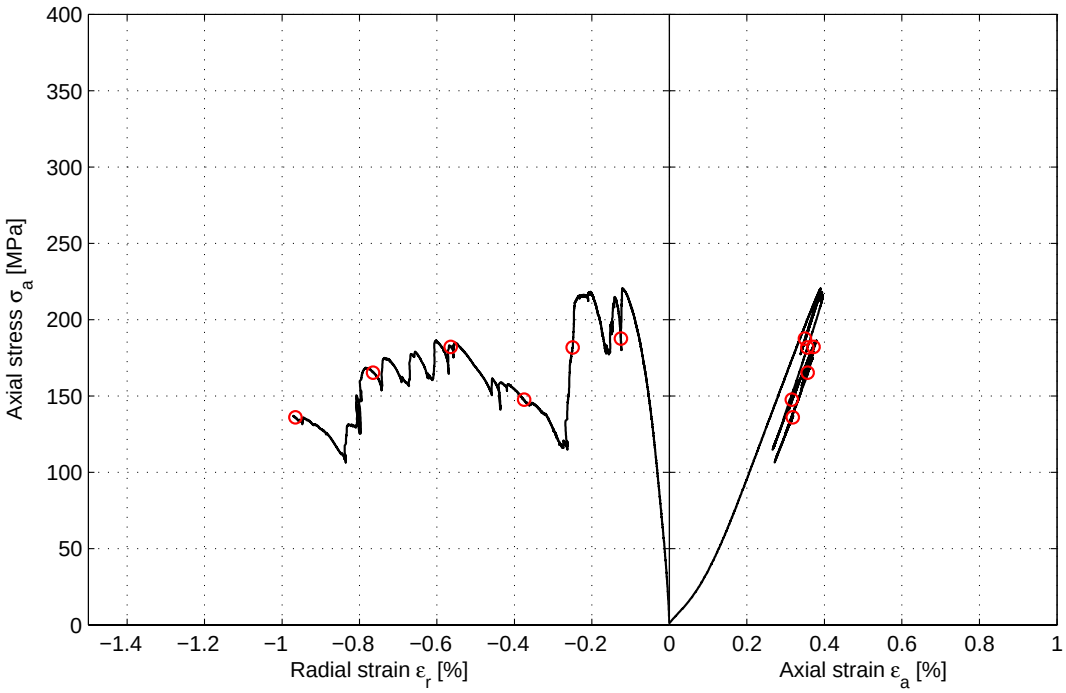

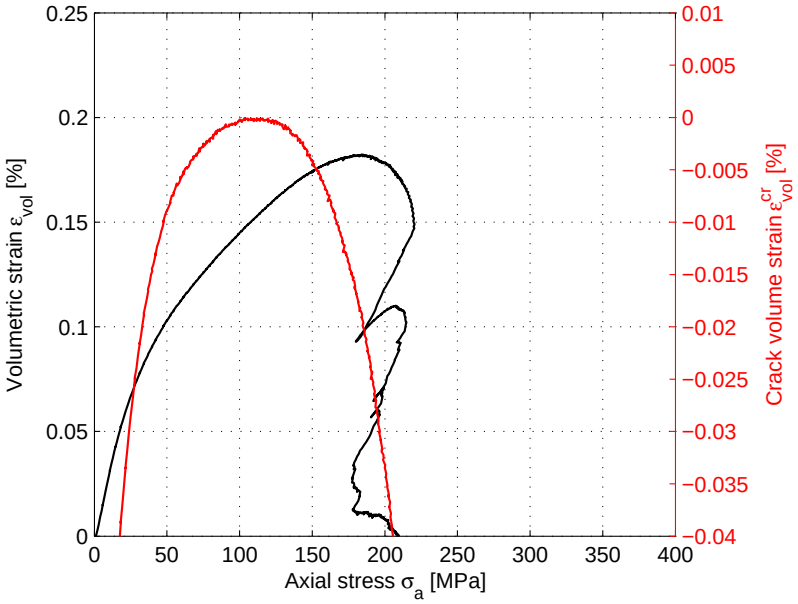

Specimen ID: 9S

Before mechanical test

After mechanical test

Diameter [mm]	**Height [mm]**	**Density [kg/m^3]**
50.9	127.0	2660

Comments Deep spalling on one side along the specimen is observed. The load started to oscillate and the test was stopped.

Specimen ID: 09S

Youngs Modulus (E):	66.5	[GPa]
Poisson Ratio (ν):	0.312	[−]
Axial peak stress (σ_c):	266	[MPa]

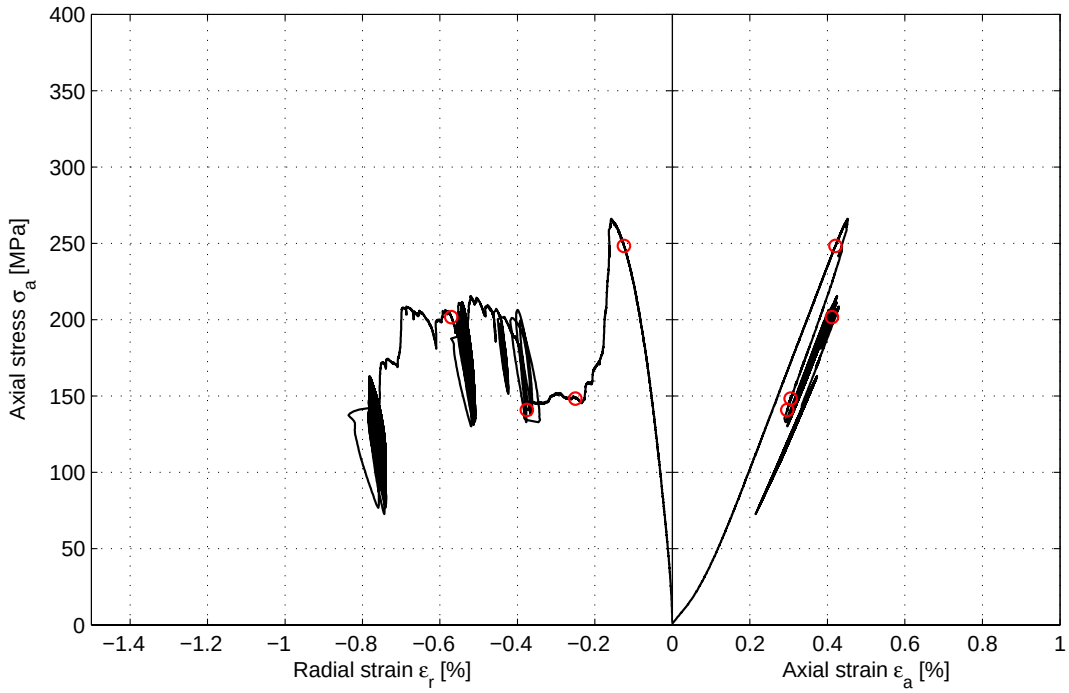

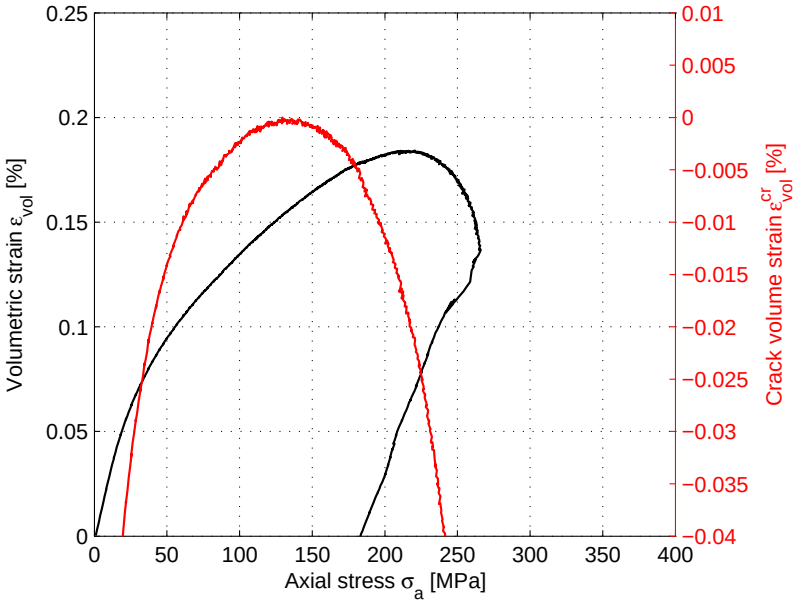

Specimen ID: 13S

Before mechanical test

After mechanical test

Diameter [mm]	Height [mm]	Density [kg/m^3]
51.0	127.1	2680

Comments Spalling on one side along the specimen is observed. The load started to oscillate and the test was stopped. The specimen had a curvature larger than what is recommended in /ISRM, 1999/.

Specimen ID: 13S

Youngs Modulus (E):	67.8	[GPa]
Poisson Ratio (ν):	0.303	[−]
Axial peak stress (σ_c):	234.2	[MPa]

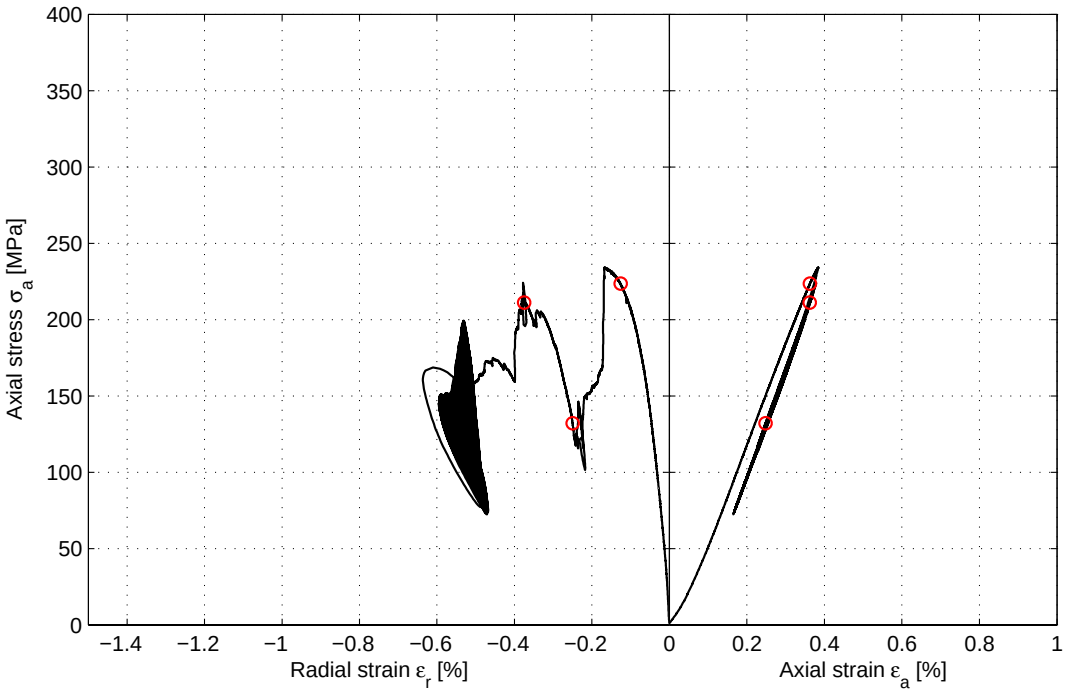

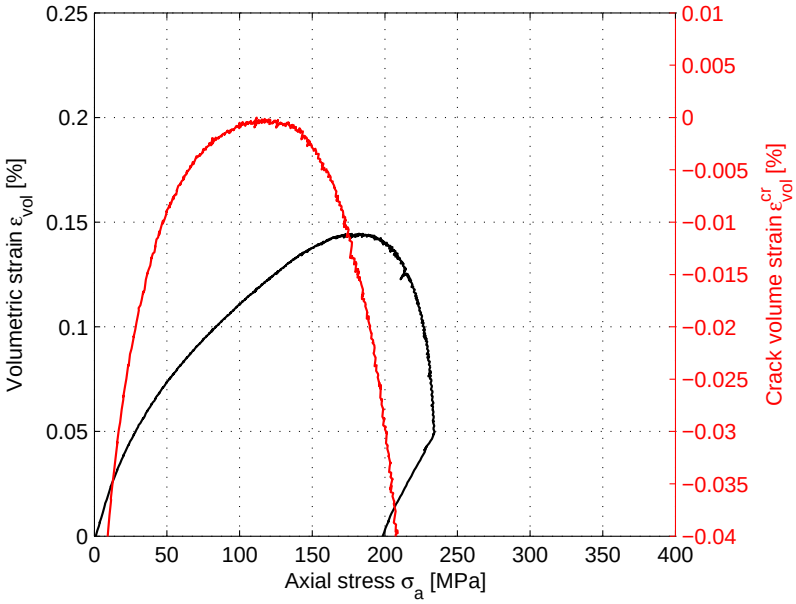

Specimen ID: 17S

Before mechanical test

After mechanical test

Diameter [mm]	**Height [mm]**	**Density [kg/m^3]**
50.8	127.5	2680

Comments A main vertical crack is going along the specimen plus secondary vertical cracks are observed. The load started to oscillate and the test was stopped.

Specimen ID: 17S

Youngs Modulus (E):	63.8	[GPa]
Poisson Ratio (ν):	0.258	[−]
Axial peak stress (σ_c):	188.1	[MPa]

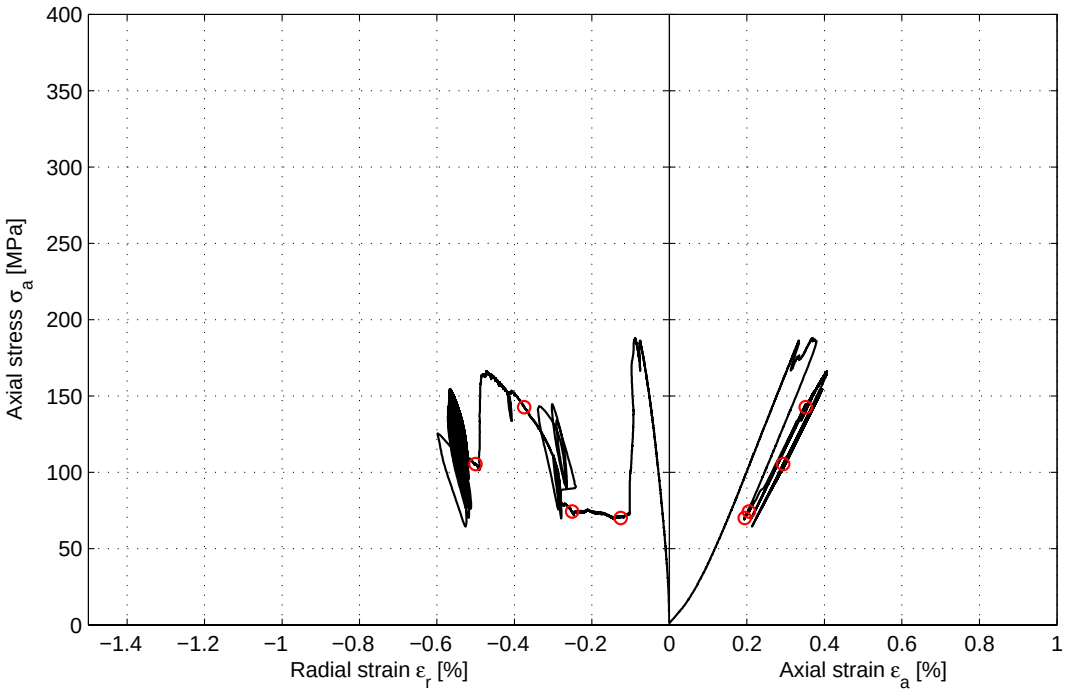

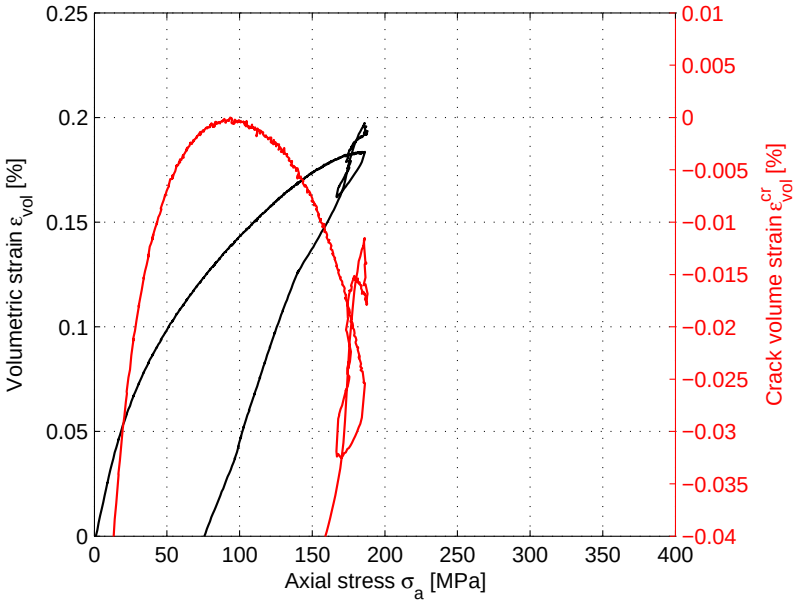

Specimen ID: 21S

Before mechanical test

After mechanical test

Diameter [mm]	**Height [mm]**	**Density [kg/m^3]**
50.6	126.8	2670

Comments Spalling on one side along the specimen is observed.

Specimen ID: 21S

Youngs Modulus (E):	65.1	[GPa]
Poisson Ratio (ν):	0.277	[−]
Axial peak stress (σ_c):	277	[MPa]

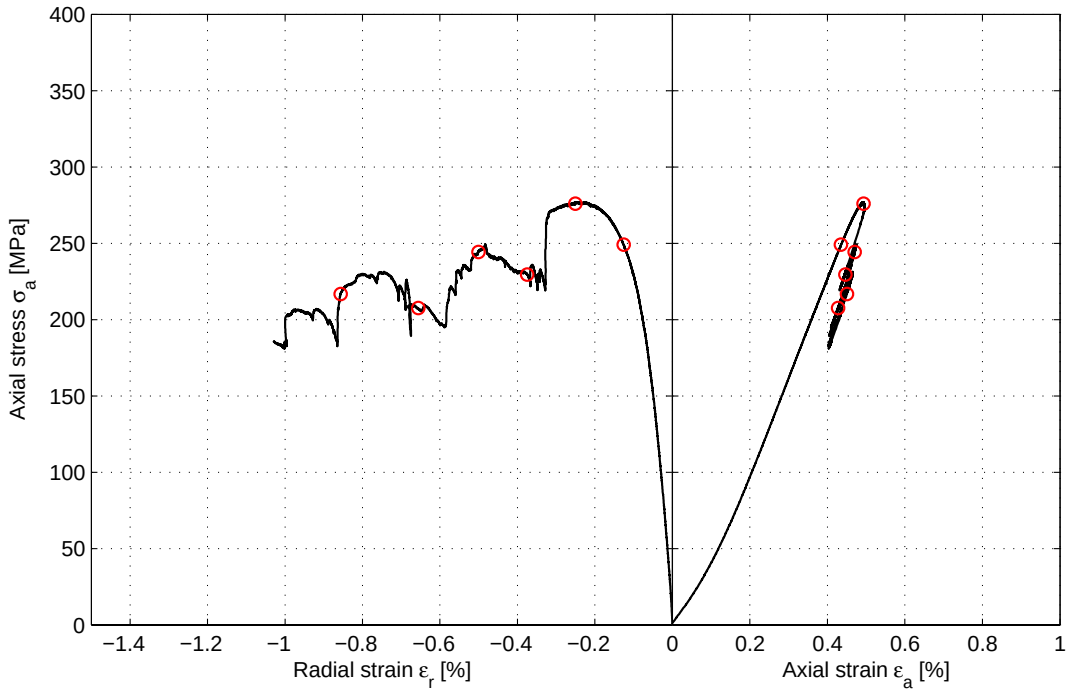

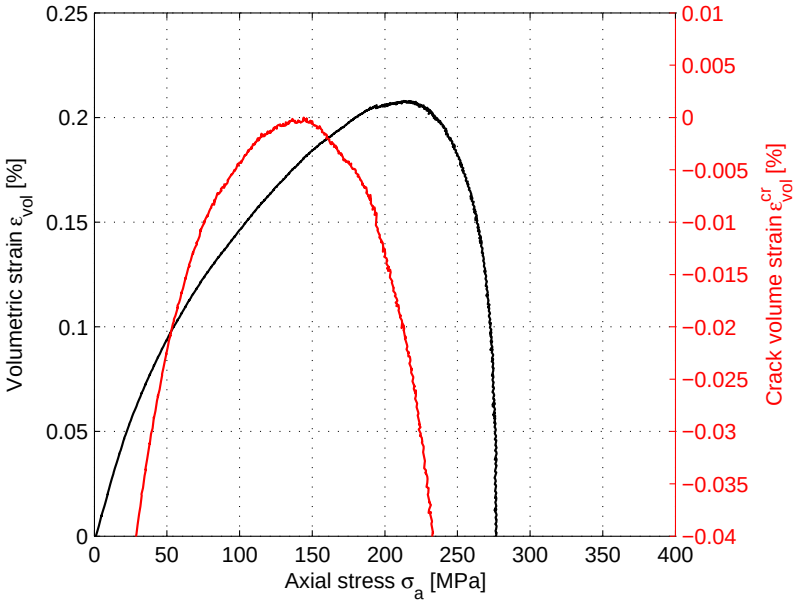

6.2 Results for the entire test series

A summary of the test results is shown in Tables 5-1 and 5-2. The density, uniaxial compressive strength, the tangent Young's modulus and the tangent Poisson ratio versus sampling depth are shown in Figures 5-1 to 5-4.

Table 5-1 Summary of results.

Identification	Density [kg/m^3]	Compressive Strength [MPa]	Young's modulus [GPa]	Poisson ratio [-]	K_{system} [GN/m]
6T DRY	2660	335.8	71.6	0.30	9.64
31T	2680	283.6	72.0	0.29	10.39
18T	2680	295.1	70.4	0.29	9.75
25T	2690	273.9	71.2	0.29	11.28
29T	2680	323.0	72.7	0.27	12.71
Mean value	**2678**	**302.3**	**71.6**	**0.29**	**10.76**
7D DISTILLED	2660	274.7	67.5	0.30	12.18
24D WATER	2670	279.1	72.1	0.34	8.57
15D	2670	249.4	69.4	0.29	10.56
19D	2680	287.4	68.5	0.34	9.78
26D	2660	262.6	72.4	0.26	11.90
Mean value	**2668**	**270.6**	**70.0**	**0.31**	**10.60**
16F FORMATION	2680	232.8	66.1	0.31	15.98
20F WATER	2680	264.2	67.2	0.33	11.17
27F	2680	305.1	73.4	0.26	10.72
28F	2690	291.6	71.8	0.28	9.99
30F	2690	297.7	73.1	0.29	9.77
Mean value	**2684**	**278.3**	**70.3**	**0.29**	**11.53**
4S SALINE	2670	220.4	67.6	0.28	8.12
9S WATER	2660	266.0	66.5	0.31	12.72
13S	2680	234.2	67.8	0.30	12.96
17S	2680	188.1	63.8	0.26	15.44
21S	2670	277.0	65.1	0.28	12.02
Mean value	**2672**	**237,1**	**66,2**	**0,29**	**12,25**

Table 5-2: Calculated mean values and standard deviation (Std dev) of the results.

	Density [kg/m^3]	Compressive Strength [MPa]	Young's modulus [GPa]	Poisson ratio [-]
Mean value	2672	272.1	69.5	0.29
Std dev ()	9.3	34.9	2.9	0.025

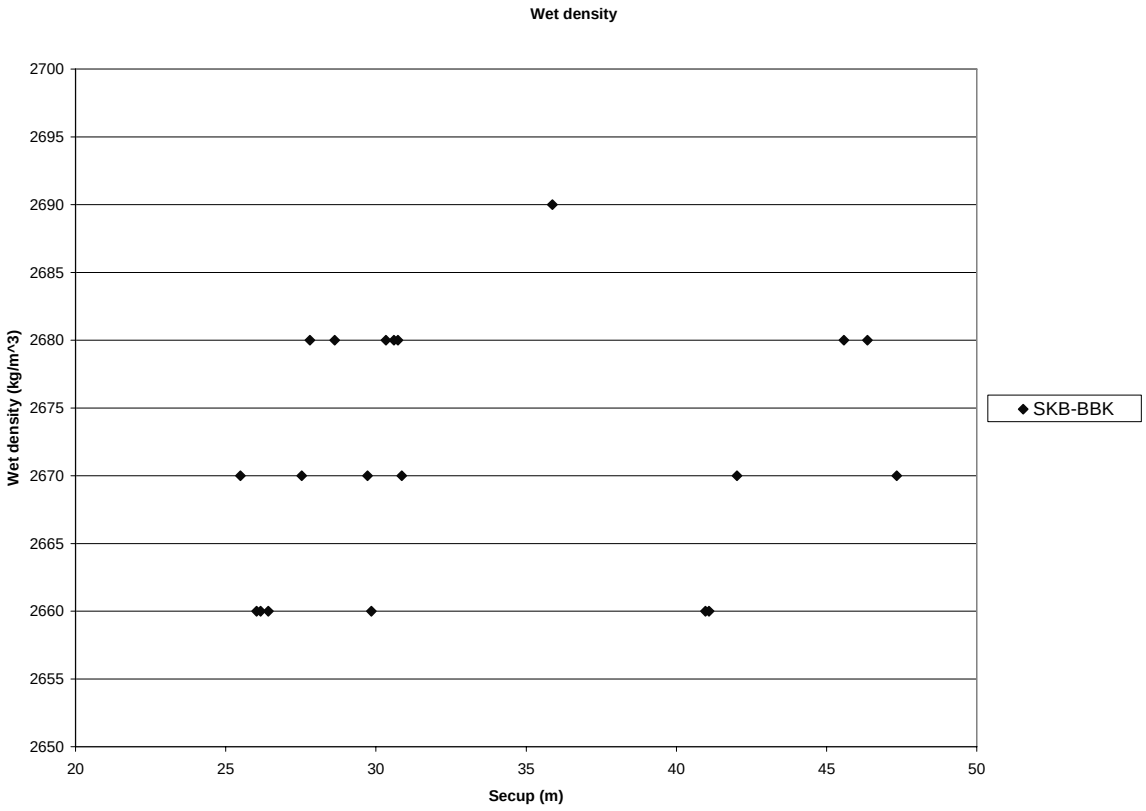

Figure 5-1: *Density versus sampling depth.*

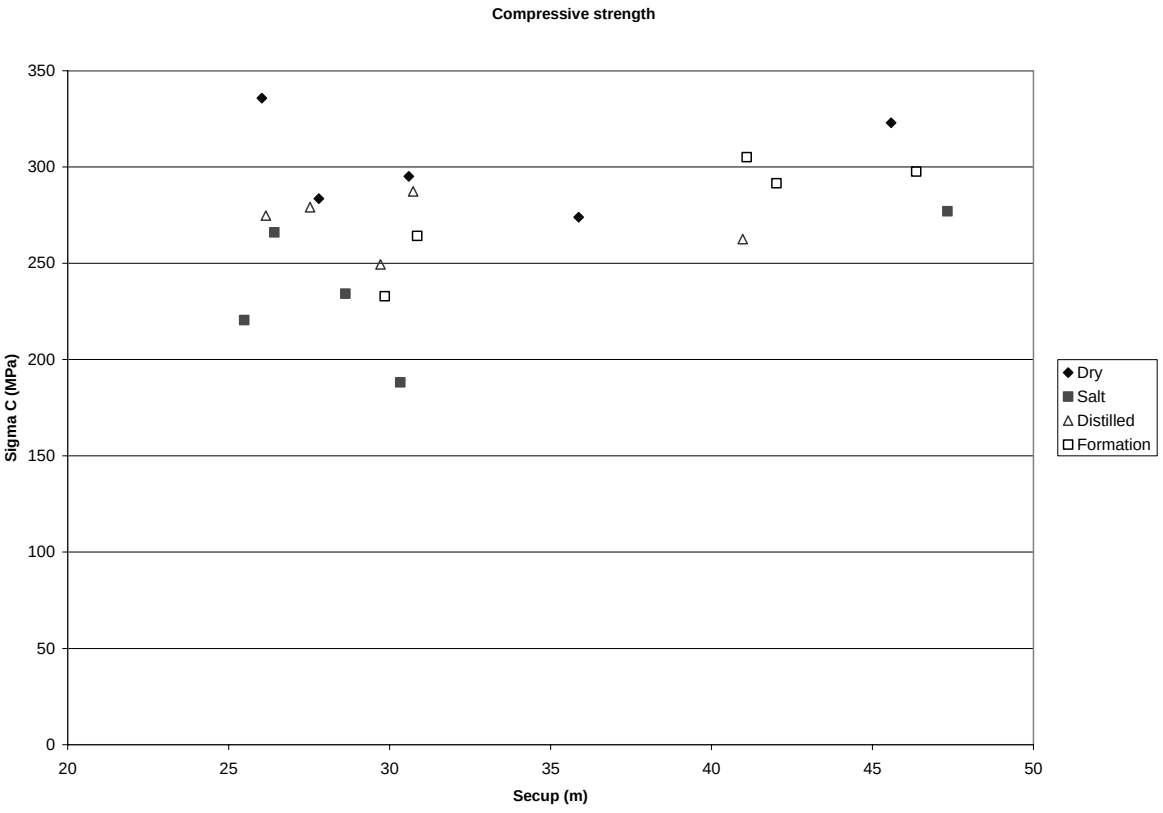

Figure 5-2: *Uniaxial compressive strength versus sampling depth.*

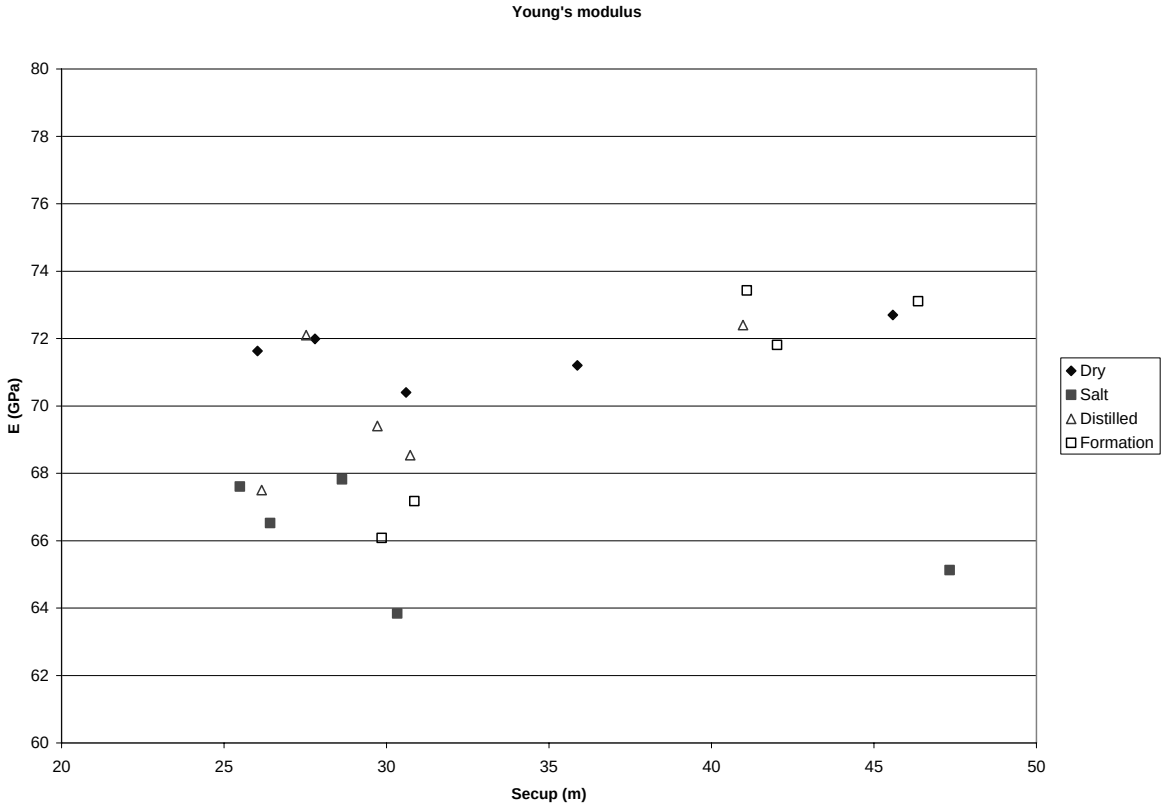

Figure 5-3: *Tangent Young's modulus versus sampling depth.*

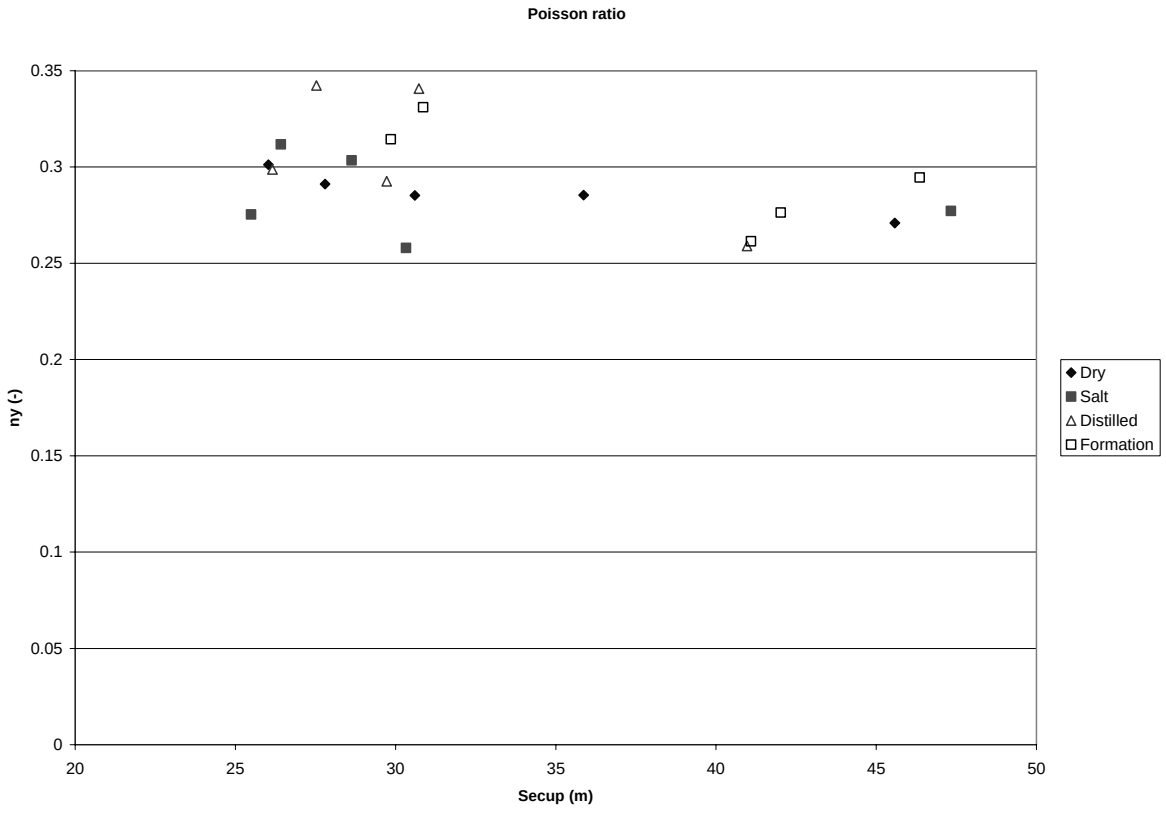

Figure 5-4: *Tangent Poisson ratio versus sampling depth.*

6.3 Nonconformities

The testing was conducted according to the method description with some deviations. The circumferential strains have been determined within a relative error of 1.5%, which is larger than what is specified in the ISRM-standard /ISRM, 1999/. Further, double systems for measuring the axial deformation have been used, which is beyond the specifications in the method description. This was conducted as development of the test method specially aimed for high-strength brittle rock.

The first shipment of specimens was pre-cut when they arrived to SP. However, many of the specimens were cut too short and had to be excluded from the testing program. Other specimens were sampled nearby in order to replace the excluded specimens. Moreover, it was also found that the core KF0066A01 was not straight piecewise. Due to this, some of the specimen had a curvature that exceeds the shape recommendations in /ISRM, 1999/. In order to keep the same number of specimens as specified in the activity plan, some specimens that had a curvature outside what is recommended in /ISRM, 1999/ had to be included in the testing program.

A summary of departures from the activity plan and additional comments are listed in Table 5-3.

Table 5-3 Summary of deviations from the activity plan and comments.

Borehole	Id	Secup [m]	Seclow [m]	Testing condition/comment	Specification in activity plan
KF0066A01		24.71	24.84	not tested (too short)	
KF0066A01		24.84	24.97	not tested (too short)	
KF0066A01		24.97	25.10	not tested (too short)	
KF0066A01	4S	25.49	25.62	according activity plan	
KF0066A01		25.83	25.96	not tested (too short)	
KF0066A01	6T	26.03	26.16	according activity plan (*)	
KF0066A01	7D	26.16	26.29	according activity plan (*)	
KF0066A01		26.29	26.42	not tested (too short)	
KF0066A01	9S	26.42	26.55	according activity plan (*)	
KF0066A01	24D	27.53	27.66	new specimen (*)	
KF0066A01	31T	27.80	27.95	new specimen	
KF0066A01		27.98	28.11	not tested (too short)	
KF0066A01		28.36	28.50	not tested (too short)	
KF0066A01		28.50	28.63	not tested (too short)	
KF0066A01	13S	28.63	28.76	according activity plan (*)	
KF0066A01		29.26	29.39	not tested (too short)	
KF0066A01	15D	29.72	29.85	distilled water (*)	dry specimen
KF0066A01	16F	29.85	29.98	formation water (*)	distilled water
KF0066A01	17S	30.33	30.46	saline water	formation water
KF0066A01	18T	30.60	30.73	dry specimen (*)	saline water
KF0066A01	19D	30.73	30.86	distilled water	dry specimen
KF0066A01	20F	30.86	31.00	formation water	distilled water
KF0066A01	25T	35.87	36.00	new specimen (*)	
KF0069A01	26D	40.97	41.09	new specimen	
KF0069A01	27F	41.09	41.22	new specimen	
KF0069A01	28F	42.02	42.15	new specimen	
KF0069A01	29T	45.58	45.71	new specimen	
KF0069A01	30F	46.36	46.49	new specimen	
KF0069A01	21S	47.33	47.47	according activity plan	Secup-low 47.13-47.27
KF0069A01		47.47	47.60	not tested (too short)	Secup-low 47.27-47.40
KF0069A01		47.60	47.73	not tested (too short)	Secup-low 47.40-47.53

(*) denotes specimens with a curvature exceeding the recommendations in /ISRM, 1999/.

7 Discussion

Similar to other tests, (e.g. Feng et al., 2001; Feucht and Logan, 1990) the samples tested in dry conditions display a higher uniaxial compressive strength than samples saturated with liquids.

The tests in this report indicated that chemical corrosion induced reduction of uniaxial compressive peak load in the samples subject to liquids with high salinity. The same effect can be seen on the elastic modulus of the specimens. To prevent a superimposing of the effects from structural differences in the samples on the chemical effect, the samples were taken in a cyclic order. The post peak behaviour of samples subjected to highly saline water is radically different to that of the other tested groups. The inclination of the post peak part of the stress-strain curve is about 50 % steeper for samples subjected to highly saline water compared to the dry samples. The other groups do not show such large difference in the inclination of the post peak curve with respect to the dry samples.

When examining the failure of the samples the mode of failure is found to be a mix of type a and b according to /Vutukuri et al., 1974/. The visual inspection does not indicate differences between the groups of samples, but in several samples, an indication that the fractures may have followed the biotite minerals can be discerned.

Earlier experiments of chemical effects on rock samples have shown that the mineral composition and the crystal array of the test specimen are quite important. The main minerals in the samples are; quarts, potassium-feldspar, plagioclase and biotite (about 10%) /Wikman & Kornfält, 1995/. None of these minerals are strongly reactive in a saline environment compared to many other minerals. It has been shown that the reaction rate for biotite is strongly dependant of the ionic concentration in the solution /Malmström et al., 1995/. The sodium ions might react more readily with the biotite than with the other minerals causing the samples to show a diminishing of the peak strength with higher sodium chloride concentration.

References

ASTM 4543-01, 2001. Standard practice for preparing rock core specimens and determining dimensional and shape tolerance.

Eberhardt E, Stead D, Stimpson B, Read R S, 1998. Identifying crack initiation and propagation thresholds in brittle rock. Can. Geotech. J. 35, pp. 222-233.

Feng, X-T., Chen, S. and Li, S., 2001. Effects of water chemistry on microcracking and compressive strength of granite. Int. J. Rock Mech. Min. Sci., 38, 557-568.

Feucht, L. J. and Logan, J. 1990. Effects of chemically active solutions on shearing behavior of a sandstone. Tectonophysics 175, 159-176.

Hoek, E., 1968. Brittle failure of rock. In Rock Mechnics in Engineering Practice. (eds. Stagg, K. G., Zienkiewicz, O. C.). John Wiley & sons, London, 442.

ISRM, 1979. Suggested Method for Determining Water Content, Porosity, Density, Absorption and Related Properties and Swelling and Slake-durability Index Properties. Int. J. Rock. Mech. Min. Sci. & Geomech. Abstr. 16(2), pp. 141-156.

ISRM, 1999. Draft ISRM suggested method for the complete stress-strain curve for intact rock in uniaxial compression. Int. J. Rock. Mech. Min. Sci. 36(3), pp. 279-289.

Malmström, M., Banwart, S., Duro, L., Wersin, P., Bruno, J., 1995. Biotite and chlorite weathering at 25ºC TR-95-01. Swedish Nuclear Fuel and Waste Management Company (SKB). 128.

Martin C D, Chandler N A, 1994. The progressive fracture of Luc du Bonnet granite. Int. J. Rock. Mech. Min. Sci. & Geomech. Abstr. 31(6), pp. 643-659.

MATLAB, 2002. The Language of Technical computing. Version 6.5. MathWorks Inc.

Savukoski M, 2005. Drill hole KF0066A01 and KF0069A01. Determination of porosity by water saturation and density by buoyancy technique, SKB IPR-05-XXX, xx pp.

Seto, M., Utagawa, M., Feng, X.-T., 1998. Change of chemical environment to change of strength and cracking properties of rocks. Japan Association of Rock Mechanics. 41-46.

SS-EN 13755. Natural stone test methods – Determination of water absorption at atmospheric pressure.

SS-EN 1936. Natural stone test methods – Determination of real density and apparent density, and of total and open porosity.

Stråhle A, 2001. Definition och beskrivning av parametrar för geologisk, geofysisk och bergmekanisk kartering av berg, SKB-01-19. svensk kärnbränslehantering AB. In Swedish.

Vutukuri, V. S., Lama, R. D., Saluja, S. S., 1974. Handbook on mechanical properties of rocks, vol. 1. Trans Tech publications, Germany. 280.

Wikman, H., Kornfält, K-A., 1995. Updating of a lithological model of the bedrock of the Äspö area. SKB report (PR. 25-95-04), 42.

Appendix A

The following equations describe the calculation of radial strains when using a circumferential deformation device, see Figure A-1.

$$\varepsilon_r = \frac{\Delta C}{C_i}$$

where

$C_i = 2\ \pi R_i$ = initial specimen circumference

ΔC = change in specimen circumference = $\dfrac{\pi \cdot \Delta X}{\sin\left(\dfrac{\theta_i}{2}\right) + \left(\pi - \dfrac{\theta_i}{2}\right)\cos\left(\dfrac{\theta_i}{2}\right)}$

and

ΔX = change in LVDT reading = X_i - X_f

(X_i = initial chain gap; X_f = current chain gap)

θ_i = initial chord angle = 2π - $\dfrac{L_c}{R_i + r}$

L_c = chain length (measured from center of one end roller to center of other end roller)

r = roller radius

R_i = initial specimen radius

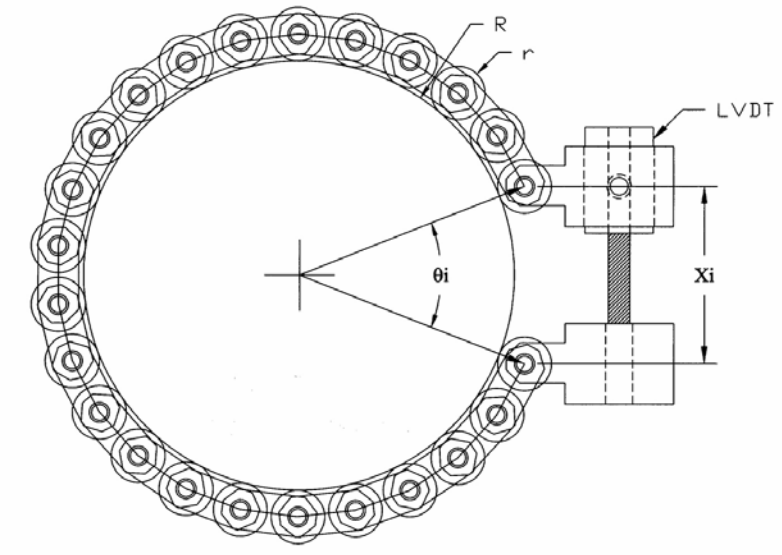

Figure A-1: *Chain for radial deformation measurement.*

Appendix B

This Appendix contains results showing the unprocessed data and values on the computed system stiffness K_{system} that was used for the data processing, cf. Section 4.4. In addition graphs showing the volumetric strain ε_{vol} versus the axial strain ε_a and the actual radial strain rate $d\varepsilon_r/dt$ versus time are also displayed.

B.1 Dry specimens

Specimen ID: 06T

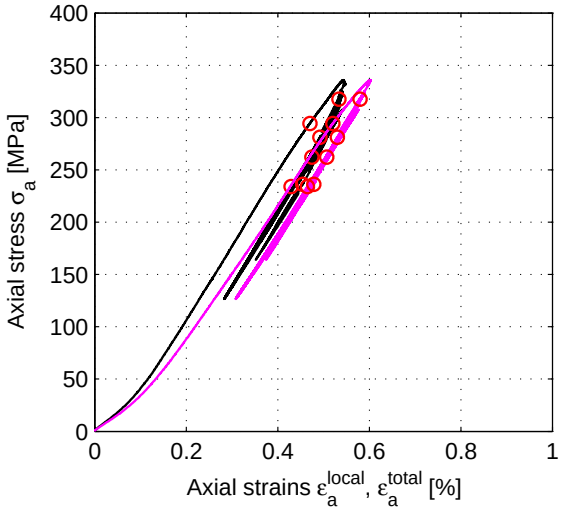

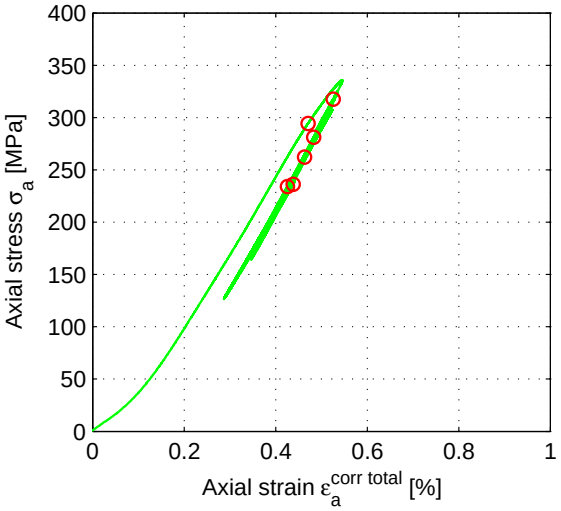

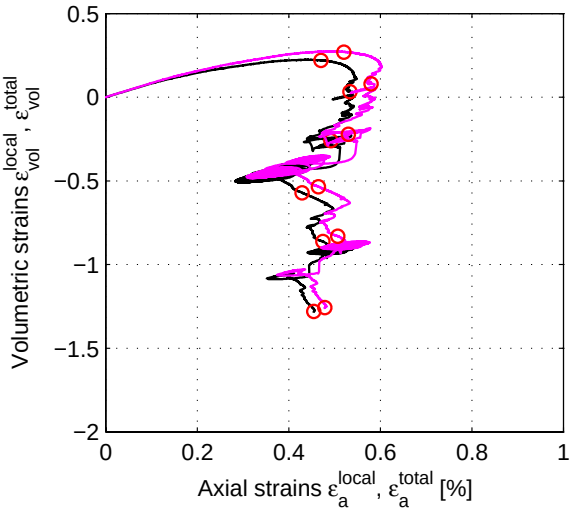

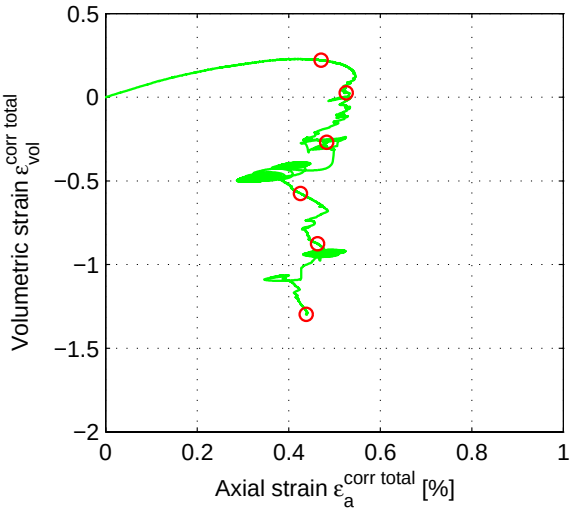

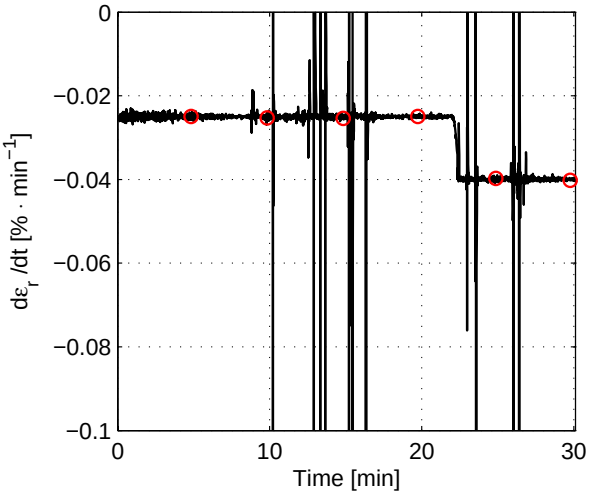

Explanation to curves above:

Based on local deformation (black)

Based on total deformation (mangenta)

Based on corrected deformation (green)

Calculated system stiffness:

K_{system} = 9.6443 [GN/m]

Specimen ID: 31T

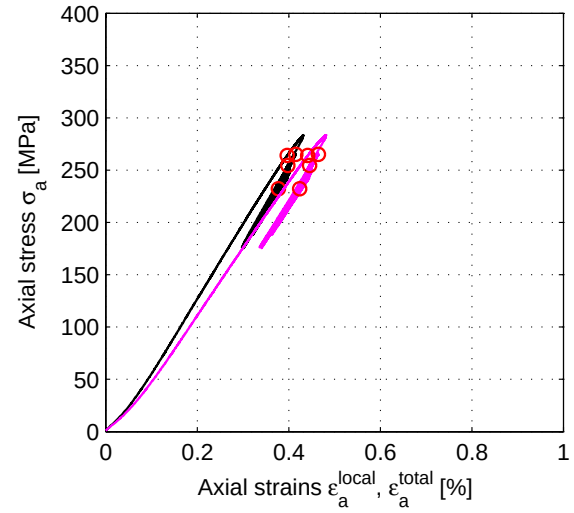

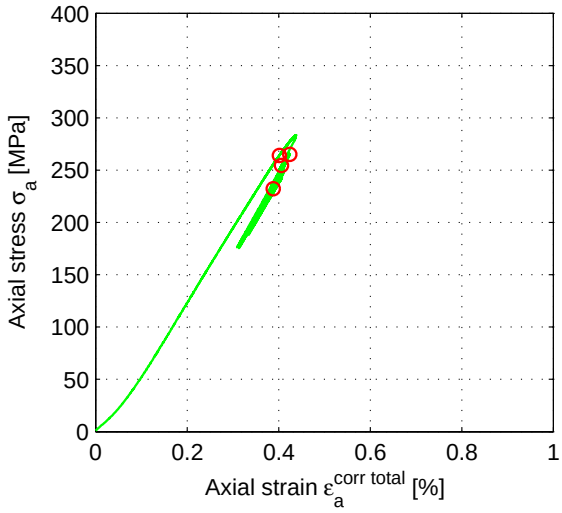

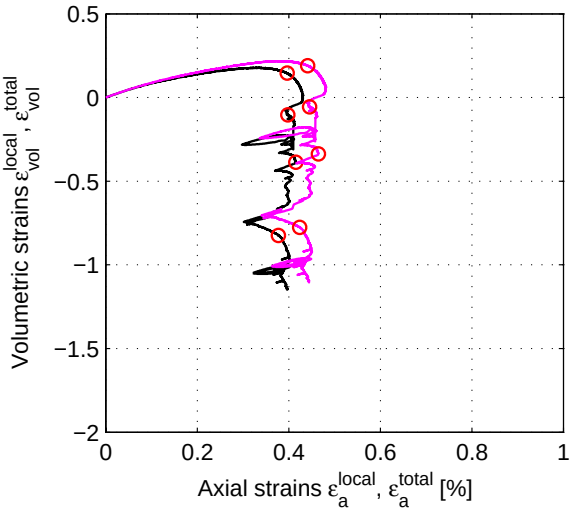

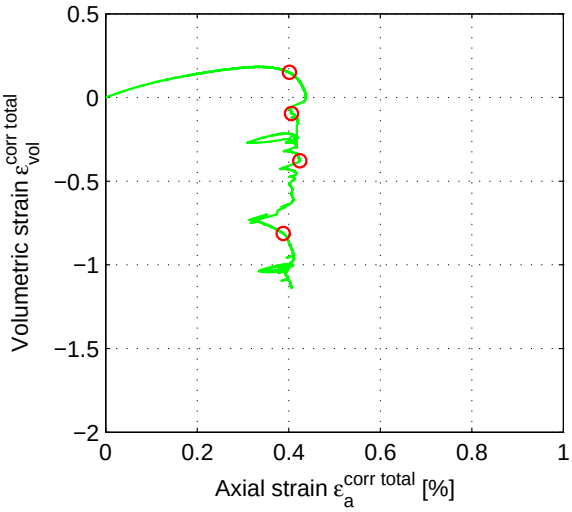

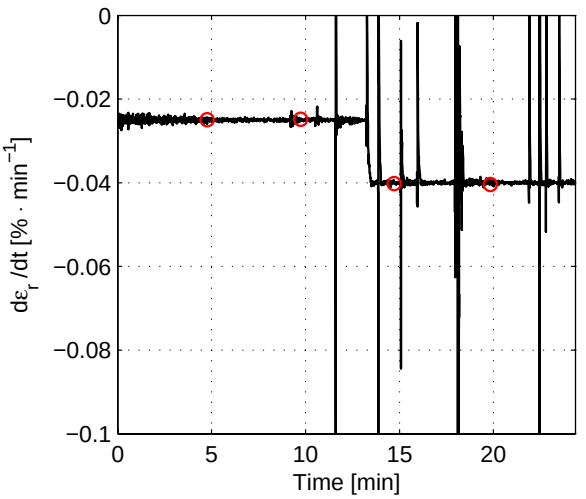

Explanation to curves above:

Based on local deformation (black)

Based on total deformation (mangenta)

Based on corrected deformation (green)

Calculated system stiffness:

K_{system} = 10.3936 [GN/m]

Specimen ID: 18T

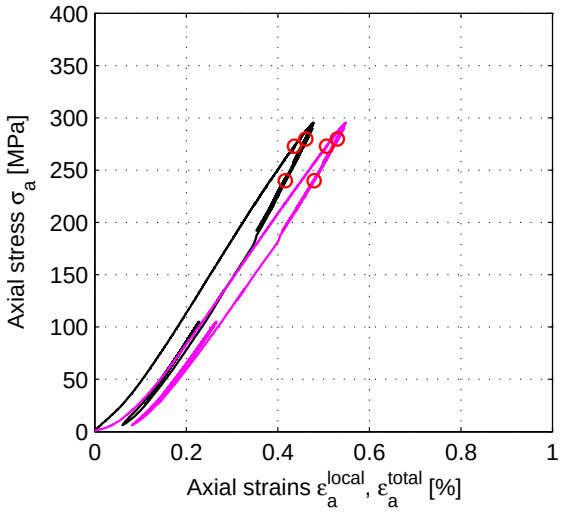

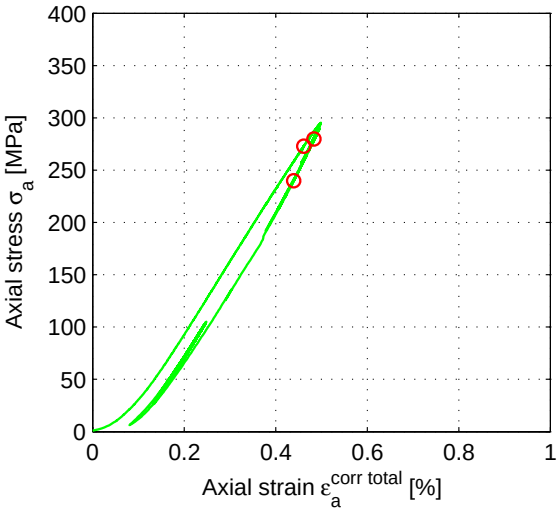

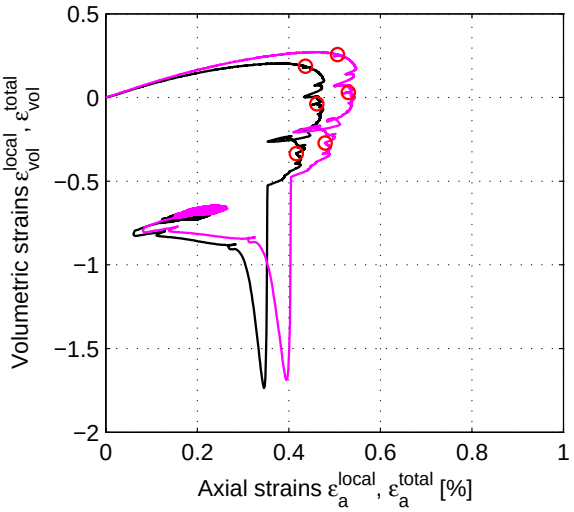

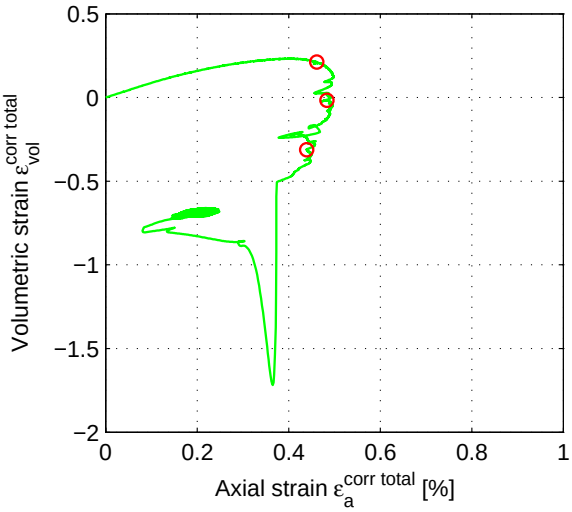

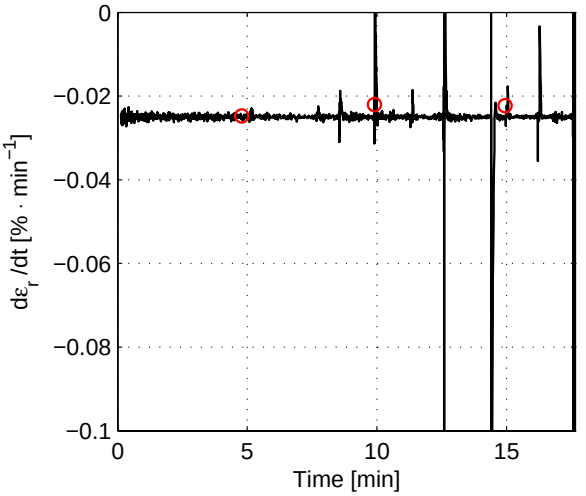

Explanation to curves above:

Based on local deformation (black)

Based on total deformation (mangenta)

Based on corrected deformation (green)

Calculated system stiffness:

K_{system} = 9.7515 [GN/m]

Specimen ID: 25T

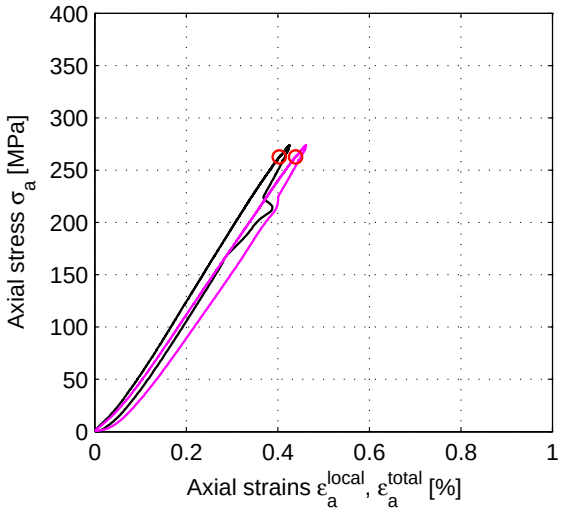

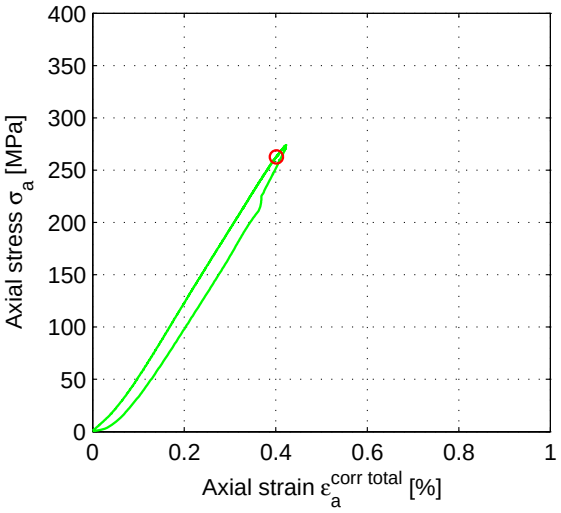

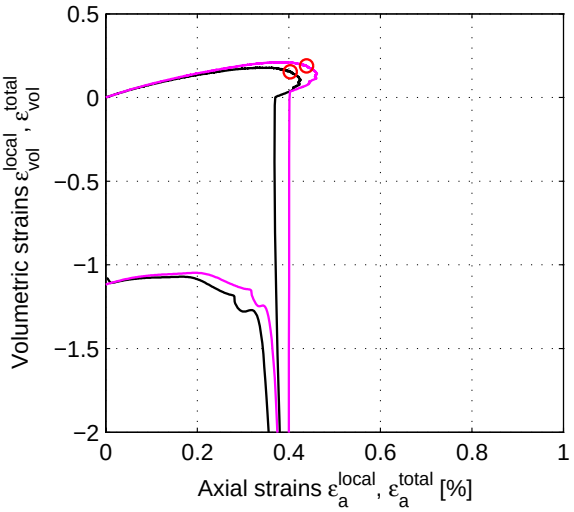

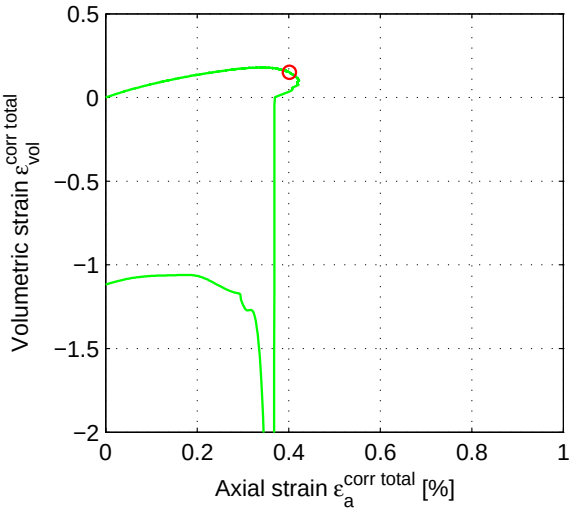

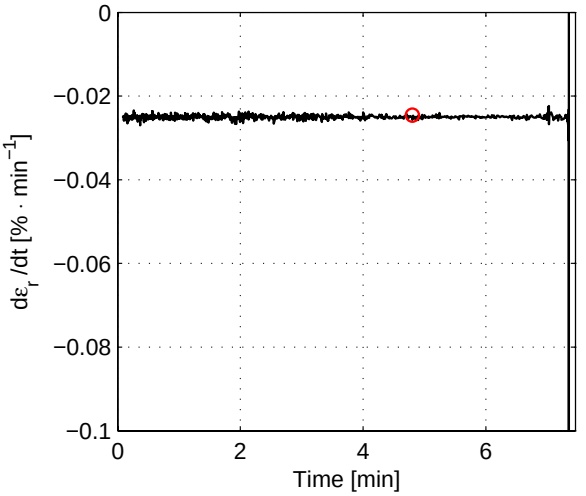

Explanation to curves above:

Based on local deformation (black)

Based on total deformation (mangenta)

Based on corrected deformation (green)

Calculated system stiffness:

K_{system} = 11.2806 [GN/m]

Specimen ID: 29T

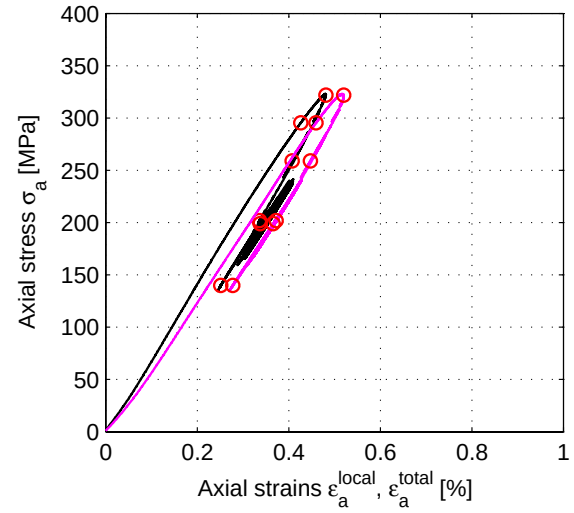

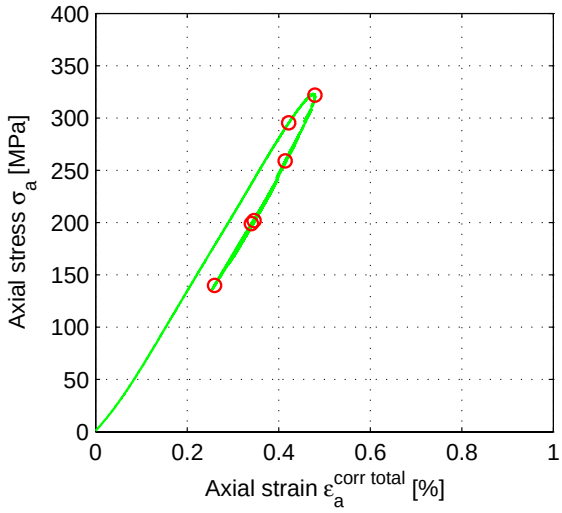

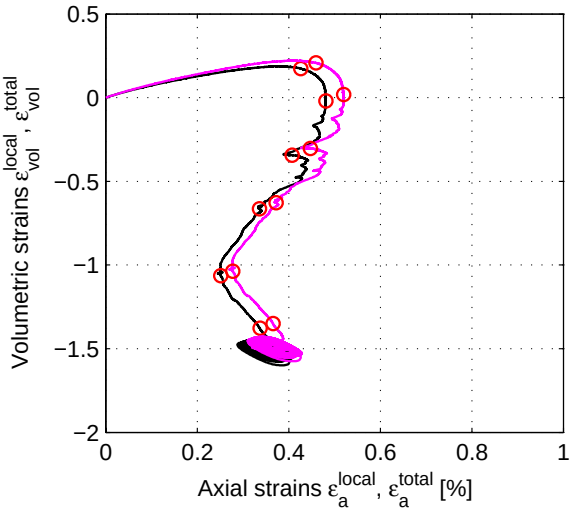

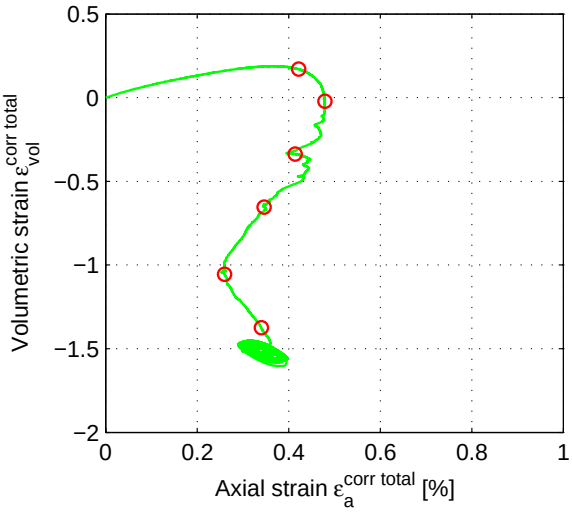

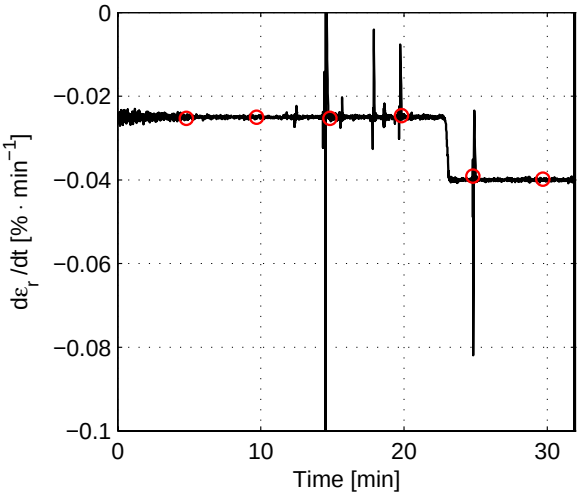

Explanation to curves above:

Based on local deformation (black)

Based on total deformation (mangenta)

Based on corrected deformation (green)

Calculated system stiffness:

K_{system} = 12.7059 [GN/m]

B.2 Specimens saturated with distilled water

Specimen ID: 07D

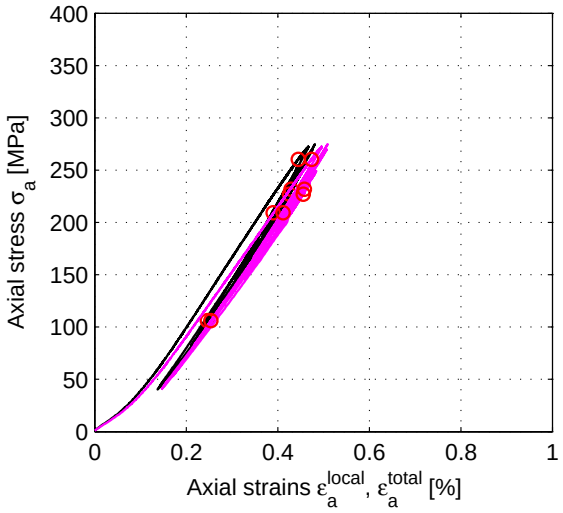

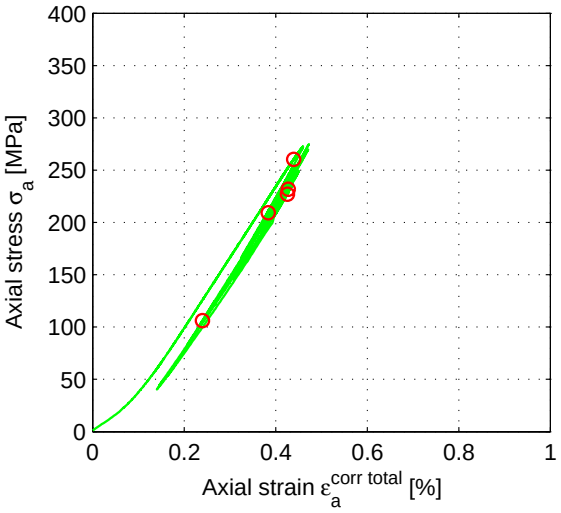

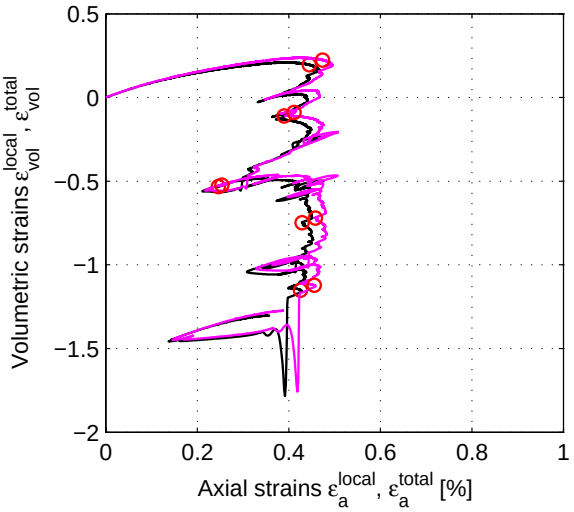

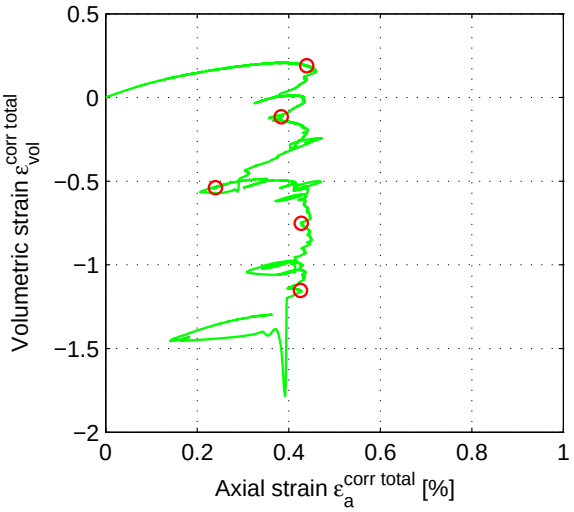

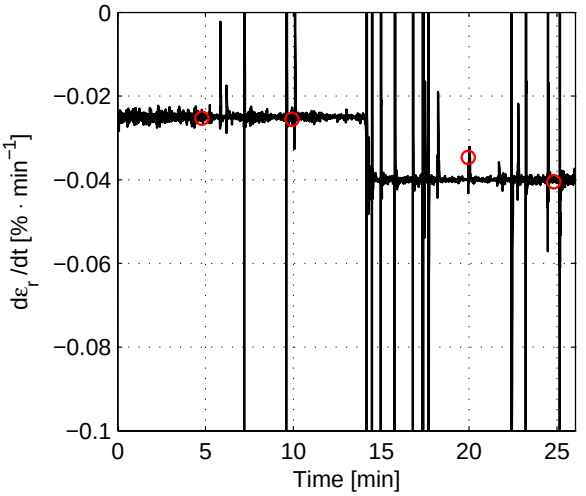

Explanation to curves above:

Based on local deformation (black)

Based on total deformation (mangenta)

Based on corrected deformation (green)

Calculated system stiffness:

K_{system} = 12.1774 [GN/m]

Specimen ID: 24D

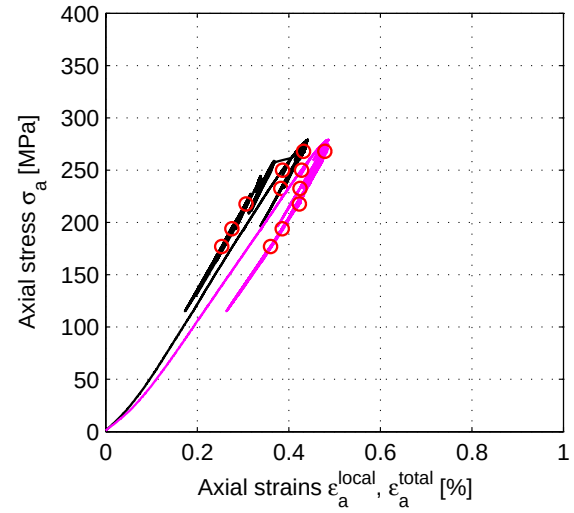

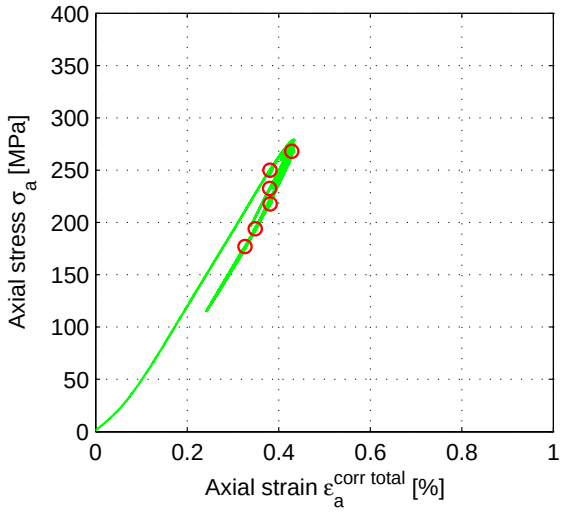

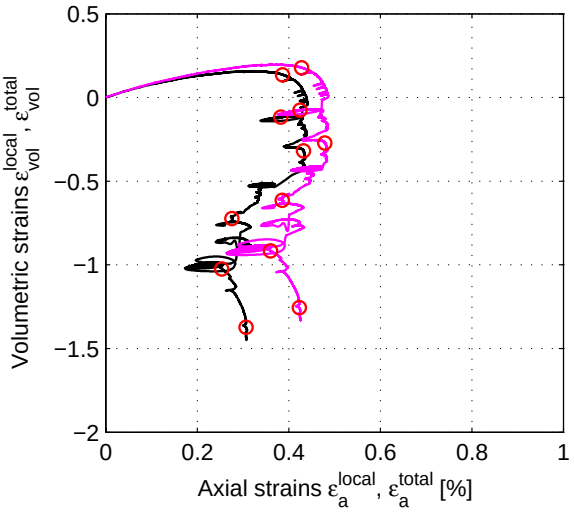

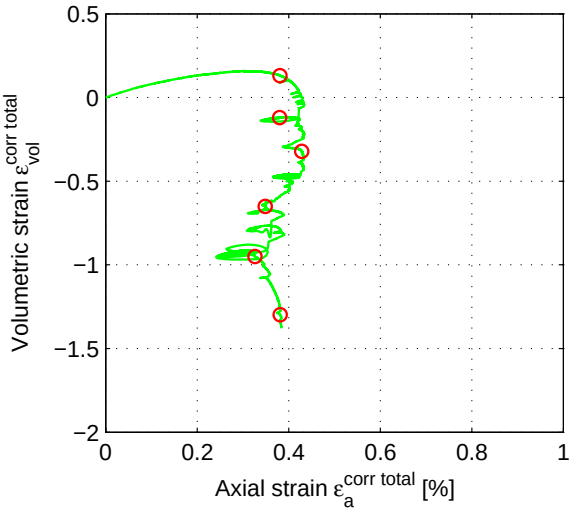

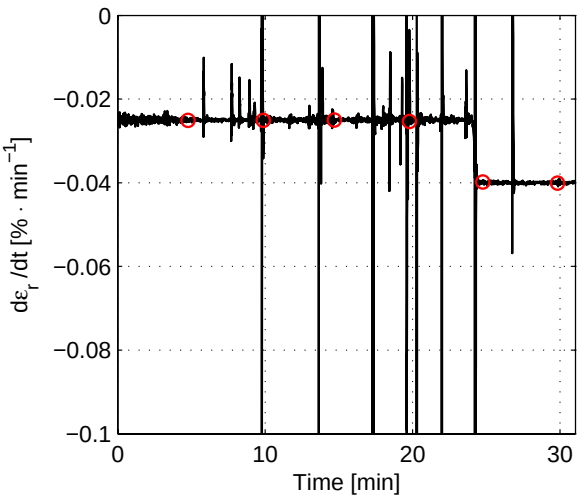

Explanation to curves above:

Based on local deformation (black)

Based on total deformation (mangenta)

Based on corrected deformation (green)

Calculated system stiffness:

K_{system} = 8.5721 [GN/m]

Specimen ID: 15D

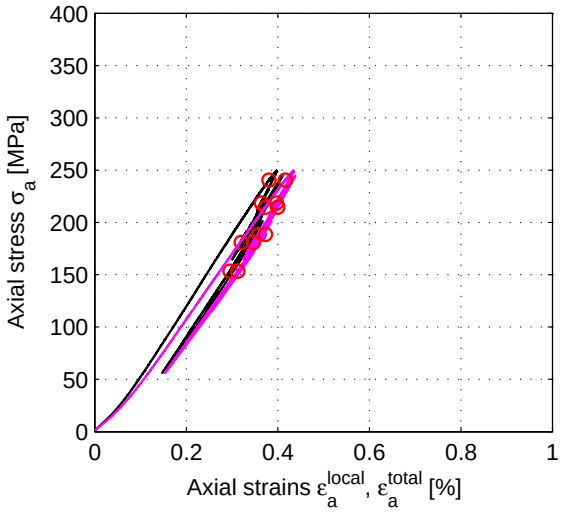

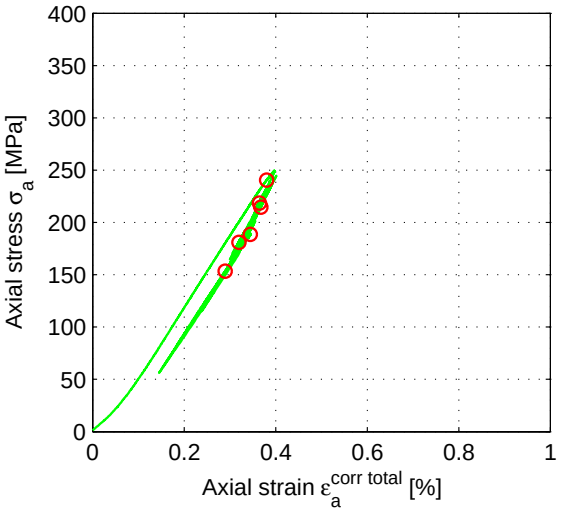

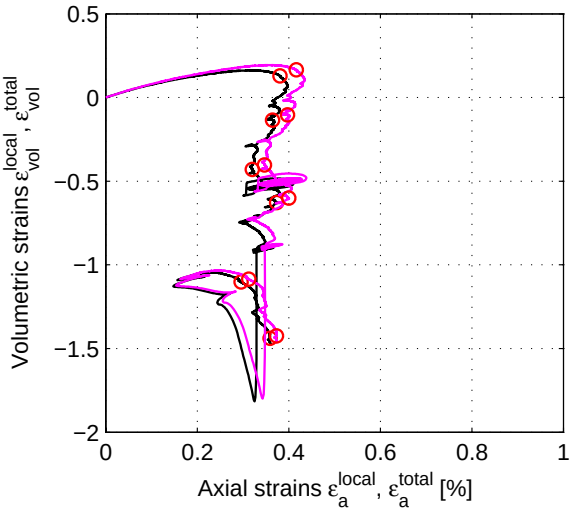

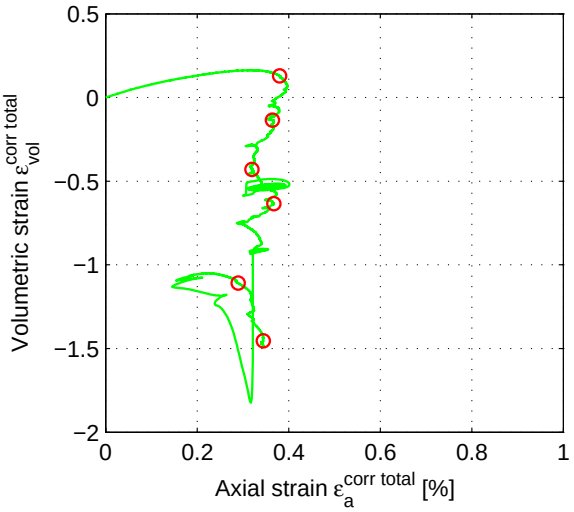

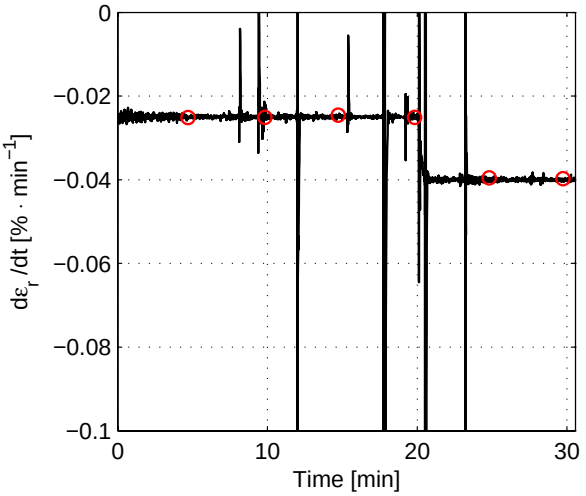

Explanation to curves above:

Based on local deformation (black)

Based on total deformation (mangenta)

Based on corrected deformation (green)

Calculated system stiffness:

K_{system} = 10.5577 [GN/m]

Specimen ID: 19D

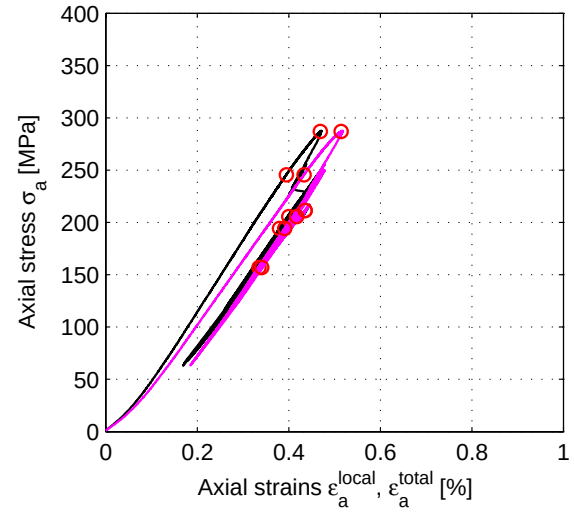

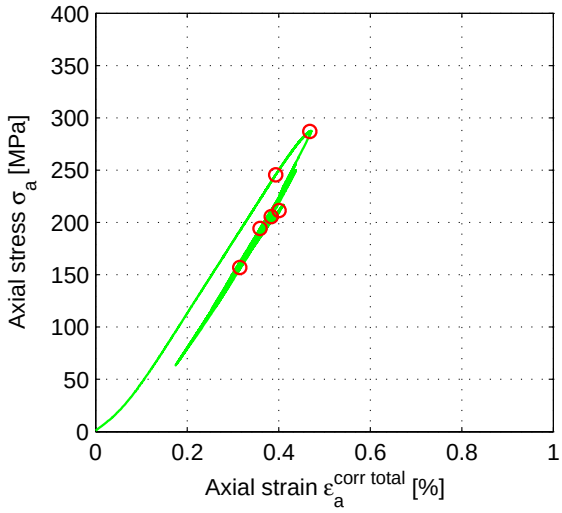

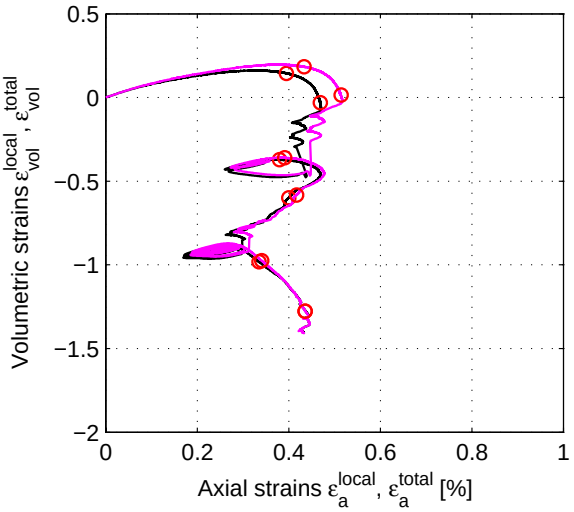

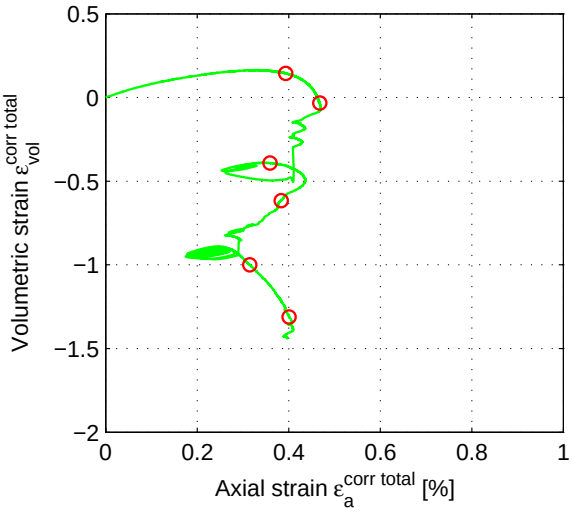

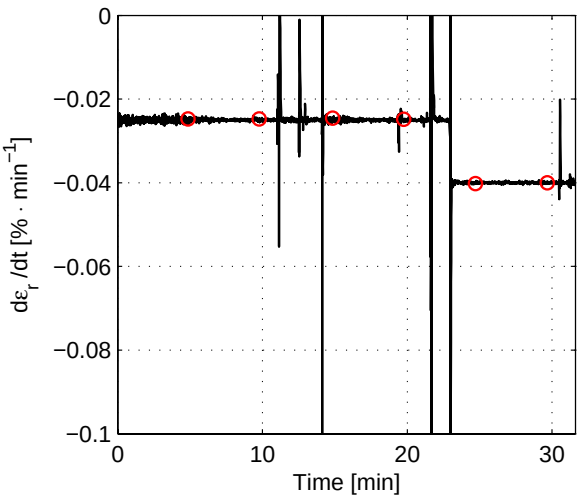

Explanation to curves above:

Based on local deformation (black)

Based on total deformation (mangenta)

Based on corrected deformation (green)

Calculated system stiffness:

K_{system} = 9.7845 [GN/m]

Specimen ID: 26D

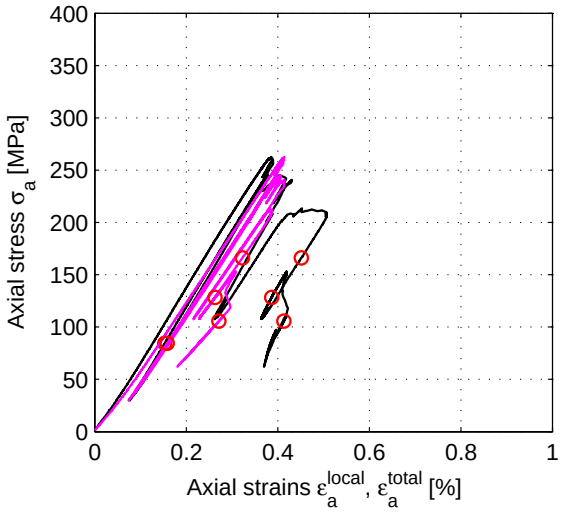

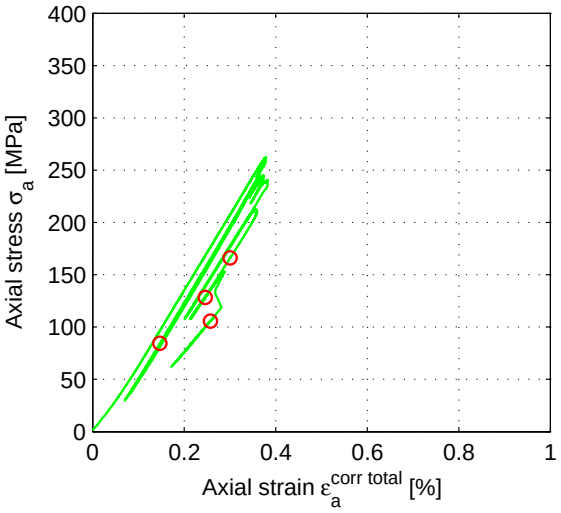

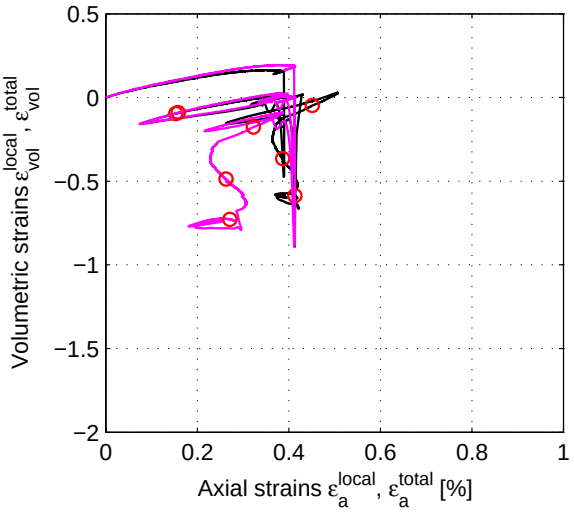

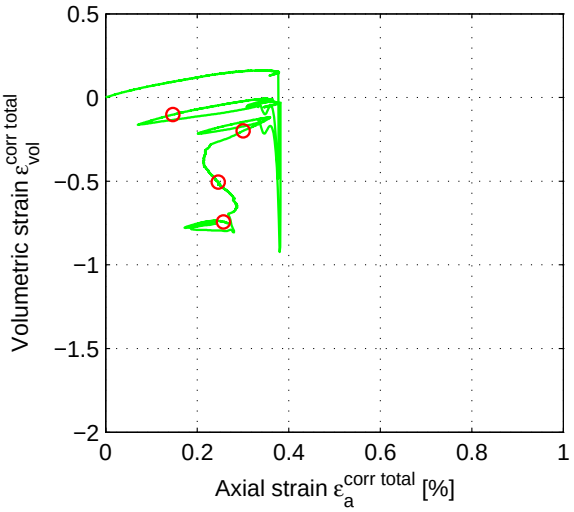

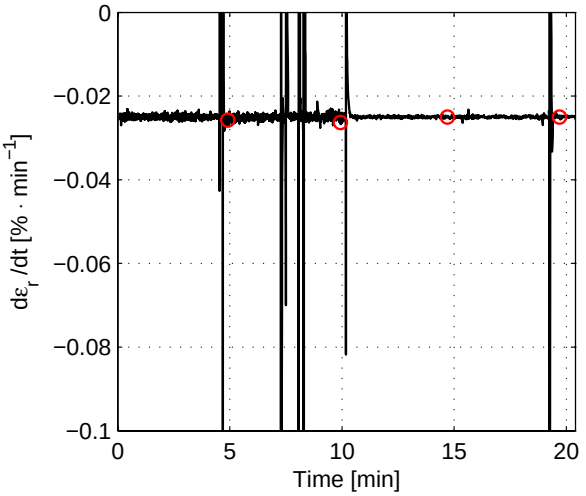

Explanation to curves above:

Based on local deformation (black)

Based on total deformation (mangenta)

Based on corrected deformation (green)

Calculated system stiffness:

K_{system} = 11.8997 [GN/m]

B.3 Specimens saturated with formation water

Specimen ID: 16F

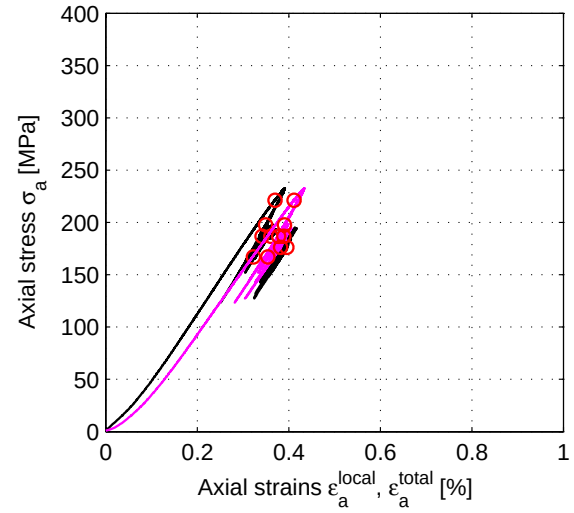

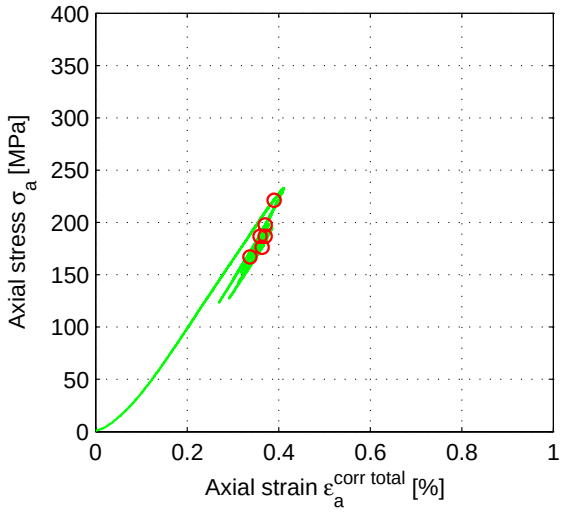

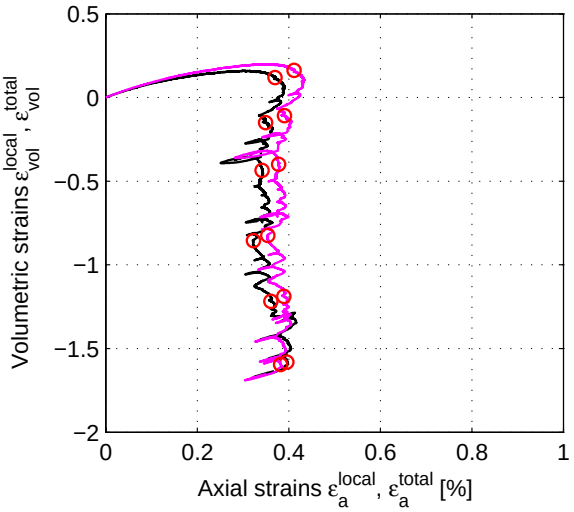

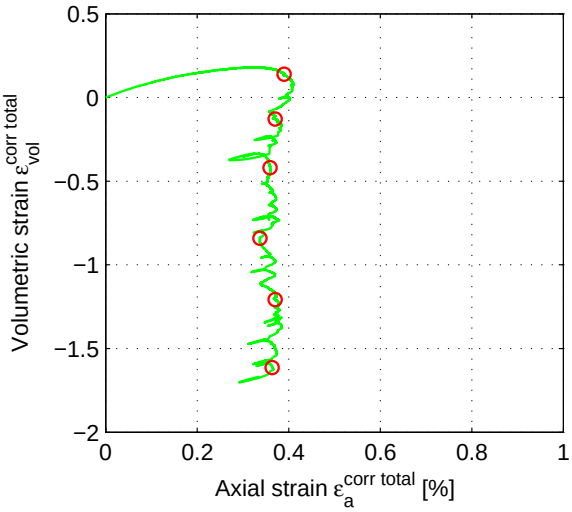

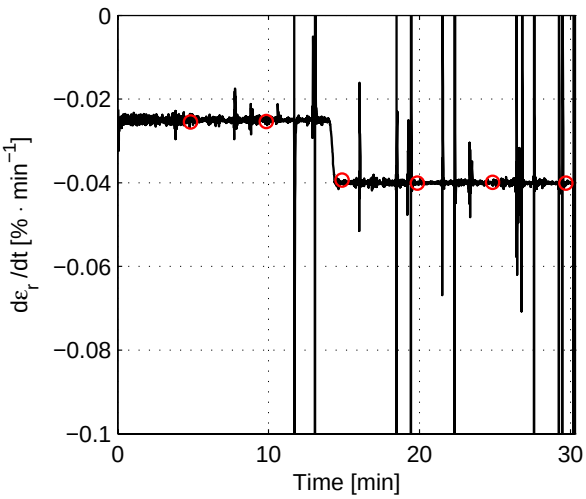

Explanation to curves above:

Based on local deformation (black)

Based on total deformation (mangenta)

Based on corrected deformation (green)

Calculated system stiffness:

K_{system} = 15.9847 [GN/m]

Specimen ID: 20F

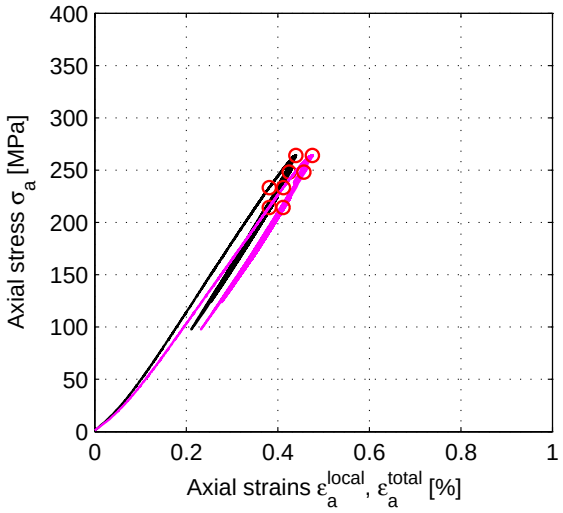

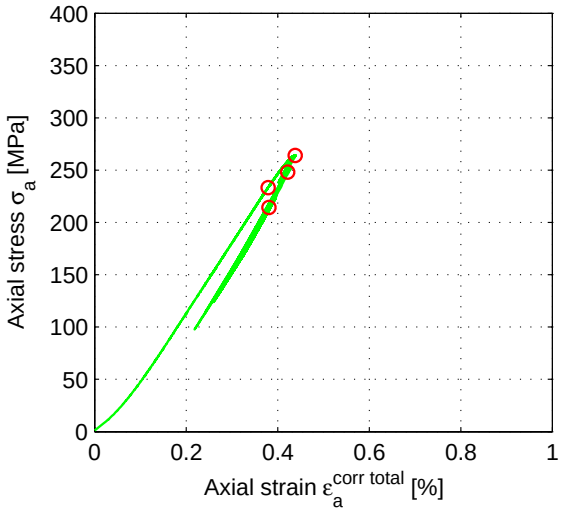

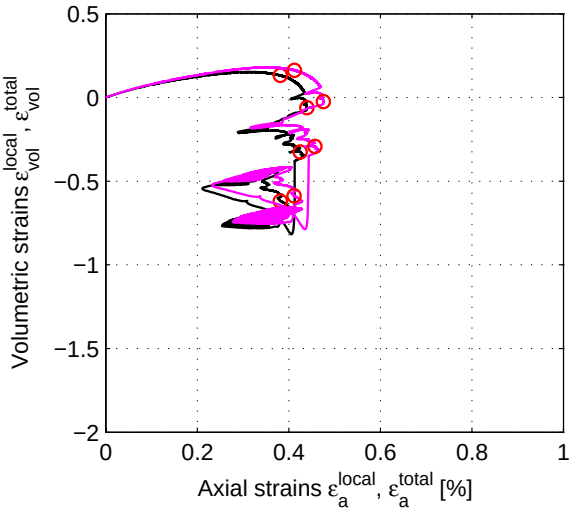

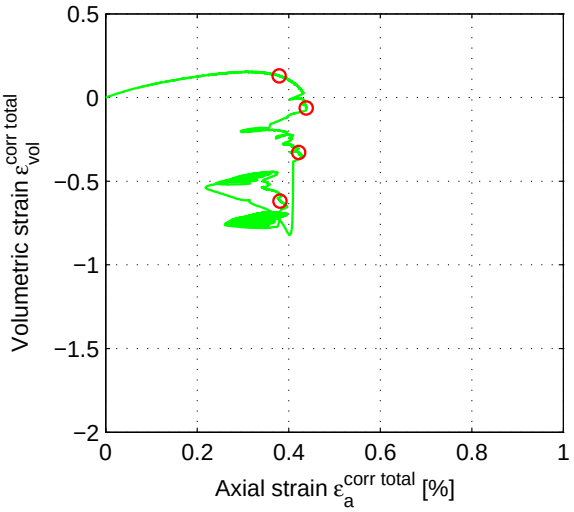

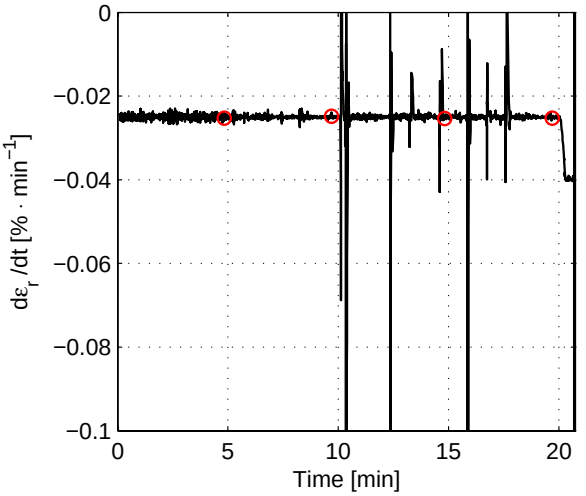

Explanation to curves above:

Based on local deformation (black)

Based on total deformation (mangenta)

Based on corrected deformation (green)

Calculated system stiffness:

K_{system} = 11.1678 [GN/m]

Specimen ID: 27F

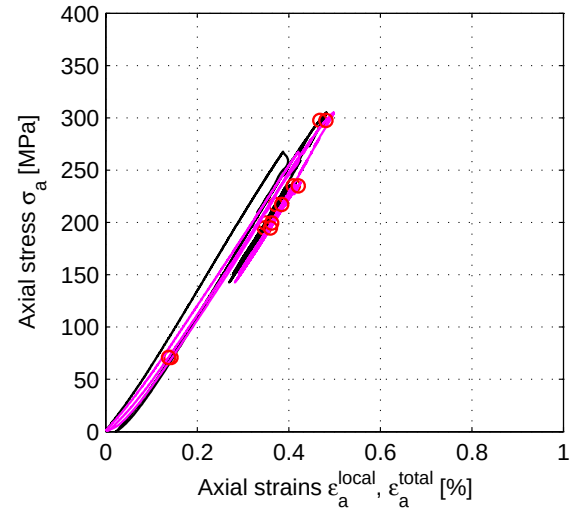

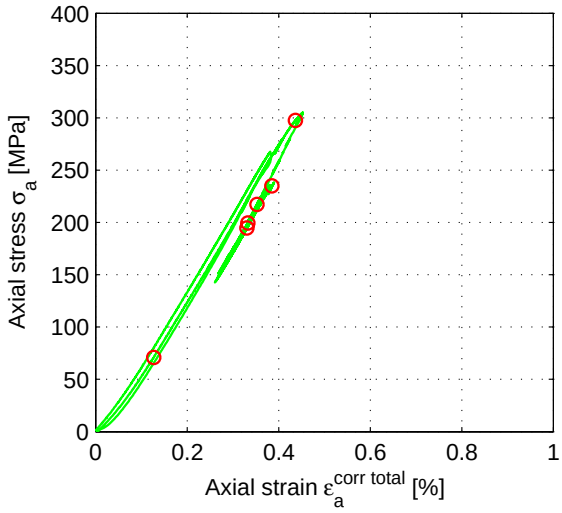

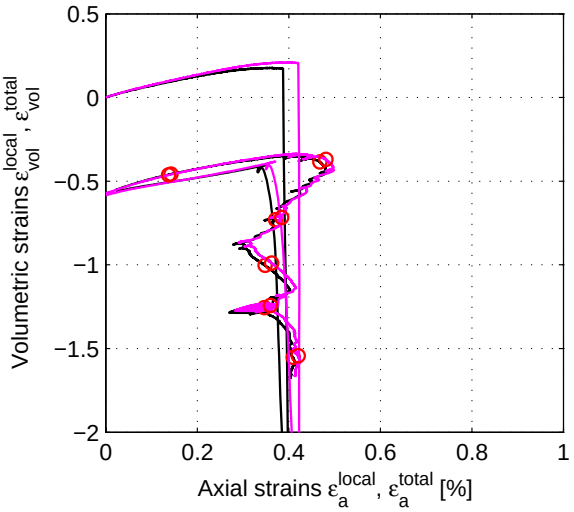

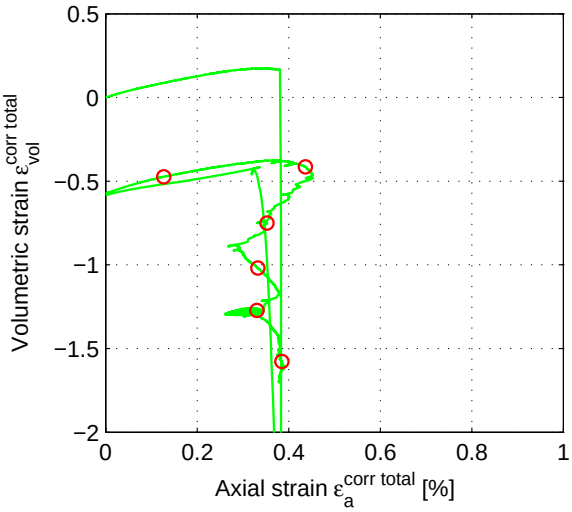

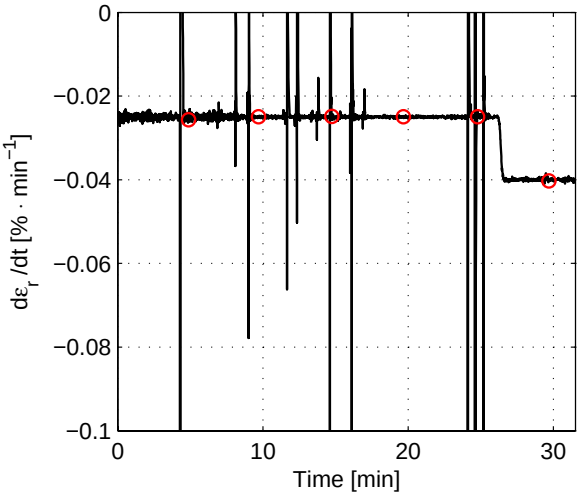

Explanation to curves above:

Based on local deformation (black)

Based on total deformation (mangenta)

Based on corrected deformation (green)

Calculated system stiffness:

K_{system} = 10.7198 [GN/m]

Specimen ID: 28F

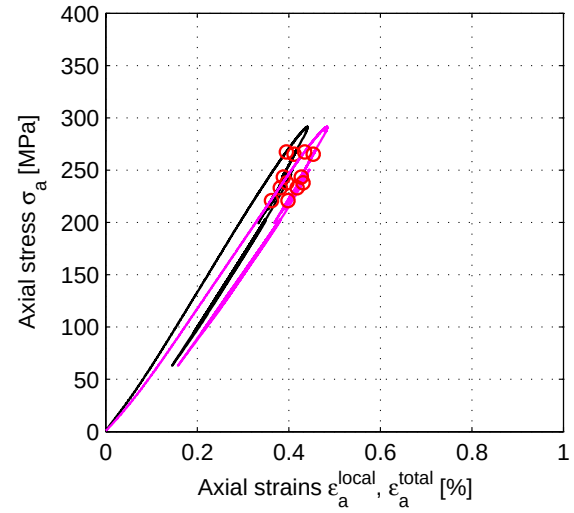

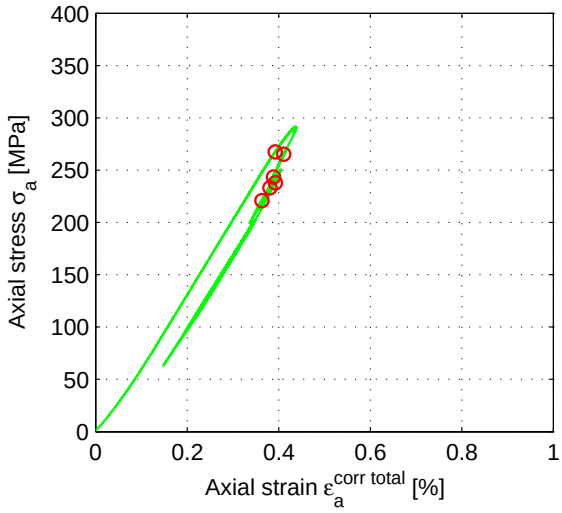

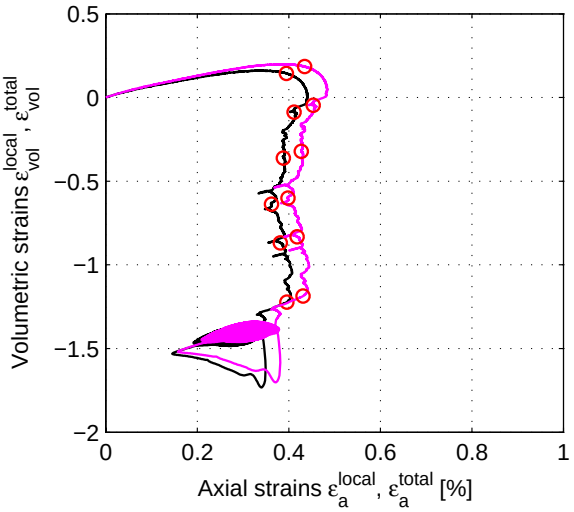

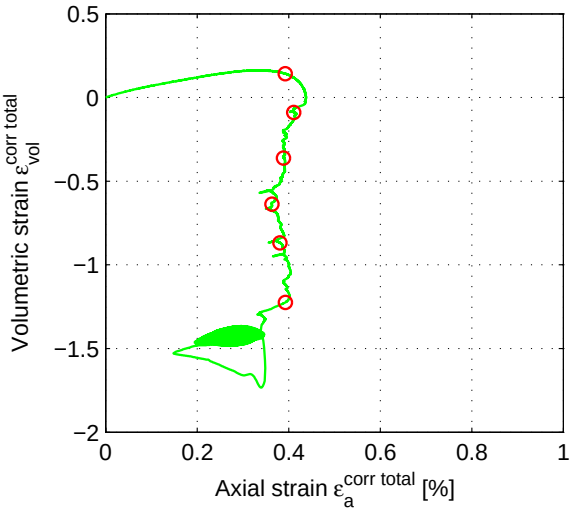

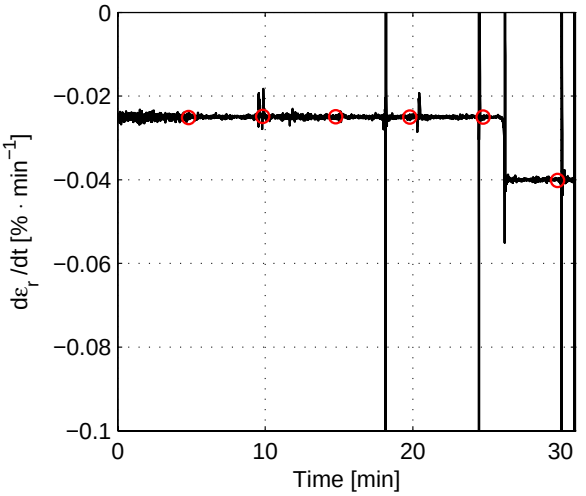

Explanation to curves above:

Based on local deformation (black)

Based on total deformation (mangenta)

Based on corrected deformation (green)

Calculated system stiffness:

K_{system} = 9.9881 [GN/m]

Specimen ID: 30F

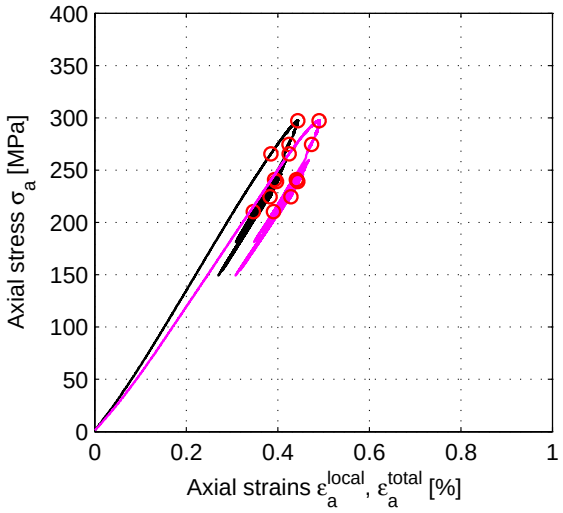

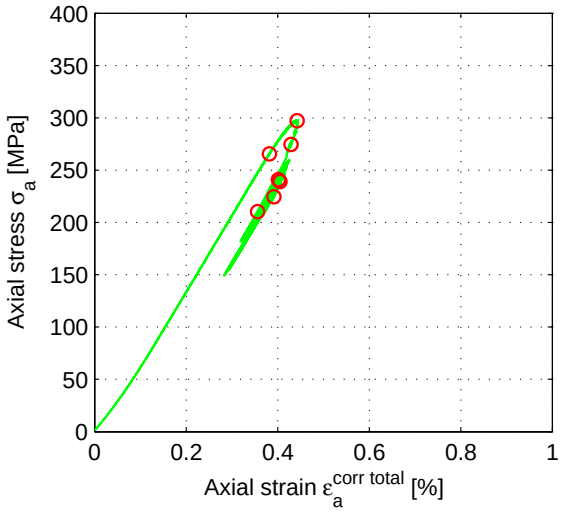

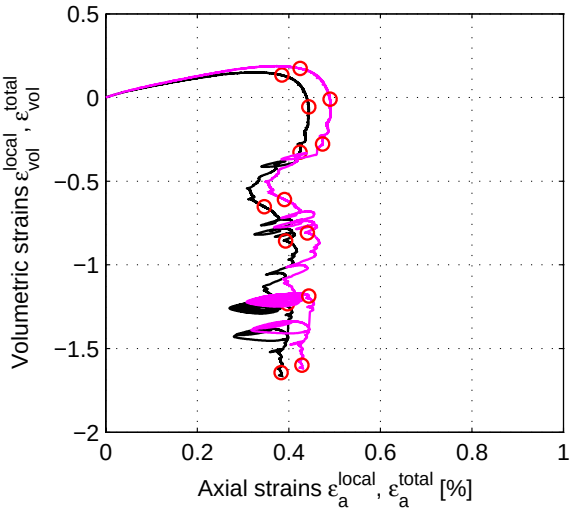

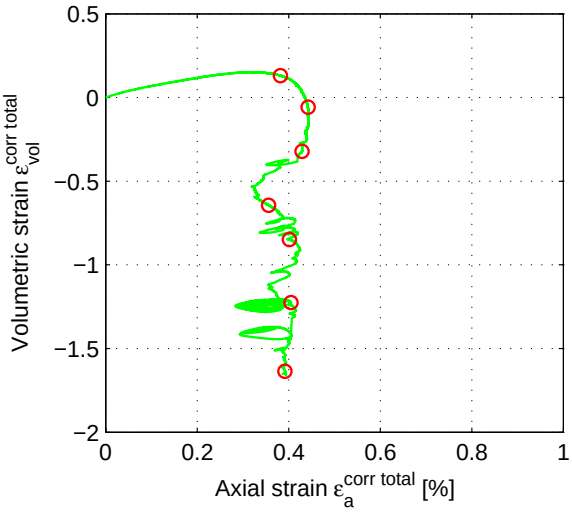

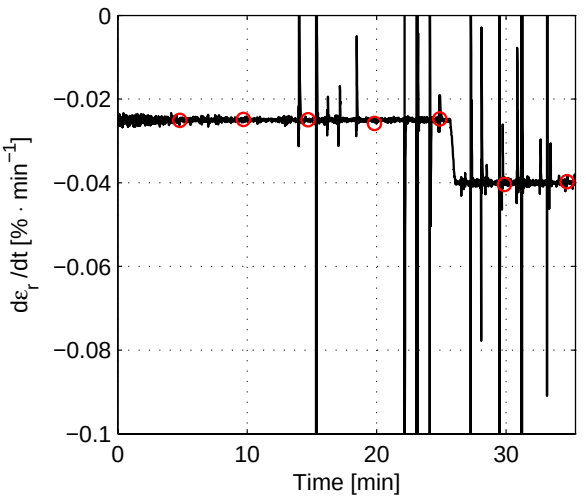

Explanation to curves above:

Based on local deformation (black)

Based on total deformation (mangenta)

Based on corrected deformation (green)

Calculated system stiffness:

K_{system} = 9.7749 [GN/m]

B.4 Specimens saturated with saline water

Specimen ID: 04S

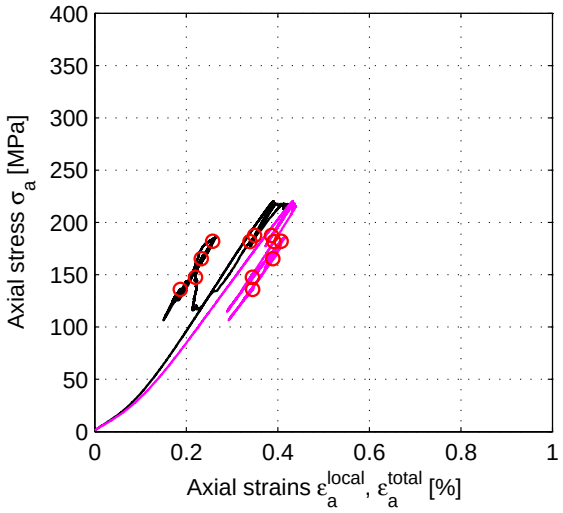

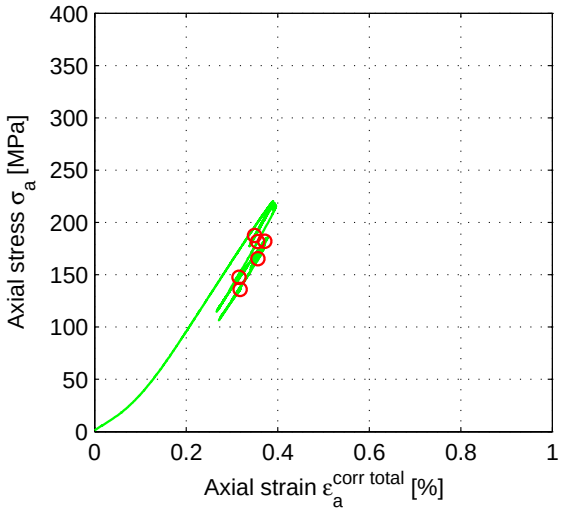

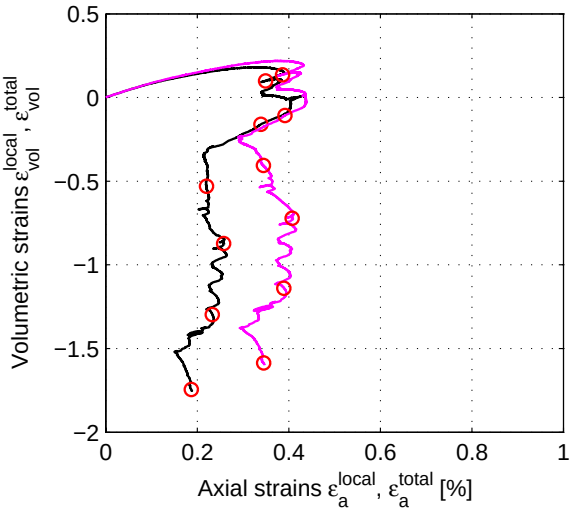

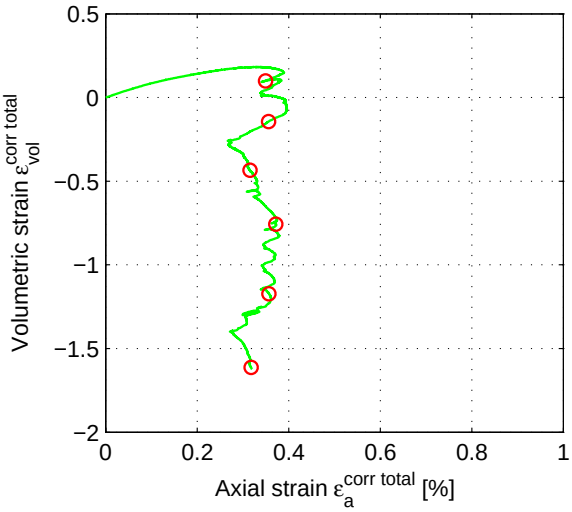

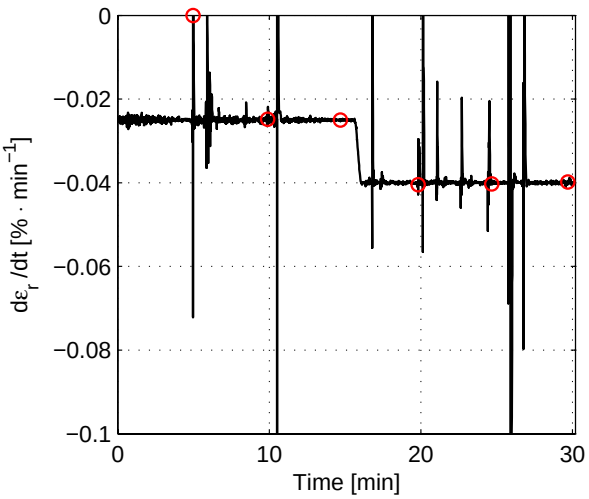

Explanation to curves above:

Based on local deformation (black)

Based on total deformation (mangenta)

Based on corrected deformation (green)

Calculated system stiffness:

K_{system} = 8.1204 [GN/m]

Specimen ID: 09S

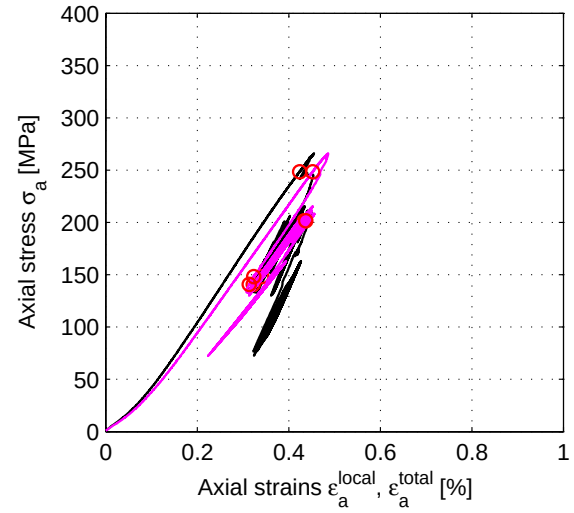

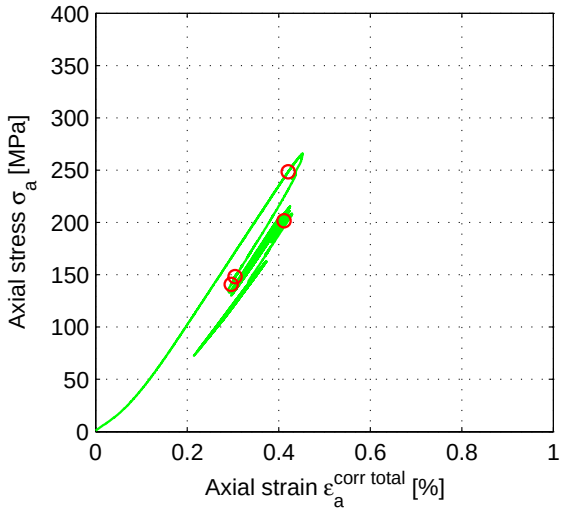

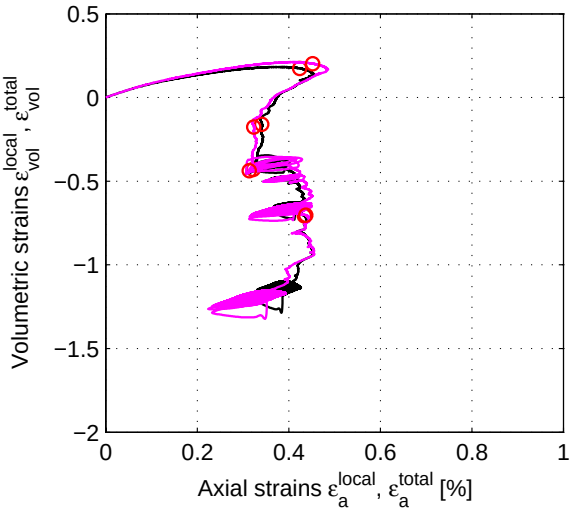

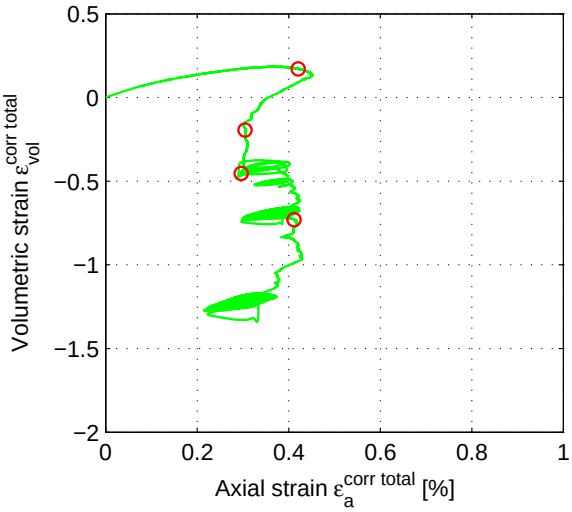

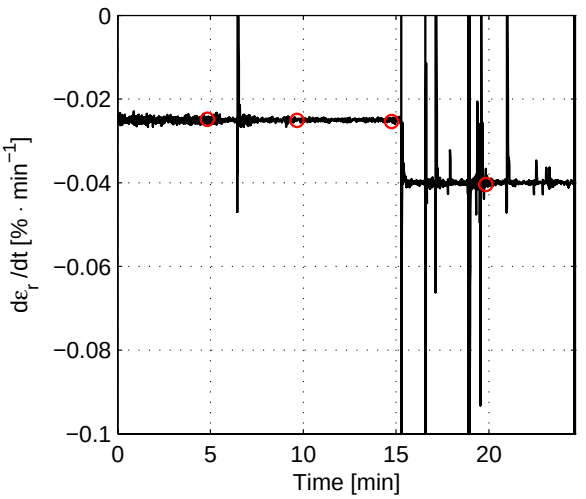

Explanation to curves above:

Based on local deformation (black)

Based on total deformation (mangenta)

Based on corrected deformation (green)

Calculated system stiffness:

K_{system} = 12.7227 [GN/m]

Specimen ID: 13S

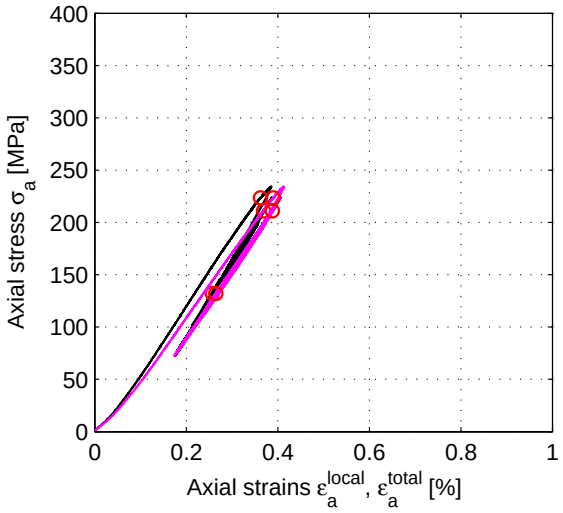

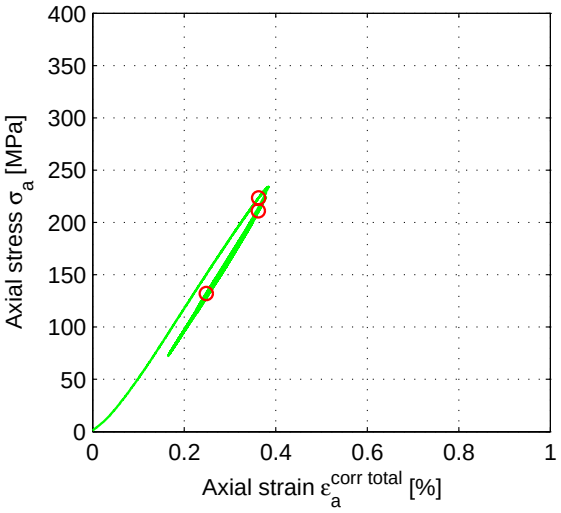

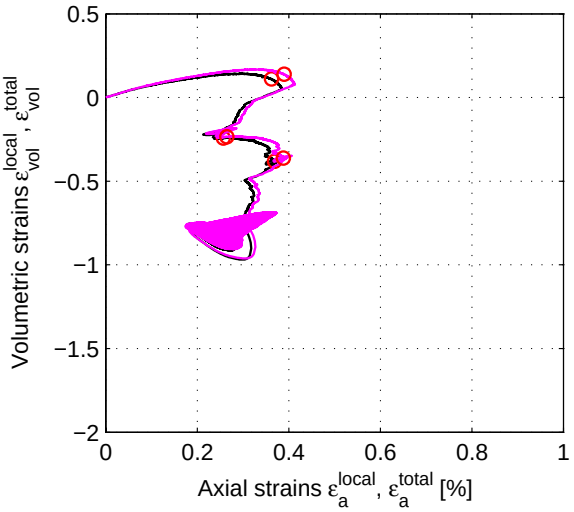

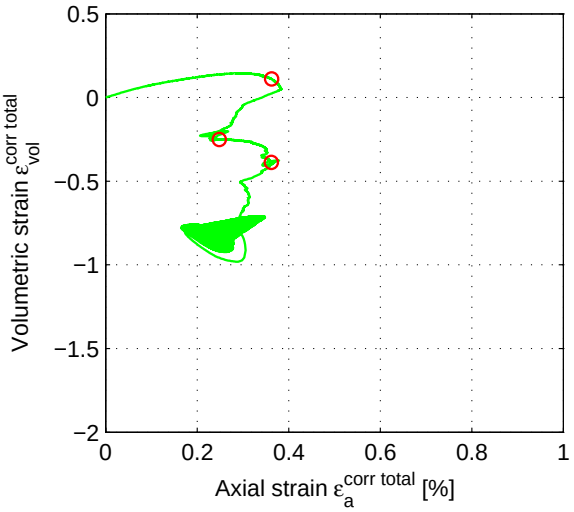

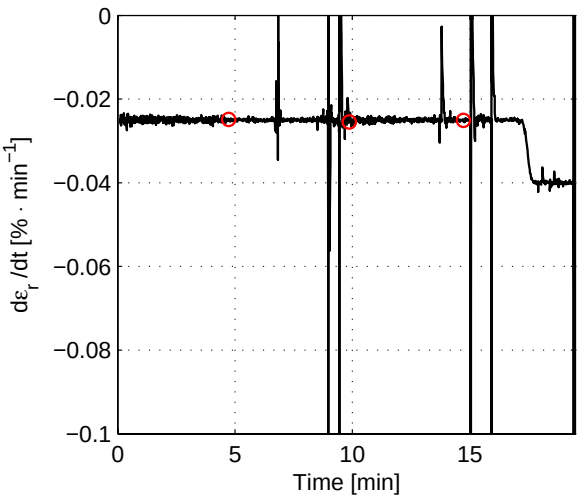

Explanation to curves above:

Based on local deformation (black)

Based on total deformation (mangenta)

Based on corrected deformation (green)

Calculated system stiffness:

K_{system} = 12.957 [GN/m]

Specimen ID: 17S

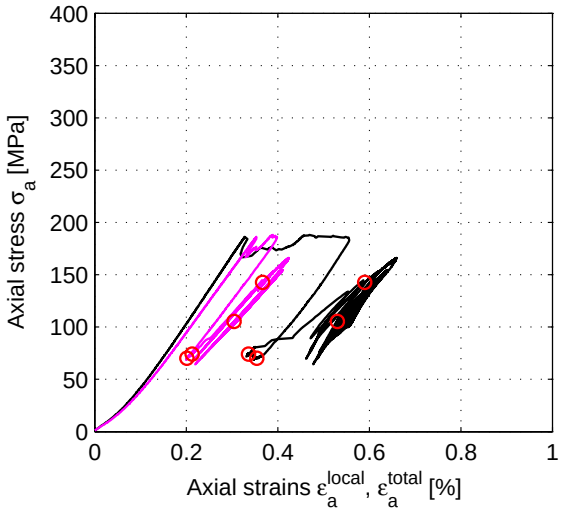

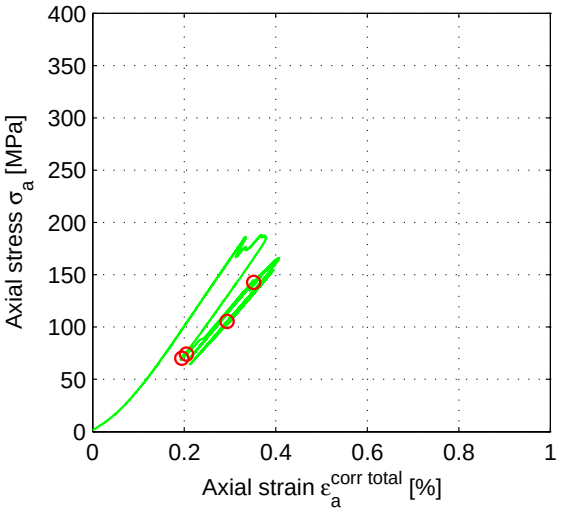

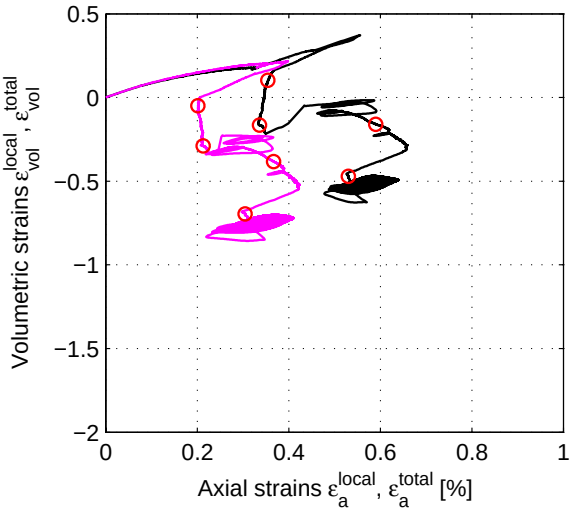

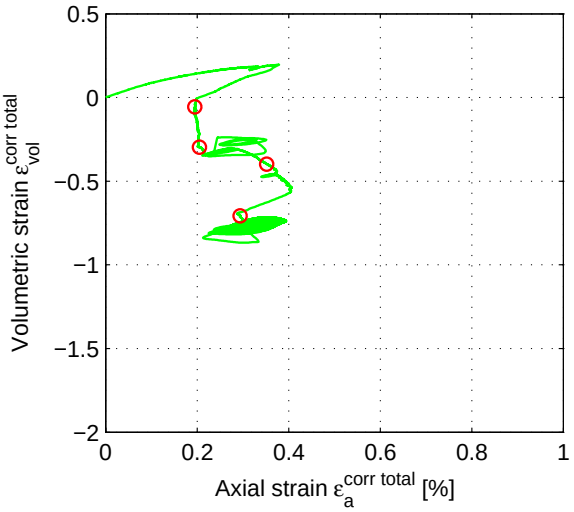

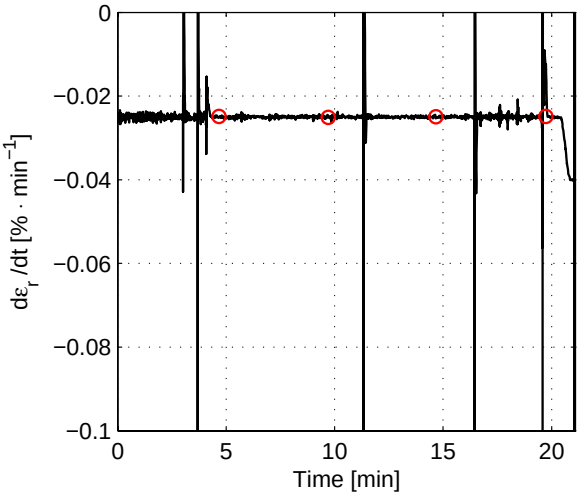

Explanation to curves above:

Based on local deformation (black)

Based on total deformation (mangenta)

Based on corrected deformation (green)

Calculated system stiffness:

K_{system} = 15.4365 [GN/m]

Specimen ID: 21S

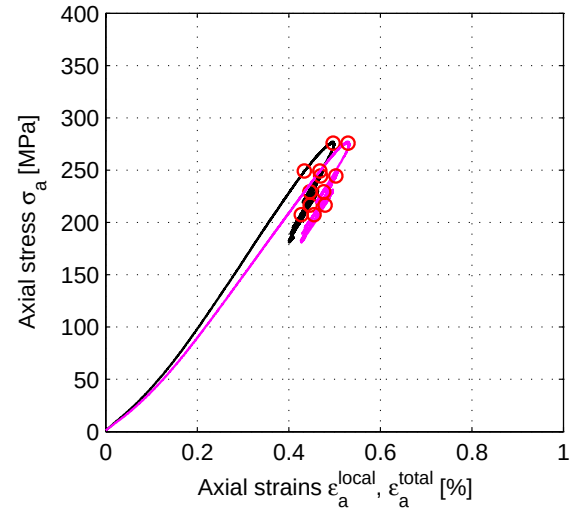

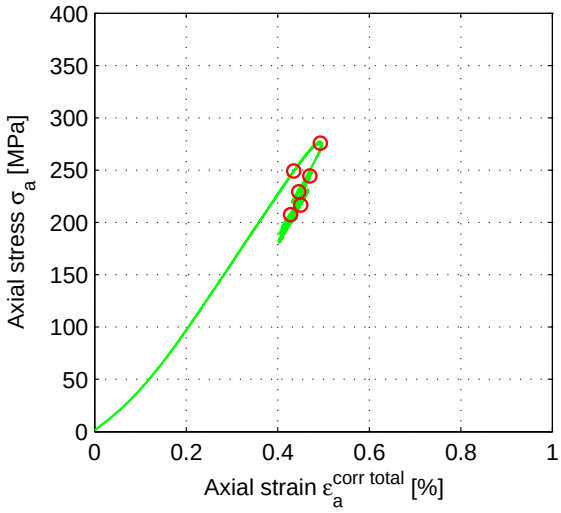

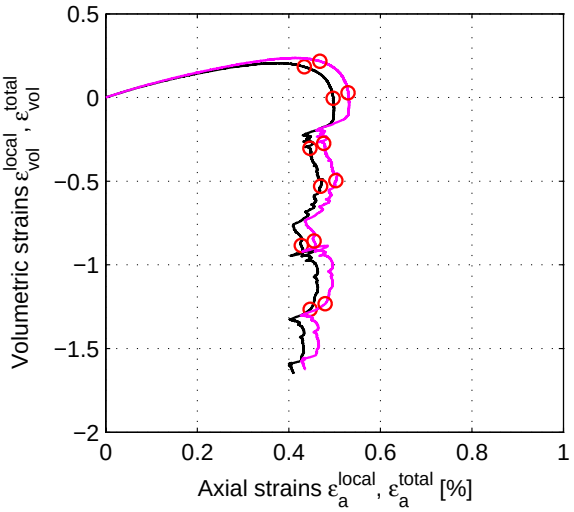

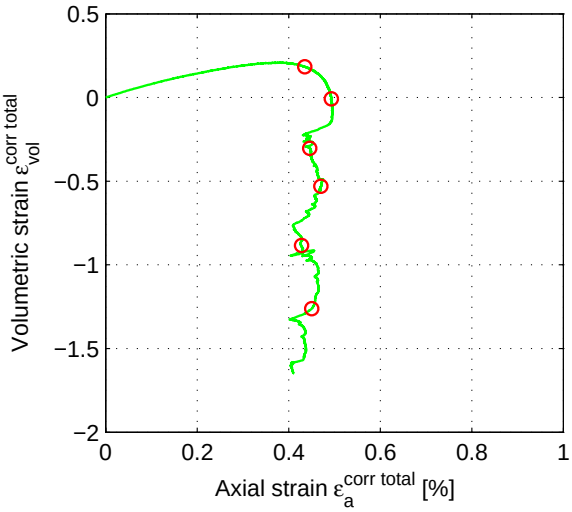

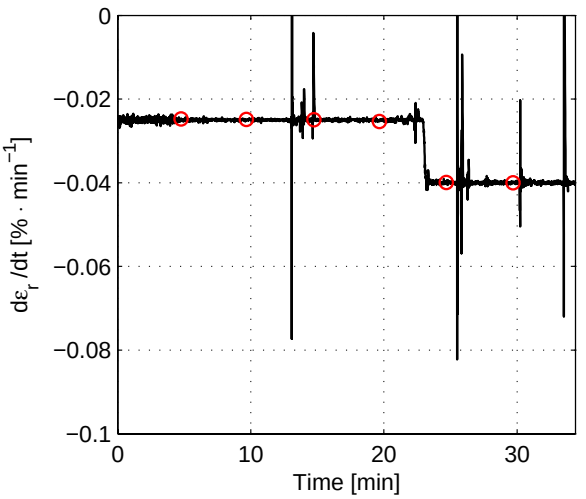

Explanation to curves above:

Based on local deformation (black)

Based on total deformation (mangenta)

Based on corrected deformation (green)

Calculated system stiffness:

K_{system} = 12.016 [GN/m]